การพัฒนาและประยุกต์ใช้เชิงตัวเลขของแบบจำลองดินที่อ้างอิงกฎอุณหพลศาสตร์

นายเด็ดดิ อาพริอาดิ

วิทยานิพนธ์นี้เป็นส่วนหนึ่งของการศึกษาตามหลักสูตรปริญญาวิศวกรรมศาสตรดุษฎีบัณฑิต

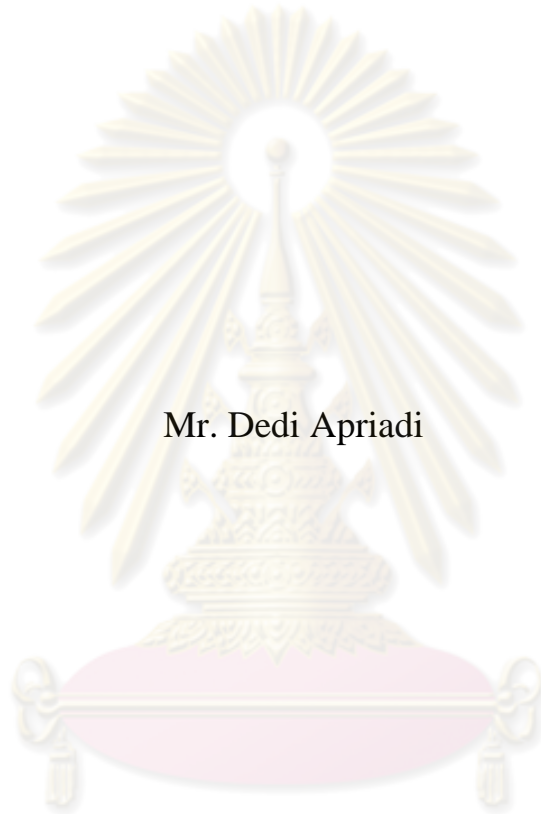สาขาวิชาวิศวกรรมโยธา ภาควิชาวิศวกรรมโยธา

คณะวิศวกรรมศาสตร์ จุฬาลงกรณ์มหาวิทยาลัย

ปีการศึกษา 2552

DEVELOPMENT AND NUMERICAL IMPLEMENTATION
OF THERMODYNAMICS-BASED SOIL MODEL

Mr. Dedi Apriadi

A Dissertation Submitted in Partial Fulfilment of the Requirements

for the Degree of Doctor of Philosophy in Civil Engineering

Department of Civil Engineering

Faculty of Engineering

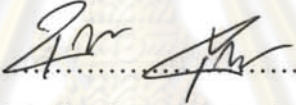Chulalongkorn University

Academic Year 2009

Thesis Title   DEVELOPMENT AND NUMERICAL IMPLEMENTATION
                 OF THERMODYNAMICS-BASED SOIL MODEL

By   Mr. Dedi Apriadi

Field of Study   Civil Engineering

Thesis Advisor   Assistant Professor Suched Likitlersuang, D.Phil

---

Accepted by the Faculty of Engineering, Chulalongkorn University in
Partial Fulfilment of the Requirements for the Doctoral Degree

....................................Dean of the Faculty of Engineering

(Associate Professor Boonsom Lerdhirunwong, Dr. Ing.)

THESIS COMMITTEE

.... Chairman

(Associate Professor Boonchai Ukritchon, Sc. D.)

.... Thesis Advisor

(Assistant Professor Suched Likitlersuang, D.Phil)

.... Thesis Co-advisor

(Associate Professor Thirapong Pipatpongsa, D.Eng)

.... Examiner

(Associate Professor Tirawat Boonyatee, D. Eng.)

.... External Examiner

(Assistant Professor Siam Yimsiri, Ph.D.)

เด็ดดี อาพริอาดิ: การพัฒนาและประยุกต์ใช้เชิงตัวเลขของแบบจำลองดินที่อ้างอิงกฎอุณ
หพลศาสตร์. (Development and numerical implementation of thermodynamics-
based soil model) อ.ที่ปรึกษาวิทยานิพนธ์หลัก: ผศ.ดร.สุเชษฐ์ ลิขิตเลอสรวง, อ.ที่
ปรึกษาวิทยานิพนธ์ร่วม: รศ.ดร.ธีรพงษ์ พิพัฒน์พงศา 110 หน้า.

ในการวิเคราะห์และออกแบบทางวิศวกรรมธรณีเทคนิคนั้น วิศวกรนิยมเลือกใช้แบบจำลองมอร์-คู
ลอมบ์ และแบบจำลองแคมเคลย์ในการอธิบายพฤติกรรมของดิน อย่างไรก็ตามด้วยข้อจำกัดของ
แบบจำลองทั้งสองที่ยังไม่อธิบายพฤติกรรมที่ซับซ้อนของดินได้อย่างครบถ้วน ส่งผลให้มีการ
พัฒนาทฤษฎีและหลักการต่าง ๆ เพื่อใช้อธิบายพฤติกรรมดินได้ถี่ถ้วนขึ้น เช่น พฤติกรรมที่
ความเครียดระดับต่ำ และผลของประวัติความเค้นก่อนหน้า ตัวอย่างหลักการที่มีชื่อเสียงเช่น
หลักการพื้นผิวครากเชิงซ้อน หลักการพื้นผิวบาวดิง และหลักการไฮโพพลาสติกซิตี เป็นต้น
นอกเหนือจากนั้นยังมีผลการทดสอบในห้องปฏิบัติการชี้ให้เห็นว่า ลักษณะความเค้นและ
ความเครียดของดินเป็นแบบไม่เชิงเส้นขึ้นกับระดับความเค้น และยังแสดงพฤติกรรมไม่คืนตัว การ
พัฒนาสมการความสัมพันธ์ระหว่างความเค้นกับความเครียดของดินควรจะต้องสอดคล้องกับ
พฤติกรรมเชิงกายภาพของดิน ยกตัวอย่างเช่น แบบจำลองดินอย่างน้อยไม่ควรที่จะละเมิดกฎ
พื้นฐานทางฟิสิกส์ ดังนั้นแบบจำลองที่อ้างอิงกฎพื้นฐานทางฟิสิกส์น่าจะเป็นแนวทางที่เหมาะจะ
นำมาใช้อธิบายพฤติกรรมความสัมพันธ์ระหว่างความเค้นกับความเครียดของดิน แบบจำลอง
ไคเนมาติกฮาร์ดเดนนิงโมดิฟายด์แคมเคลย์ซึ่งถูกพัฒนาขึ้นจากกฎอุณหพลศาสตร์ถูกเลือก
นำมาใช้ศึกษา โดยงานวิจัยนี้ได้ปรับปรุงและขยายความแบบจำลองรุ่นก่อนหน้า โดยเน้นปรับปรุง
ในส่วนความสัมพันธ์ไม่เชิงเส้นที่ความเครียดระดับต่ำ และขยายความแบบจำลองให้อยู่ใน
รูปแบบสมการทั่วไป ตลอดจนพัฒนาวิธีการคำนวณเชิงตัวสำหรับวัสดุที่ขึ้นกับอัตรา เพื่อ
ประโยชน์ในการคำนวณเชิงตัวเลขด้วยวิธีไฟไนต์อิลิเมนต์ แบบจำลองและวิธีการคำนวณเชิงตัว
เลขที่ปรับปรุงขึ้นนี้ได้มีการตรวจสอบกับผลข้อมูลการทดสอบในห้องปฏิบัติการหลายแห่ง เช่น มี
การสอบเทียบกับโปรแกรมการทดสอบผลของประวัติความเค้นด้วยการทดสอบแรงอัดสามแกน
ของดินเหนียวแข็งลอนดอน ตลอดจนสอบเทียบค่าพารามิเตอร์ดินเหนียวอ่อนกรุงเทพฯ จากผล
การทดสอบแรงอัดสามแกนแบบไม่ระบายน้ำ และผลการทดสอบเฉือนอย่างง่าย แบบจำลองดินที่
นำเสนอนี้สามารถอธิบายพฤติกรรมไม่เชิงเส้นที่ระดับความเค้นต่ำ พฤติกรรมไม่คืนตัว พฤติกรรม
ที่ขึ้นกับประวัติความเค้น และพฤติกรรมที่ไม่ขึ้นกับทิศทาง

ภาควิชา	วิศวกรรมโยธา	ลายมือชื่อนิสิต
สาขาวิชา	วิศวกรรมโยธา	ลายมือชื่อ อ.ที่ปรึกษาวิทยานิพนธ์หลัก
ปีการศึกษา	2552	ลายมือชื่อ อ.ที่ปรึกษาวิทยานิพนธ์ร่วม

4971869721: MAJOR CIVIL ENGINEERING
KEYWORDS: HYPERPLASTICITY / SMALL-STRAIN / RATE-DEPENDENT / NON-LINEAR STIFFNESS / KINEMATIC HARDENING
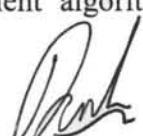
DEDI APRIADI: DEVELOPMENT AND NUMERICAL IMPLEMENTATION OF THERMODYNAMICS-BASED SOIL MODEL. ADVISOR: ASST. PROF. SUCHED LIKITLERSUANG, D.Phil., THESIS CO-ADVISOR: ASSOC. PROF. THIRAPONG PIPATPONGSA, 110 pp.
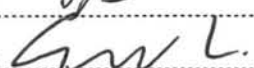
In practical geotechnical engineering analysis and design, a well-known Mohr-Coulomb and Cam-clay models have been widely used for simplifying complex behaviours of soils. Several advanced frameworks have been further proposed to include some important aspects of soil behaviours, such as small-strain stiffness or the effects of immediate past stress by introducing multiple or nested surface model (Mroz & Norris, 1982), bounding surface model (Dafalias & Hermann, 1982), and hypoplasticity framework (Kolymbas, 1977). The interpretation of the experimental data shows that the stress-strain characteristic of soils is non-linear function of the mean effective stress and irreversible, in that the small-strain tangent stiffness depends on the stress level. Since constitutive models relate to physical phenomena, they must obey certain principles or axioms that govern the physical phenomena such as conservation of mass, conservation of energy, and laws of thermodynamics. To include these certain physical principles, Likitlersuang (Likitlersuang, 2003; Likitlersuang and Houlsby, 2006) proposed the hyperplasticity kinematic hardening Modified Cam-clay (KHMCC) model based on the thermodynamics principles. This research aims to extend the previous research of Likitlersuang and Houlsby (2006) by incorporating small-strain stiffness in form of power function of pressure into energy function. Correspondingly, the numerical implementation and piece-wise multisurface is enhanced to address a higher degree of non-linearity and loading history. A numerical implementation of the hyperplasticity non-linear KHMCC model based on triaxial and general stress condition using strain-driven forward-Euler integration scheme is employed. Some important issues on the numerical implementation of the continuous hyperplasticity non-linear KHMCC model are presented. Some numerical demonstrations are also carried out to illustrate several key features of the model. Furthermore, model validation using single element calculation against analytical solution of ideal undrained triaxial test response, small-strain experimental on clay soils and two experiments from Bangkok Clay i.e.: response of K_0-consolidated Undrained Direct Simple Shear (CK_0UDSS) test and anisotropic undrained compression behaviour of Bangkok Clay are made. Finally, rate dependent continuous hyperplasticity finite element algorithm is employed.

Department : _____Civil Engineering_____   Student's Signature _____

Field of Study : __Civil Engineering__   Advisor's Signature _____

Academic Year : _2009_____   Co-Advisor's Signature_____

ACKNOWLEDGEMENTS

Alhamdulillah, praise and glory be to *Allah*, the supreme sovereign of the skies and the earth, I can completely finish this work. Greetings and salutations on our messenger Muhammad, his family, friends and all believers until the end of time.

Seldom is anything accomplished without the encouragement of others. This dissertation is no exception. Sometimes, I felt a need to pursue this research in my own way. Yet, without the advice, guidance and encouragement of Dr. Suched Likitlersuang and Dr. Thirapong Pipatpongsa, there were times when this research might have gone no further. I thank them for giving their valuable time to guide me.

This research could not be well performed without financial support. Thank to AUN/SEED-Net JICA for the grant. Special appreciation is expressed for Professor Hideki Ohta, whose difficult questions for this research have been inspiring me during Terakoya seminar and one year study in Tokyo Institute of Technology. In addition, I thank Dr. Tomohide Takeyama from Ohta Laboratory for his assistance.

Of course, thank to my dear friends Rhandley, Bil-*san*, Hossein-*san*, Bot, Sochan, Soksan, Omar and *Pak* Harry who gave me encouragement and assistance, when I faced the difficulties.

Much appreciation goes to *mama* and *papa Palembang*, *mama* and *Alm. papa Bandung*, and the rest of my family; their support and belief in me have always inspired me in my endeavours. Last, but certainly not least, I thank my wife, Irma Noerhaty, whose love gave me strength and encouragement to follow the path that I felt was right, and whose infinite patience and unselfishness allowed me the freedom to complete this work. My sons, Nawal Fairuz Dinan and Nawal Faiza Malihan, this dissertation is lovingly dedicated to them.

CONTENTS

ศูนย์วิทยทรัพยากร

จุฬาลงกรณ์มหาวิทยาลัย

LIST OF TABLES

LIST OF FIGURES

ศูนย์วิทยทรัพยากร
จุฬาลงกรณ์มหาวิทยาลัย

LIST OF SYMBOLS

α	direction of the major principal stress
α_{ij}	kinematic internal variable
α_p	volumetric kinematic internal variable
α_q	deviatoric (shear) kinematic internal variable
$\hat{\alpha}_{ij}$	kinematic internal variable function
$\chi_{ij}, \overline{\chi}_{ij}$	generalised stress
γ	engineering shear strain
δ	distance between the stress and image points
ε_{ij}	strain tensor
$\varepsilon_{ij}^{(e)}$	elastic strain tensor
$\varepsilon_{ij}^{(p)}$	plastic strain tensor
$\dot{\varepsilon}$	strain rate
ε_p	volumetric strain
ε_q	deviatoric (shear) strain
ε_a	axial strain
ε_r	radial strain
ϕ	internal friction angle
η	(1) stress ratio
	(2) internal coordinate
κ	slope of swelling line in consolidation plot
λ	slope of compression line in consolidation plot
$\lambda^{(n)}$	an *n-th* scalar (non-negatif) multiplier
μ	viscosity coefficient
ν	poisson ratio
ψ	exponent of hardening modulus

σ_I	major principle stress
σ'_{vm}	past maximum vertical effective stress
σ'_{v0}	current vertical effective stress
$\overset{\circ}{\sigma}$	Jaumann stress rate
σ_a	axial stress
σ_r	radial stress
σ_{ij}	stress tensor
$\dot{\omega}$	rotation rate
$\langle\,\rangle$	Macaulay brackets
a	kinematic hardening parameter
c	undrained shear strength
$\hat{c}$	yield stress
c_{ijkl}	compliance matrix
d	dissipation function or dissipation functional
d_{ijkl}	stiffness matrix
E	(1) elastic modulus
	(2) Gibbs free energy
e	void ratio
f	(1) yield surface
	(2) specific Helmholtz free energy
G	elastic shear modulus
g	(1) dimensionless material constant, shear modulus constant
	(2) specific Gibbs free energy
H	plastic modulus, kinematic hardening
$\hat{H}$	kinematic hardening function
h	(1) hardening modulus
	(2) enthalpy
J	coupling modulus
K_0	coefficient of earth pressure at rest

K	elastic bulk modulus
k	dimensionless material constant, bulk modulus constant
M	slope of critical state line in p', q plot
N	the number of variables, number of yield surfaces
n	dimensionless material constant
OCR	overconsolidation ratio $OCR = \sigma'_{vm} / \sigma'_{v0}$
p'_m	past maximum mean effective stress
p'	current mean effective stress
p	pressure, mean (effective) compressive stress
p_a	atmospheric pressure
p_r	reference pressure
p_c	preconsolidation pressure in term of mean stress
p_e	equivalent stress variable
$\dot{Q}$	heat supply
q	stress deviator
R_o	overconsolidation ratio $R_o = p'_m / p'$
R_η	overconsolidation ratio with respect to the anisotropic stress condition
s	specific entropy
T, S	ratio of the extent of the effect of recent stress history
$\dot{W}$	rate of work input
w	flow potential
y	yield function
y^e	yield function corresponding to the energy function e

CHAPTER I. INTRODUCTION

1.1 Background and Motivations

In practical geotechnical engineering analysis and design, a well-known Mohr-Coulomb and Cam-clay models (Roscoe and Burland, 1968) have been widely used for simplifying complex behaviours of soils. Several advanced frameworks have been further proposed to include some important aspects of soil behaviours, such as small-strain stiffness or the effects of immediate past stress by introducing multiple or nested surface model (Mroz & Norris, 1982), bounding surface model (Dafalias & Hermann, 1982), and hypoplasticity framework (Kolymbas, 1977). Another important issue is the stress-strain characteristic of soils is non-linear and irreversible, in that the initial soil stiffness or small-strain tangent stiffness depends on the stress level. The interpretation from experimental observations of bender element test shows that the small-strain stiffness of soils is a non-linear function of the mean effective stress for isotropically consolidated samples as reported by Tanizawa et. al. (1994), Kohata et. al. (1997), Pennington et. al. (1997), and Techavorasinskun et. al. (2002) and depend on the stress ratio (Rampello et. al., 1997) for anisotropically consolidated samples. The stiffness also affected by other variables, such as the voids ratio, anisotropic stress state, and/or the preconsolidation pressure (Hardin, 1978; Houlsby & Wroth, 1991; Viggiani, 1992; Rampello et al., 1994; and Soga, 1995).

Since constitutive models relate to physical phenomena, they must obey certain principles or axioms that govern the physical phenomena such as conservation of mass, conservation of energy, and laws of thermodynamics. All models mentioned above do not referred to the Laws of Thermodynamics and they may violate one or the other of fundamental laws. Models that violate thermodynamics may not be used with any confidence to describe material behaviour (Houlsby & Puzrin, 2006).

Likitlersuang (Likitlersuang, 2003; Likitlersuang and Houlsby, 2006) proposed the hyperplasticity kinematic hardening modified Cam-clay (KHMCC) model to address small-strain stiffness based on the thermodynamics principles. The kinematic hardening function was included in the energy and yield functions to characterise small-strain stiffness and accommodate smooth transition of stiffness in corresponding to loading conditions and stress histories. Hyperbolic function recommended by Puzrin and Houlsby (2001) was employed to express the continuous kinematic hardening function in order to fit with the observed non-linear stress-strain responses. Continuous kinematic hardening function was piece-wised into a finite number of multiple yield functions. Therefore, combined responses of activated yield surfaces can represent non-linear kinematic hardening behaviours. Calibration of the model in triaxial stress-strain

space was carried out by Likitlersuang, and Houlsby (2007) on Bangkok clay. Stress-strain responses under monotonic and cyclic loadings were simulated to show the advantage of hyperplasticity KHMCC model.

Though the formulation of hyperplasticity KHMCC model has been already proposed in the earlier researches, the numerical implementation and simulation are restricted to linear stress-strain relationship with stiffness proportional to isotropic pressure. Further, small-strain stiffness study of Bangkok Clay using bender element test on the isotropically consolidated samples clearly show that the shear modulus is a power function of pressure (Teachavorasinskun, et. al., 2002) rather than linear function of pressure. Therefore, the numerical implementation for hyperplasticity KHMCC model with non-linear elastic stiffness has not been explored.

This research aims to extend the previous research of Likitlersuang and Houlsby (2006) by incorporating small-strain stiffness in form of power function of pressure in to energy function. Correspondingly, the numerical implementation and piece-wise multisurface plasticity described by Likitlersuang, and Houlsby (2007) is enhanced to address a higher degree of non-linearity and loading history. An approach to determine the necessary parameters obtained from small-strain experimental tests for regulating small-strain stiffness characteristic of the hyperplasticity KHMCC model is presented.

This study is expected to provide a theoretical background and numerical implementation for those who are interested in the advancement of critical state soil model under the framework of hyperplasticity. The results of this research may give a light to model the complicated behaviours of soils observed from advanced small-strain laboratory testing.

1.2   Objectives

The objectives of this study are summarised in the following:

- To develop and implement numerically a continuous hyperplasticity non-linear Kinematic Hardening Modified Cam Clay soil model in triaxial and general stress-strain by:
    - Incorporating small-strain stiffness in form of power function of pressure into energy function (Houlsby and Puzrin, 2005).
    - Integrating the incremental stress-strain relation using rate-dependent strain driven forward-Euler integration scheme.
- To validate the developed model with some experimental data of:
    - Loading Path Dependence and Non-Linear Stiffness at Small-Strain (Stallebrass and Taylor, 1997).
    - K_0-consolidated Undrained Direct Simple Shear (CK_0UDSS) test of Bangkok Clay (Konkong, 2007).

$-$ Small-strain undrained compression test of Bangkok Clay (Yimsiri, et al., 2009; Ratananikom, 2009).

- To implement the developed model into rate-dependent continuous hyperplasticity finite element algorithm.

1.3 Methodology and Structure of Thesis

This research will be divided into two parts, dealing respectively with a analytical and numerical study of the non-linear Kinematic Hardening Modified Cam Clay model using continuous hyperplasticity framework.

The analytical study of the research activities consists of model development in triaxial and general stress condition based on the thermomechanical principles. In this part, stiffness and/or compliance matrix of the model will be derived before implemented into numerical algorithm.

The numerical study of the research activities consist of numerical review and implementation of the developed model into rate-dependent strain driven forward-Euler integration scheme by incorporating a non-linear dependence of initial stiffness on pressure. Several numerical demonstrations are performed to show features of the developed model. The study also consists of identification and determination of soil model parameters from experimental test data. Furthermore, the model parameters will be back predicted to the experimental laboratory testing from which the soil parameters are obtained.

Chapter 2 presents some recent issues in advanced soil behaviours or commonly called as pre-failure deformation behaviour. Explanation will be emphasised on experimental investigations. A brief review and comparison some advanced soil constitutive models are also presented.

Chapter 3 explains a development and numerical implementation of the hyperplasticity non-linear KHMCC model based on triaxial stress-strain variables and general stress using strain-driven forward-Euler integration scheme. Further, some important issues on the numerical implementation of this model is discussed, including incremental stress-strain response algorithm, numerical integration of hardening functions, as well as effect of time increment and number of yield surfaces. Several numerical demonstration and validations with analytical solution are presented.

Chapter 4 presents some comparisons to experimental data of clay soils. Two experiments of K_0-consolidated Undrained Direct Simple Shear (CK_0UDSS) test and small-strain undrained compression behaviour of Bangkok Clay are selected.

Chapter 5 explains implementation of the developed model into rate-dependent continuous hyperplasticity finite element algorithm.

Finally, some conclusions on the development of this model are discussed in Chapter 6 including development for future research.

CHAPTER II. SOME RECENT ISSUES ON THE SOIL BEHAVIOUR AND CONSTITUTIVE MODELING

2.1 Soil Behaviour

Soil is natural material which behaves very complex manner. When dealing with geotechnical engineering problems, the understanding of the real soil behaviour is very important to obtain accurate prediction, for instance, of stress-strain characteristic.

The study of soil behaviour is now over three hundred years old, since Coulomb in 1773 analysing the failures mechanism of soil mass. Progressive developments of advanced soil laboratory tests, for instance, with capability to accurately control and monitor stresses and strains during rotation of principal stresses such as directional shear cell (Arthur & Menzies, 1972) and the hollow cylinder apparatus (High et al., 1983); and the instrumented soil tests such as strain gauges, electrolevels, proximity and local-deformation transducer making the study of soil behaviour more interesting in quality and increasing in intensity.

This chapter presents some recent issues in advanced soil behaviours or commonly called as pre-failure deformation behaviour. Explanation will be emphasised on experimental investigations.

2.1.1 Anisotropic

Soil behaviour is affected by orientation or its deposited direction, so that soil is classified as an anisotropic material. Seah (1990) presented the influence of the orientation of the major principle stress (σ_l) to the direction of soil deposition against the undrained shear strength of reconsolidated Boston Blue Clay. The data shows that the undrained shear strength drops by 50% as the angle of σ_l to the deposited direction increases from 0^0-90^0 as shown in Figure 2.1.

Some recent laboratory tests on a silt soil performed in a large hollow cylinder apparatus also show that soil strength is very anisotropic (Zdravkovic, 1996; Zdravkovic & Jardine, 2000).
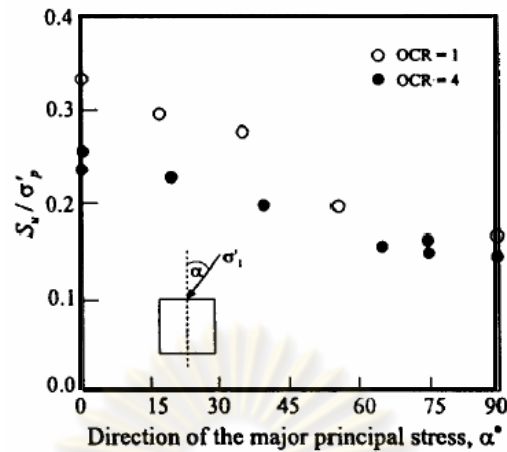
Figure 2.1 An anisotropic behavior of soils (Seah, 1990)
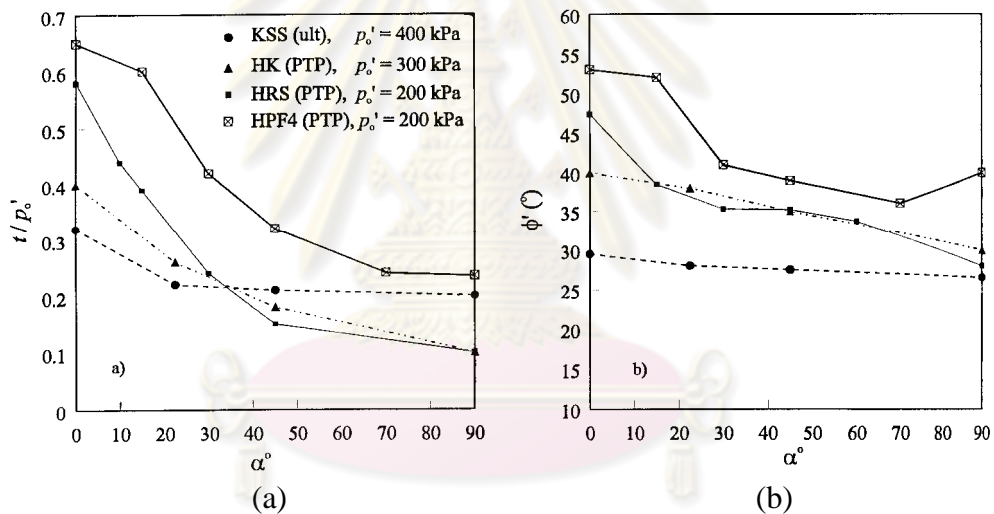
Figure 2.2 Initial strength anisotropic of four K_0 consolidated materials (Kolymbas, 2000)

Figure 2.2(a) and (b) show the change of deviatoric stress normalised by the mean effective stress at the end of K_0 consolidation and effective internal friction angle against the direction of the major principal stress, α.

2.1.2 Stress History

Soil has a "memory", so that any of the stress and other changes that have occurred during their history, and these changes is preserved in the soil structure (after Casagrande, 1932; Holtz & Kovacs, 1981). When the soil is subjected to a stress level greater than it ever "experienced" in the past, the soil is no longer able to sustain the increased stress and it start to break down. In the other words, the stress-stain behaviour of soil is depends on the current state and stress history or consolidation history, and

which is best described by the overconsolidation ratio (R_o) as shown in Figure 2.3, i.e. ratio by which the current mean effective stress in the soil was exceeded in the past ($R_o = p'_m / p'$ where p'_m is the past maximum mean effective stress and p' is the current mean effective stress). The definition of R_o is more general than definition OCR that usually used in practical i.e. ratio between past maximum vertical effective stress (σ'_{vm}) over current vertical effective stress (σ'_{v0}).
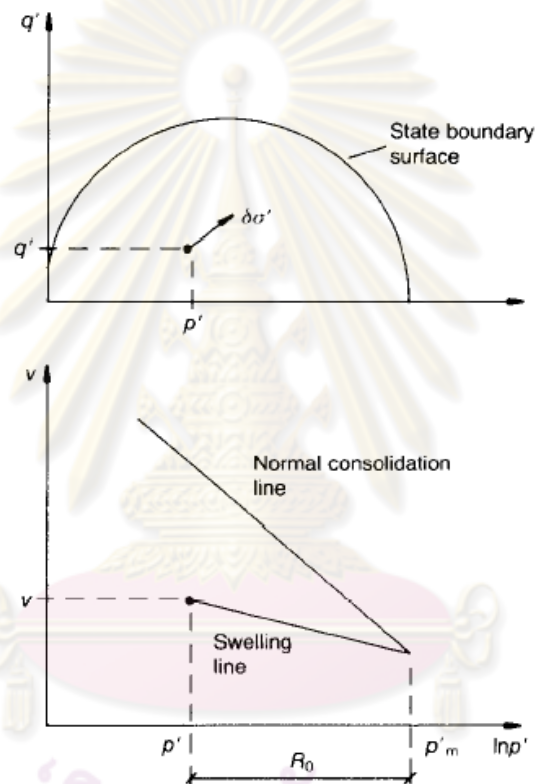
Figure 2.3 Current state and consolidation history of the soil (Atkinson, 1990)

Som (1968) and Atkinson (1973, 1990) observed, one additional influence on its stress strain behaviour that is the recent stress history of the soil described by the most recent loading, which may take the form of an extended period of rest or a sudden change in the direction of the stress path. Later, Houlsby (1999) also found this phenomenon particularly in the second causal factor, and call it as immediate stress history. They showed that the stiffness of soils in triaxial and plane strain tests was increased following a sudden change in the direction of the stress path as illustrated in Figure 2.4.
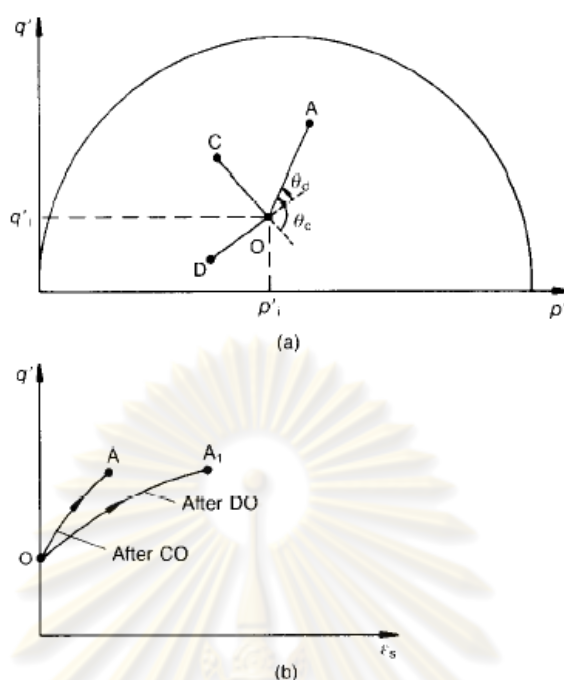
Figure 2.4 Effect of recent stress history on current stiffness of the soil (Atkinson, 1990)

Figure 2.4(a) illustrates effect of stress path rotation for conditions of axial symmetry and loading paths, inside the state boundary. Along the different paths CO and DO, soil brought to the same initial state q'_i and p'_i at O, and then loaded along the same path OA. θ_c and θ_d are the rotations of the stress paths relative to the new stress path OA at point O. Figure 2.4(b) illustrates the stress-strain curves for the same loading path OA. In this figure, the different stiffness is related to the different stress path rotations, since the soil had identical states, equal periods of time and overconsolidation ratio at O.

2.1.3 *Small-Strain Behaviour of Soils*

In the settlement and displacement problems of soil-structure interaction, the contribution of (very) small-strain zones to boundary displacement can be larger than that of zones of contained failure (see, for instance, Burland, 1989). Recent back analysis of field measurement and laboratory studies using local strain-measuring techniques such as strain gauges, electrolevels, proximity and local-deformation transducer, show that the initial stress-strain behaviour of many soils is much stiffer than indicated by conventional strain (intermediate to large strain) measurement. It also exhibits a non-linear behaviour (Jardine, Symes and Burland, 1984).
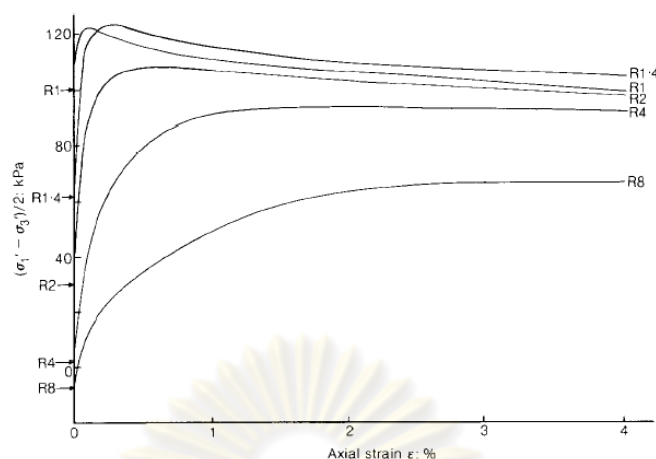
Figure 2.5 Measured undrained stress-strain behaviour of a reconstituted clay by using local strain measuring techniques (Jardine, Symes and Burland, 1984)

Figure 2.5 shows the measured undrained stress-strain behaviour of reconstituted clay various with OCR values using local strain measuring techniques performed by Jardine et al. (1984). It can be seen that the strains over the initial range of stresses are extremely small.

Sensitivity studies to investigate the significance of non-linearity at small-strain and local failure have been performed by Jardine et al. (1986), it shows that in all practical case studied, the modelling of realistic small-strain non-linearity and the consideration of local failure have important implications in considering soil-structure interactions at working loads. Figure 2.6 shows the current understanding of soil stiffness in relating to laboratory test and structure types.
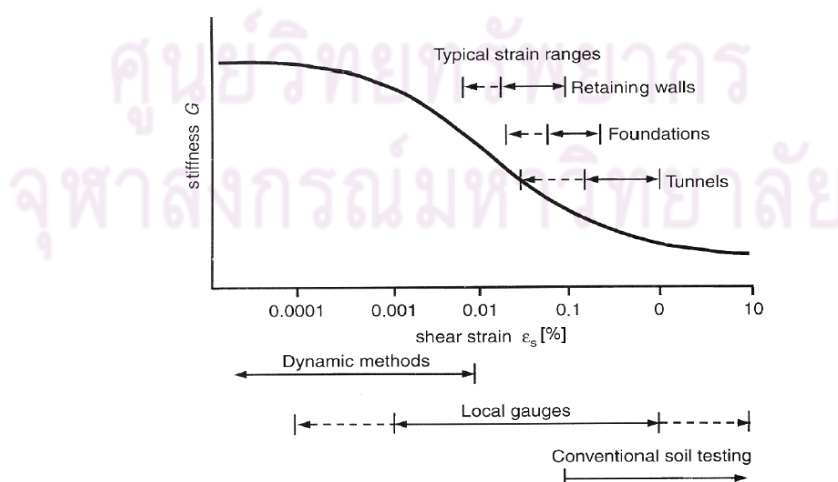
Figure 2.6 Characteristic stiffness-strain behavior of soils with typical strain range for laboratory tests and structures (Mair, 1993)

2.1.4 Initial Stiffness Dependence on Pressure

The stress-strain characteristic of soils is non-linear and irreversible, in that the initial soil stiffness or small-strain tangent stiffness depends on the stress level. It is also affected by other variables, such as the voids ratio, anisotropic stress state, and/or the preconsolidation pressure. Soga et al. (1995) present the variation of stiffness with strain from torsional tests on isotropically normally consolidated kaolin varied with the stress level as shown in Figure 2.7.
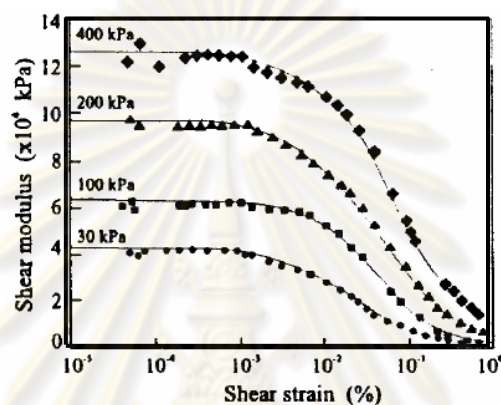
Figure 2.7 Non-linear dependence of initial soil stiffness on stress level (Soga et al, 1995)

Many published experimental data on the small-strain stiffness of soils are carried out from dynamic laboratory tests on natural or reconstituted clays, or reconstituted sands samples, in triaxial conditions and under isotropic stress state.

Hardin (1978) proposed the following form on sands:

$$\frac{G}{p_a} = S f(e) \left(\frac{p}{p_a} \right)^n OCR^k$$

(2.1)

where $f(e)$ is an empirically defined decreasing function of the void ratio e; p_a is the atmospheric pressure as reference stress; and S, n and k are dimensionless experimentally determined parameters. Since the sand soil does not experience a significant variation of the void ratio or of the OCR, this leads to the simplified expression for equation (2.1):

$$\frac{G}{p_a} = g \left(\frac{p}{p_a} \right)^n$$

(2.2)

and also for the corresponding bulk stiffness:

$$\frac{K}{p_a} = k \left(\frac{p}{p_a} \right)^n \tag{2.3}$$

where g and k are dimensionless constant. Constant n in shear and bulk modulus is not necessary the same.

For clay soils, several experimental observations and interpretations have indicated that, for isotropic stress condition, the small-strain shear stiffness can be expressed as in the following equation (Houlsby & Wroth, 1991; Viggiani, 1992; Rampello *et al*., 1994):

$$\frac{G}{p_a} = S * \left(\frac{p}{p_a} \right)^{n*-k*} \left(\frac{p_c}{p_a} \right)^{k*} \tag{2.4}$$

Under anisotropic stress condition, it is necessary to modify expression developed entirely from isotropic condition (e.g. Ni, 1987; Hardin and Blandford, 1989; Jamiolkowski e*t al*., 1994; Rampello *et al*., 1997; Jovicic & Coop, 1998). For example, empirical expression for sands from Ni (1987) and Hardin and Blandford (1989):

$$\frac{G}{p_a} = S_{ij} f(e) \frac{(\sigma_i \sigma_j)^{n/2}}{p_a^n} OCR^k \tag{2.5}$$

in which σ_i and σ_j are the principles stresses in the plane in which G is measured.

Furthermore, based on experimental results obtained on a reconstituted clay compressed under anisotropic stress condition, Rampello et al. (1997) proposed:

$$\frac{G}{p_a} = S_\eta^* \left(\frac{p}{p_a} \right)^{n*} R_\eta^{k*} \tag{2.6}$$

where R_η is the overconsolidation ratio with respect to the anisotropic stress condition, defined in term of mean effective stress $R = p'_c / p'$. The anisotropic stress conditions are defined at any particular stress ratio $\eta = q / p$. The notation * is for distinguishing the S, n and k values from the equation (2.1).

2.1.5 Rate Effect

Soils exhibit time dependent behaviour as well as plastic deformation, so that soils are also called as viscous material.

The viscous properties of the material define a time dependence of the state of stress and strain. On the other hand, plastic properties make these states depend on the loading path. When soil is subjected to a constant load it will deform over time, and this phenomenon is called creep. Inverse this phenomenon is called by stress relaxation, is a

drop in stress over time after as soil subjected to a particular constant strain level. Figure 2.8 shows these two phenomena. In Figure 2.8, it is shown that rate of creep will increase as increasing of deviatoric stress level. The most active clays usually exhibit the highest rate-dependent responses. Normally consolidated soil exhibits larger magnitude of creep than overconsolidated soils.

The rate-dependent phenomena are agreeable for study as rate processes as application of the theory of absolute reaction rates (Glasstone et al., 1941), which is based on statistical mechanics. Detail adaptations this theory to soil mechanics can be found in Mitchell and Soga (2005).
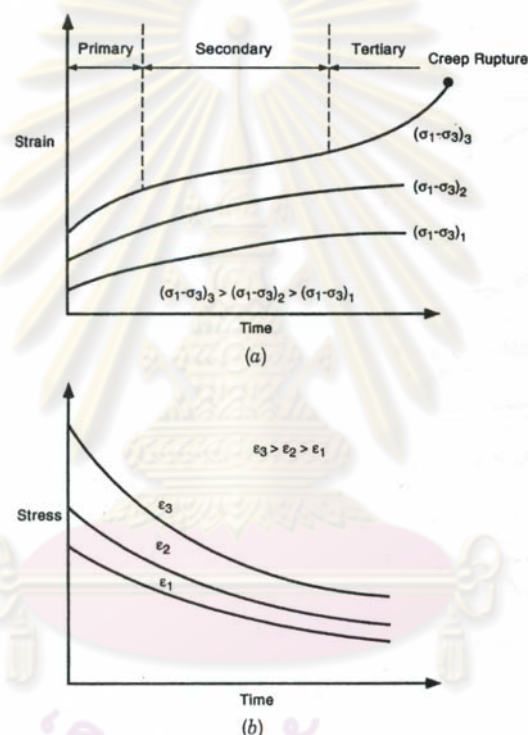
Figure 2.8 Creep and stress relaxation (Mitchell & Soga, 2005)

2.2   Review Some Advanced Soil Constitutive Models

Different advanced soil constitutive models based on different concepts have been proposed; often a particular model proclaimed its superiority over others. In fact, it is believed that each model can be valid within its own local realm, and that no universal constitutive model has yet been developed that is valid for all materials under all conditions.

It is noted that, since constitutive models relate to physical phenomena, they must obey certain principles or axioms that govern the physical phenomena such as conservation of mass, conservation of energy, and laws of thermodynamics. In the other

words, principally a good soil model must be developed without violate certain principles or axioms that govern the physical phenomena. Figure 2.9 shows place of constitutive law and physical principles in continuum mechanics.
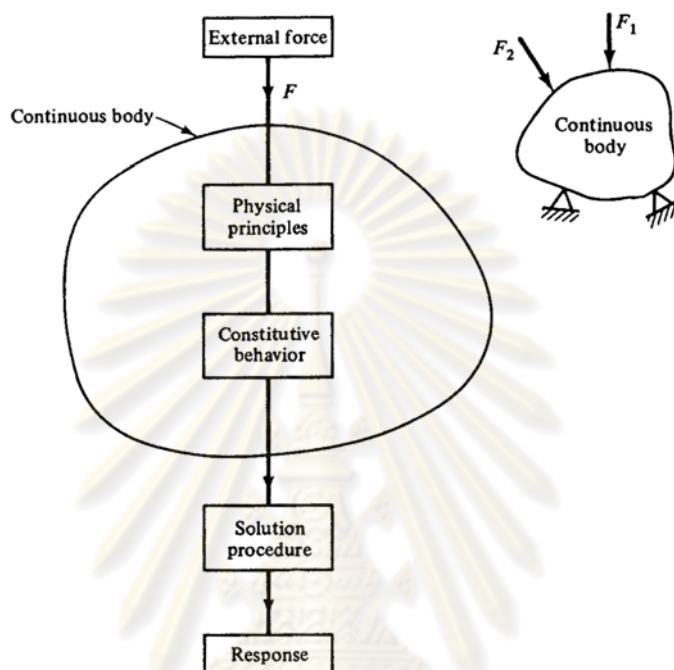
Figure 2.9 Place of constitutive laws and physical principles in continuum mechanics (Desai, 1984)

2.2.1 Multiple Surface Model

This model proposed by Mroz (1967) and Iwan (1967) consists of kinematic and isotropic hardening. Mroz (1967) explained the model using the diagrams in Figure 2.10. Figure 2.10(a) shows a uniaxial stress-strain response discretised in n linear segments or pieces. A constant tangent modulus E_i ($i = 1, 2,…, n$) or constant plastic modulus E_i^p ($i = 1, 2,…, n$) is associated with each yield surface.

Surfaces f_1, f_2,…, f_n represent specific regions of constant work hardening moduli E_i^p. It is assumed that there exists, in domain of interest from the initial state f_0 to the limit (ultimate or bounding state) f_n, a series of yield surfaces, each defining a specific part or region of the domain in the stress space. With deformation, the surfaces translate in the stress space and as soon as surface f_i touches the next surface f_{i+1} they both move together until they touch f_{i+2} and so on. The surfaces touch each other tangentially and are not permitted to intersect each other (non-intersection condition).
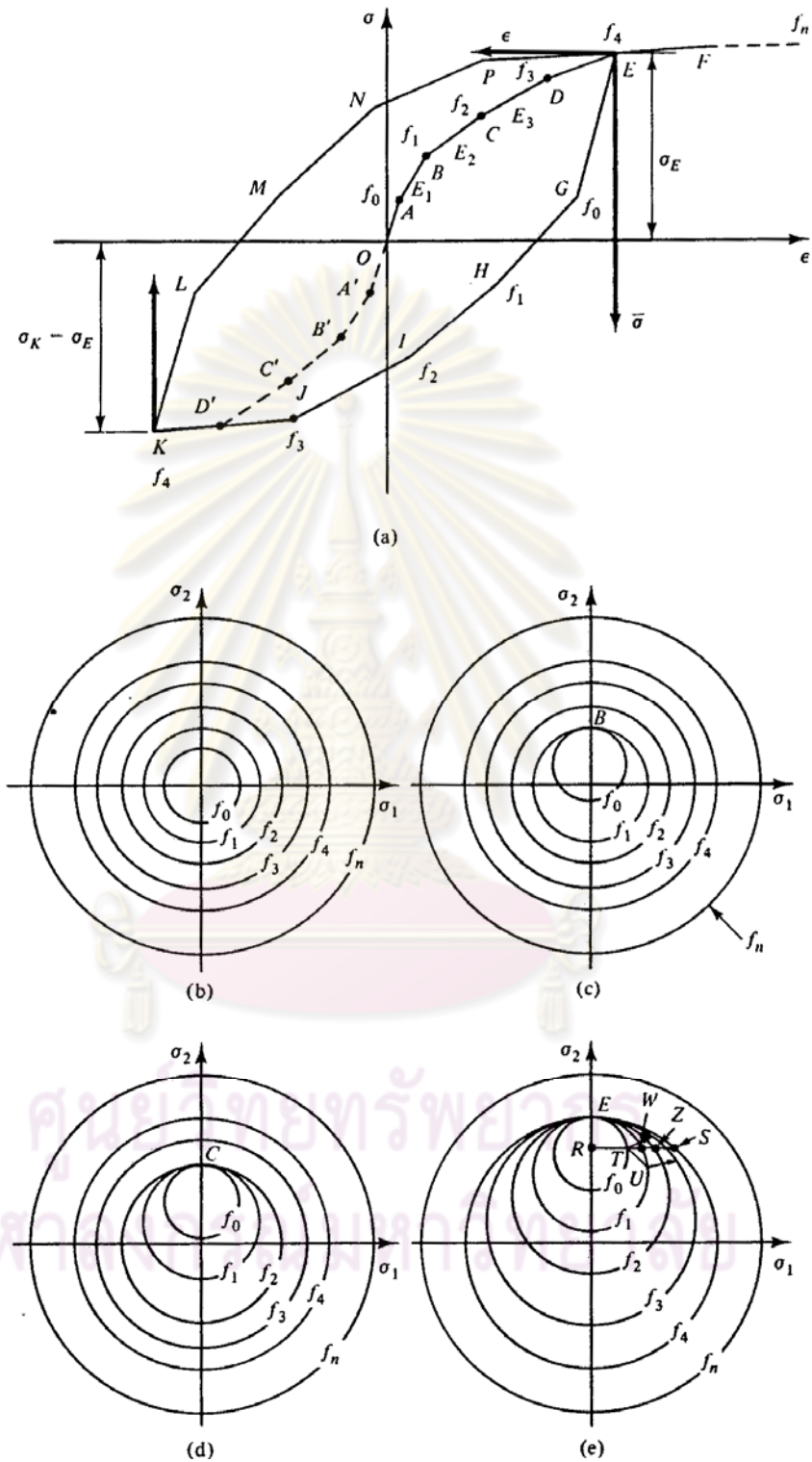
Figure 2.10 Multiple surface model: (a) stress-strain curve; (b) before straining; (c) loading A to B; (d) loading B to C; (e) loading C to D to E and nonproportional loading (Desai, 1984)

Mroz first considered proportional loading, for the uniaxial case specifically along the σ_z-axis [Figure 2.10(a)]. For an increment of stress, the stress point moves from O to A [Figure 2.10(a)], where it reaches the yield stress defined by f_0. The initial yield surface f_o moves along the σ_z-axis, and at B, during plastic straining, it touches yield surface f_1 associated with point B; this is depicted in Figure 2.10(c). The plastic strain induced during the movement from A to B is defined by the tangent modulus E_1. During this movement, all other surfaces remain fixed.

When the stress point moves from B to C, the surfaces f_0 and f_1 translate together until at C they touch f_2 associated with C [Figure 2.10(d)]. The plastic strain during this movement is defined by modulus E_2. Similarly, during subsequent loadings the yield surfaces translate, taking with them the previous surfaces and touching the next ones during changes or increments in the state of stress. For the case in Figure 2.10(e), the end or final state of the particular loading history up to E is represented by the surface f_4.
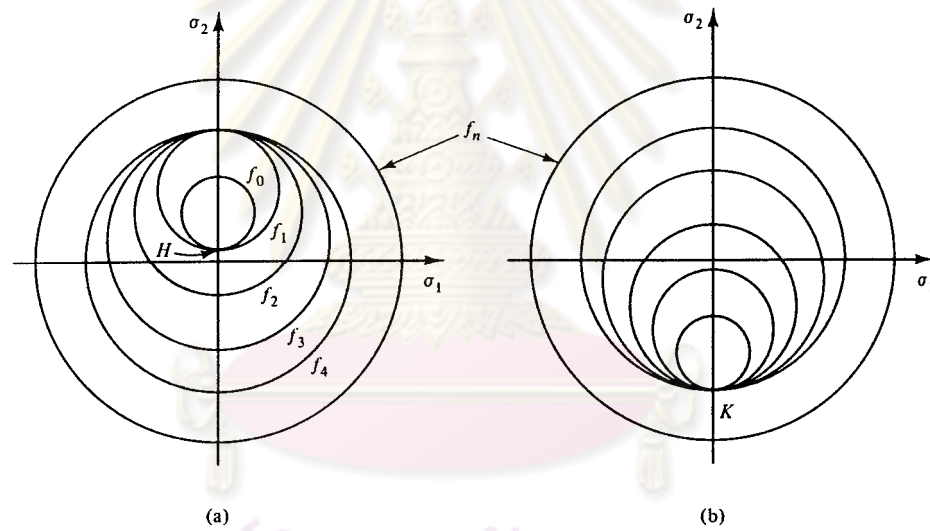
Figure 2.11 Unloading behavior: (a) unloading G to H; (b) unloading H to I, I to J, and J to K (Desai, 1984)

Consider unloading from E along path EGHIJK [Figure 2.10(a)]. At G, (inverse) plastic flow occurs, and then the surface f_0 translates downward until it touches f_1 corresponding to point H [Figure 2.11(a)]. Since this movement of f_0 is twice that for its movement from A to B during the loading, the stress difference between H and G is twice that between A and B. With subsequent unloading along HI, IJ, and JK corresponding to loadings BC, CD, and DE, respectively, the yield surfaces move and finally touch f_4 on the opposite side [Figure 2.11(b)].

The total strain is the sum of the elastic strain and plastic strain components:

$$\varepsilon_{ij} = \varepsilon_{ij}^{(e)} + \sum_{n=1}^{N} \varepsilon_{ij}^{(p)(n)} \tag{2.7}$$

Each yield surface is specified in the form $f^{(n)}\left(\sigma_{ij}, \varepsilon_{ij}^{(p)(n)}\right) = 0$, where for simplicity the yield surface depends only on the plastic strain associated with that surface, and is not coupled to other yield surfaces. Non-associated flow rule can be introduced by defining plastic potential different with the yield surfaces so that $\dot{\varepsilon}_{ij}^{(p)(n)} = \lambda^{(n)} \dfrac{\partial g^{(n)}}{\partial \sigma_{ij}}$, where $\lambda^{(n)}$ is scalar multiplier and $g^{(n)}$ is plastic potential functions associated to $f^{(n)}$.

At the same time, Iwan (1967) formulated his multiple surface models without the non-intersection condition. His model built from one spring with elastic coefficient E and a series of sliding elements with slip stresses k_n, each in parallel with a spring with corresponding elastic coefficient H_n (Figure 2.12).
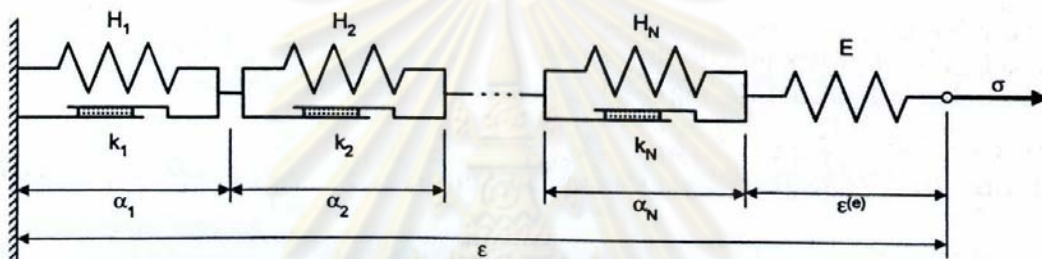
Figure 2.12 Schematic layout of the Iwan model (Houlsby & Puzrin, 2006)

An elongation of the E spring gives elastic strain $\varepsilon^{(e)}$, whereas an elongation of each of the H_n springs contributes the plastic strain an to the total plastic strain; the sum of elastic and all plastic strains gives the total strain ε. After the stress reaches the value of slip stress k_N, the *Nth* sliding element slips and the H_N spring becomes active. The corresponding behavior is elastoplastic with linear hardening characterised by tangent modulus E_N, which can determined from the relationship $\dfrac{1}{E_n} = \dfrac{1}{E} + \sum\limits_{n=1}^{N} \dfrac{1}{H_n}$

In its application, relocation of each yield surface has proved as a very convenient framework for modelling the pre-failure behaviour of soils, allowing a realistic treatment of issues such as non-linearity at small-strain and the effects of recent stress history.

2.2.2 Bounding Surface Model

The original concept this model proposed by Dafalias (1975) and Dafalias and Hermann (1980). As implied in the name, strictly no plastic strain is allowed inside a yield surface. Further, the domain enclosed by the bounding surface is not elastic;

though for some incremental stress trajectories within this surface, an elastic response can be obtained. Following is simplified of this concept taken from Houlsby & Puzrin (2006).

For every stress point A in Figure 2.13 an image of point B on a "bounding surface" is determined using mapping rule. The stress point A(σ_{ij}) always lies within or on the bounding surface. It is assumed that if the incremental stress vector at the point A(σ_{ij}) is directed inside this surface, the behaviour is elastic.

If the incremental stress vector at each point A(σ_{ij}) is directed outward from the loading surface, the behaviour is elastoplastic. The plastic strain in a conventional plasticity model with an associated flow rule and a yield locus $f\left(\sigma_{ij}, \varepsilon_{ij}^{(p)}\right) = 0$ is given by:

$$\dot{\varepsilon}_{ij}^{(p)} = \frac{1}{h} \frac{\partial f}{\partial \sigma_{ij}} \frac{\partial f}{\partial \sigma_{kl}} \dot{\sigma}_{kl} \qquad (2.8)$$

where h is a hardening modulus. In the bounding surface f is interpreted as the bounding surface and σ_{ij} in equation (2.8) as the stress at the image point. The value of h is then given by:

$$h = h_0 + h_1 \frac{\delta}{\left(p_c' - \delta\right)} \qquad (2.9)$$

where δ is shown on Figure 2.13.
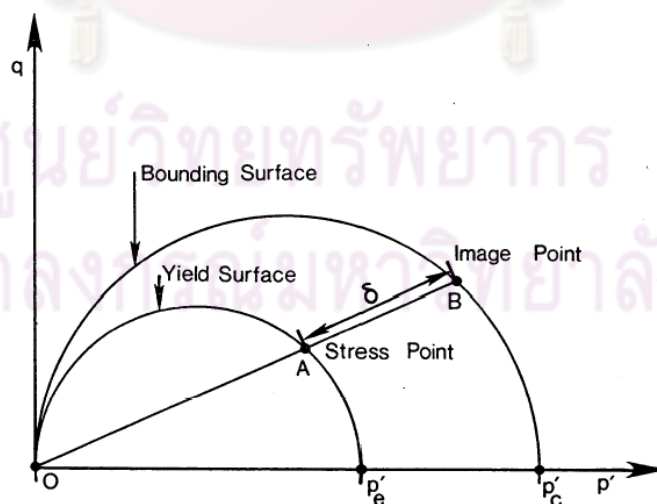
Figure 2.13 Bounding surfaces model of Dafalias and Hermann (1980) (Houlsby, 1981)

The result is that when the stress point is on the bounding surface conventional plastic behaviour is given, inside the surface a reduced plastic strain occurs if the quantity $p_e^{'}$ is increasing.

Bounding surface model can be successful in describing hysteresis for large unload-reload loops, typically those which involve complete load reversal. For small unload-reload loops, however, the prediction is not realistic. It is also incapable to incorporate the effects of recent stress history on the stiffness of the response.

2.2.3 Hypoplasticity Model

This name referring to the plastic model, in which the direction of the plastic strain rate, unlike in the conventional plastic models, depends on the stress rate. The formal definition this model provided by Wu and Kolymbas (1990).

Hypoplastic constitutive model assume that there exists a tensorial function H, such that:

$$\overset{\circ}{\sigma} = H(\sigma, \dot{\varepsilon}) \tag{2.10}$$

where $\dot{\varepsilon}$ denotes the stretching (strain rate) and $\overset{\circ}{\sigma}$ is the Jaumann stress rate, in which defined as follows

$$\overset{\circ}{\sigma} = \dot{\sigma} + \sigma\dot{\omega} - \dot{\omega}\sigma \tag{2.11}$$

where $\dot{\omega}$ is the rotation rate (spin). Furthermore, it is assumed that the function H in (2.10) is continuously differentiable for all $\dot{\varepsilon}$ except at $\dot{\varepsilon} = 0$. Some restriction on the function H in (2.10) was introduced to make the model more concrete constitutive equations, and then final equation of this model is:

$$\overset{\circ}{\sigma} = L(\sigma, \dot{\varepsilon}) + N(\sigma)\|\dot{\varepsilon}\| \tag{2.12}$$

where L is linear in $\dot{\varepsilon}$ and N is nonlinear in $\dot{\varepsilon}$, $\|\dot{\varepsilon}\| = \sqrt{tr\dot{\varepsilon}^2}$ stands for the Euclidean norm.

One important conceptual in hypoplasticity, distinguish with elastoplasticity, is that in elastoplasticity, yield function and material state parameters define the yield surface, which bounds the elastic domain, but not in hypoplasticity. As we have already seen, within the elastic domain only elastic deformation occurs, the material is more rigid. The yield surface is a kind of material memory. In hypoplasticity there is no yield function, no elastic domain. All past information is concentrated in the current stress.

Indeed, there are today new versions of hypoplastic equations involving the void ratio and a structural tensor that are more sensible to past deformation history.

The hypoplasticity framework, however, is not a simple model and have no some physical meaning in deriving the formulation. And still need to be improved and extended to make simpler.

2.3 Hyperplasticity Model

This model derived based on generalized thermodynamics principles. Some people contribute to build this framework are Ziegler (1983), Houlsby (1981); Collins and Houlsby (1997). Further extension and generalization of this approach can be found in Houlsby and Puzrin (2006).

In this model incremental response is derived from two scalar potential functions: an energy function and a dissipation function (or yield function). The energy function can be used in any of four alternative forms related by Legendre transformations. An alternative to the dissipation function is a yield surface, related to the dissipation function by a degenerate Legendre transformation.

For small-strain continuum mechanics in Cartesian coordinates, energy functions are defined in Table 2.1, u is the specific internal energy function of strain tensor ε_{ij} and specific entropy s, defined as a potential for stress tensor σ_{ij} and temperature θ. The function f is the specific Helmholtz free energy function of strain tensor and temperature, a potential for stress and specific entropy; h is the specific enthalpy function of stress and specific entropy, a potential for strain and temperature. The function g is the specific Gibbs free energy function of stress and temperature, a potential for strain and specific entropy.

In the hyperplasticity formulation, the second potential function required is the dissipation function, which allows the Second Law of Thermodynamics to be satisfied within the proposed framework. The Second Law can be formulated as in the following:

$$\dot{s} \geq -\left(\frac{q_k}{\theta}\right)_{,k} \tag{2.13}$$

where (q_k/θ) is the entropy flux. When this inequality is rewritten in the following way:

$$\theta\dot{s} + q_{k,k} - \frac{q_k\theta_{,k}}{\theta} \geq 0 \tag{2.14}$$

the first two terms $\theta\dot{s} + q_{k,k} = d$ are called the mechanical dissipation. The third term is called the thermal dissipation and it is always non-negative. For slow processes, this term becomes small by comparison with the first two, so it is argued that the mechanical

Table 2.1 Energy function for small-strain continuum mechanics (Houlsby & Puzrin, 2006)

Internal energy	Helmholtz free energy	Enthalpy	Gibbs free energy
$u = u(\varepsilon_{ij}, s)$	$f = f(\varepsilon_{ij}, \theta)$	$h = h(\sigma_{ij}, s)$	$g = g(\sigma_{ij}, \theta)$
$\sigma_{ij} = \dfrac{\partial u}{\partial \varepsilon_{ij}}$ $\theta = \dfrac{\partial u}{\partial s}$	$\sigma_{ij} = \dfrac{\partial f}{\partial \varepsilon_{ij}}$ $s = \dfrac{\partial f}{\partial \theta}$	$\varepsilon_{ij} = \dfrac{\partial h}{\partial \sigma_{ij}}$ $\theta = \dfrac{\partial h}{\partial s}$	$\varepsilon_{ij} = \dfrac{\partial g}{\partial \sigma_{ij}}$ $s = \dfrac{\partial g}{\partial \theta}$
$u = g - s\theta - \sigma_{ij}\varepsilon_{ij}$	$f = u - s\theta$	$h = u - \sigma_{ij}\varepsilon_{ij}$	$g = h - s\theta$ $= f - \sigma_{ij}\varepsilon_{ij}$

dissipation must itself be non-negative. For dissipative materials, the internal energy is a function not only strain and entropy, but of kinematic internal variables α_{ij} as well: $u = u(\varepsilon_{ij}, \alpha_{ij}, s)$. Strain, internal variables and entropy define a thermodynamics state of material. Further, an assumption is defined that the dissipation is also a function of the thermodynamic state and the rate of change of the material state. In fact, it is sufficient to consider that the dissipation function depends only on the rate of change of the internal variables α_{ij}. The dissipation function can be written in four possible ways, depending on which form of the energy function is specified:

$$d = d^e\left(\sigma_{ij} \text{ or } \varepsilon_{ij}, \alpha_{ij}, s \text{ or } \theta, \dot{\alpha}_{ij}\right) \geq 0 \tag{2.15}$$

where e superscript in this equation represent one of the four energy functions.

To impose the First Law of Thermodynamics, the generalised and dissipative generalised stress tensor is defined. The generalised stress tensor is defined by differentiation of an energy function with respect to internal variable:

$$\bar{\chi}_{ij} = -\frac{\partial u}{\partial \alpha_{ij}} = -\frac{\partial f}{\partial \alpha_{ij}} = -\frac{\partial h}{\partial \alpha_{ij}} = -\frac{\partial g}{\partial \alpha_{ij}} \tag{2.16}$$

Whereas, the dissipative generalised stress tensor is defined by differentiation of a dissipation function with respect to internal variable rate:

$$\chi_{ij} = \frac{\partial d^e}{\partial \dot{\alpha}_{ij}} \tag{2.17}$$

where e superscript in this equation represent one of the four energy functions.

The First Law of Thermodynamics state that rate of change of internal energy is the sum of the mechanical work input and the rate of heat supply to an element of volume:

$$\dot{u} = \dot{W} + \dot{Q} \tag{2.18}$$

where $\dot{W} = \sigma_{ij}\dot{\varepsilon}_{ij}$ and $\dot{Q} = -q_{k,k}$

$$\dot{u} = \sigma_{ij}\dot{\varepsilon}_{ij} - q_{k,k} = \sigma_{ij}\dot{\varepsilon}_{ij} + \theta\dot{s} - d \tag{2.19}$$

On the other hand, the internal energy is a function of state: $u = u(\varepsilon_{ij}, \alpha_{ij}, s)$, and further that

$$\dot{u} = \frac{\partial u}{\partial \varepsilon_{ij}}\dot{\varepsilon}_{ij} + \frac{\partial u}{\partial \alpha_{ij}}\dot{\alpha}_{ij} + \frac{\partial u}{\partial s}\dot{s} \tag{2.20}$$

Noting that the increments of the variables are independent of the state and comparing (2.19) and (2.20), then using the definition of the generalised stress in (2.16), we obtain an expression for mechanical dissipation:

$$d = \overline{\chi}_{ij}\dot{\alpha}_{ij} \tag{2.21}$$

Furthermore, a yield function is defined as a degenerate special case of the Legendre transformation of the dissipation function: $y^e = \chi_{ij}\dot{\alpha}_{ij} - d^e = 0$, where

$$y = y^e\left(\sigma_{ij} \text{ or } \varepsilon_{ij}, \alpha_{ij}, s \text{ or } \theta, \chi_{ij}\right) = 0 \tag{2.22}$$

The flow rule follows from the properties of Legendre transformation:

$$\dot{\alpha}_{ij} = \lambda \frac{\partial y^e}{\partial \chi_{ij}} \tag{2.23}$$

where λ is an arbitrary non-negative multiplier. Table 2.2 summarize the hyperplasticity formulation based on Gibbs (*g*) and Helmholtz (*h*) free energy.

Most of soils do exhibit a small element of rate-dependent behaviour, i.e: measured strength are slightly increased at higher strain rates, and a small amount of creep occurred under constant stress, even for soils where such effects are negligible, the inclusion of a small 'artificial' viscosity in the model simplifies the numerical calculations considerably. Those are reasons to introduce rate-dependent hyperplasticity model. Table 2.3 shows comparison between these two models.

Some further development work on hyperplasticity in soil mechanics is explored by Likitlersuang (2003) and Likitlersuang and Houlsby (2006).

Table 2.2 Basic formulas for hyperplasticity model

Definition	Gibbs free energy (g)	Helmholtz (h) free energy
Energy function	$g = g(\sigma_{ij}, \alpha_{ij})$	$f = f(\varepsilon_{ij}, \alpha_{ij})$
Dissipation function	$d = d^g(\sigma_{ij}, \alpha_{ij}, \dot{\alpha}_{ij}) \geq 0$	$d = d^f(\varepsilon_{ij}, \alpha_{ij}, \dot{\alpha}_{ij}) \geq 0$
Generalised stress	$\overline{\chi}_{ij} = -\dfrac{\partial g}{\partial \alpha_{ij}}$	$\overline{\chi}_{ij} = -\dfrac{\partial f}{\partial \alpha_{ij}}$
Stress-strain relationship	$\varepsilon_{ij} = \dfrac{\partial g}{\partial \sigma_{ij}}$	$\sigma_{ij} = \dfrac{\partial f}{\partial \varepsilon_{ij}}$
Dissipative generalised stress	$\chi_{ij} = \dfrac{\partial d^g}{\partial \dot{\alpha}_{ij}}$	$\chi_{ij} = \dfrac{\partial d^f}{\partial \dot{\alpha}_{ij}}$
Yield function	$y = y^g(\sigma_{ij}, \alpha_{ij}, \chi_{ij}) = 0$	$y = y^f(\varepsilon_{ij}, \alpha_{ij}, \chi_{ij}) = 0$
Flow rule	$\dot{\alpha}_{ij} = \lambda \dfrac{\partial y^g}{\partial \chi_{ij}}$	$\dot{\alpha}_{ij} = \lambda \dfrac{\partial y^f}{\partial \chi_{ij}}$

Table 2.3 Comparison for rate-independent and rate –dependent hyperplasticity model (Likitlersuang, 2003)

Definition	Rate-independent model	Rate-dependent model
First potential	the same definition of energy functions (g,f,h,u)	
Second potential	Dissipation function (d) and yield function (y)	Force function (z) and flow potential (w)
Dissipative generalised stress	$\chi_{ij} = \dfrac{\partial d^e}{\partial \dot{\alpha}_{ij}}$	$\chi_{ij} = \dfrac{\partial z^e}{\partial \dot{\alpha}_{ij}}$
Legendre-Fenchel transformation	$\lambda y = \chi_{ij}\dot{\alpha}_{ij} - d = 0$	$w = \chi_{ij}\dot{\alpha}_{ij} - z = d - z$
Flow rule	$\dot{\alpha}_{ij} = \lambda \dfrac{\partial y^e}{\partial \chi_{ij}}$	$\dot{\alpha}_{ij} = \lambda \dfrac{\partial w^e}{\partial \chi_{ij}}$

2.4   Comparison of Advanced Soil Constitutive Models

Although, in principally the bounding surface models more efficient than multiple surfaces, but they still have three important shortcomings i.e: (1) They often require the choice of a number of somewhat arbitrary functions; (2) often the functions without obvious physical meaning; (3) they usually fail to describe the effects of the immediate past history.

Multiple surface models are the most promising approach, but they also still have some drawbacks, i.e.: (1) they result in a large number of material parameters to be specified; (2) they also result in considerable amount of computation; (3) many of them are inherently complex.

Hypoplasticity model, which is only developed and discussed within few researches and has two shortcomings: (1) The constitutive model basically is not based on definite physical meanings, the relation between stress rate tensor and stretching tensor is just fitted by a polynomial with some fitting parameters which have less direct relation to the physical quantities of soils that geotechnical engineers familiar with, (2) The relation between stress rate tensor and stretching tensor is nonlinear, which make it very difficult to solve boundary value problems because an explicit stiffness matrix based on this model cannot be obtained easily and it has no any evidence of solving this problem mathematically and numerically. Kolymbas (2000) stated about his own model as follows: (1) The theory should be improved and extended to fill its application portfolio; (2) They should simpler and have some physical meaning, since only in this way, they can communicate with engineering practitioners.

As we stated in the Chapter 1, and we need repeat it again, since constitutive models relate to physical phenomena, they must be developed without violate certain principles or axioms that govern the physical phenomena such as the laws of thermodynamics. Hyperplasticity framework describes the behaviour of soils both for clay and sand, associative or non associative flow within a rigorous, compact, and consistent framework.

The other reasons are this framework models could be developed without the need for additional *ad hoc* assumptions and procedures, and it makes considerable use of potential function and internal variables to predict entire stress-strain response of a material subject to a specified sequence of stress or strain increment. In addition, the framework may allow a number of competing models to be cast within a single framework, and so allow them to be more readily compared.

In the next chapter, development and numerical model implementation one of the thermodynamics-based soil model based on hyperplasticity framework i.e.: continuous hyperplasticity non-linear KHMCC model is presented.

CHAPTER III.   MODEL DEVELOPMENT AND NUMERICAL IMPLEMENTATION

3.1   Introduction

The stress-strain characteristic of soils is non-linear and irreversible, in that the initial soil stiffness or small-strain tangent stiffness depends on the stress level. The interpretation from experimental observations of bender element test shows that the small-strain stiffness of soils is a non-linear function of the mean effective stress for isotropically consolidated samples as reported by Tanizawa et. al. (1994), Kohata et. al. (1997), Pennington et. al. (1997), and Techavorasinskun et. al. (2002) and depend on the stress ratio (Rampello et. al., 1997) for anisotropically consolidated samples. The stiffness also affected by other variables, such as the voids ratio, anisotropic stress state, and/or the preconsolidation pressure (Hardin, 1978; Houlsby & Wroth, 1991; Viggiani, 1992; Rampello et al., 1994; and Soga, 1995).

In this chapter, a development and numerical implementation of the hyperplasticity non-linear KHMCC model based on triaxial stress-strain variables and general stress using strain-driven forward-Euler integration scheme is presented. A power functions of pressure proposed by Houlsby et. al. (2005) is adopted in non-linear elastic energy function. A hyperbolic function proposed by Puzrin and Houlsby (2001) is adopted in non-linear kinematic hardening function. For simplicity, the pre-consolidation pressure after the completion of isotropic consolidation is referred in the initial stiffness of kinematic hardening function. An analytical solution of ideal undrained triaxial test on normally consolidated clay (Roscoe and Burland, 1968; Potts, 1994) is used to verify numerical model implementation under single yield surface. Several numerical demonstrations are performed for monotonic, cyclic and repetitive loading under undrained condition for normally and lightly consolidated clays. The developed model is highlighted through the capabilities on characterising effect of immediate stress history (Atkinson, 1990; Houlsby 1999), dependence of effective stress path on the immediate stress history during undrained shear (Stallebrass and Taylor, 1997), smooth and irreversible unloading-reloading responses. All attempts of demonstration are to emphasize the performance of hyperplasticity framework which can contain several complicated characteristics of constitutive models under the unified framework. Further, several validations against small-strain experimental on clay soil are conducted. An experimental undrained triaxial test on Speswhite kaolin (Stallebrass & Taylor, 1997) has been selected. Model validation is performed with response of tangent stiffness against stresses. Further, the experimental result of unloading-reloading at small-strain is also compared to model prediction.

3.2   Non-linear Kinematic Hardening Modified Cam Clay Model

3.2.1   *Sign Convention and Triaxial Variables*

The standard soil mechanics sign convention of compressive stresses and strains positive is used throughout this research, and all stresses are effective. The triaxial stress variables are $p = \frac{1}{3}(\sigma_a + 2\sigma_r)$, $q = \sigma_a - \sigma_r$ where p is mean effective stress, q is stress deviator, σ_a is axial stress and σ_r is radial stress. Corresponding to them are volumetric and deviatoric (shear) strains defined by $\varepsilon_p = \varepsilon_a + 2\varepsilon_r$ and $\varepsilon_q = \frac{2}{3}(\varepsilon_a - \varepsilon_r)$ where ε_a is axial strain and ε_r is radial strain.

For more general stress states, the following notation is adopted: σ_{ij} is the effective Cauchy stress tensor; ε_{ij} is small-strain tensor; and δ_{ij} is Kronecker's delta (δ_{ij} = 1 if $i = j$, δ_{ij} = 0 if $i \neq j$ where $i, j \in \{1, 2, 3\}$). The stress invariants are $p = \frac{1}{3}\sigma_{ii}$, $q = \sqrt{\frac{3}{2}\sigma'_{ij}\sigma'_{ij}}$, where $\sigma_{ii} = \sum_{i=1}^{3} \sigma_{ii}$; $\sigma'_{ij} = \sigma_{ij} - p\delta_{ij}$ is deviatoric component of the effective stress tensor. The corresponding strain invariants are $\varepsilon_p = \varepsilon_{ii}$ and $\varepsilon_q = \sqrt{\frac{2}{3}\varepsilon'_{ij}\varepsilon'_{ij}}$, where $\varepsilon'_{ij} = \varepsilon_{ij} - \frac{1}{3}\varepsilon_{ii}\delta_{ij}$ is deviatoric component of the strain tensor. In similar way, generalised stress invariants are $\chi_p = \frac{1}{3}\chi_{ii}$, $\chi_q = \sqrt{\frac{3}{2}\chi'_{ij}\chi'_{ij}}$ where $\chi_{ii} = \sum_{k=1}^{3} \chi_{kk}$; $\chi'_{ij} = \chi_{ij} - \chi_p\delta_{ij}$ is deviatoric component of the effective generalised stress tensor. The corresponding internal variable invariants are $\alpha_p = \alpha_{ii}$ and $\alpha_q = \sqrt{\frac{2}{3}\alpha'_{ij}\alpha'_{ij}}$, where $\alpha'_{ij} = \alpha_{ij} - \frac{1}{3}\alpha_{ii}\delta_{ij}$ is deviatoric component of the internal variable tensor.

3.2.2   *Triaxial Formulation*

Under the hyperplasticity framework (see Houlsby and Puzrin (2006) for details), the entire constitutive model is fundamentally governed by two scalar functions which are energy function and yield function or dissipation function. In typical formulation, Gibbs free energy function is suggested to associate stresses, material parameters and material memories (internal variables) to a unique potential function where the referenced pressure for zero volumetric strain is defined at 1 atm. It is noticed that hyperplasticity framework employs a total energy instead of rate form of energy which is commonly used in classical plasticity theory. Since Gibbs free energy is equivalent to a complementary energy, then negative elastic stored energy, negative dissipation energy and positive hardening energy are combined. According to Houlsby et al. (2005), a non-linear version of KHMCC is created to allocate non-linear elastic moduli at small-

strain into the Gibbs free energy which is expressed in the form $E = E(p, q, \alpha_p, \alpha_q, \hat{\alpha}_p, \hat{\alpha}_q)$ by adding the hyperelastic expression using triaxial stress variables.

$$E = -\frac{p_e^{2-n}}{p_r^{1-n}k(1-n)(2-n)} + \frac{p}{k(1-n)} - (p\alpha_p + q\alpha_q) + \int_0^1 \left(\frac{1}{2}\hat{H}_p\hat{\alpha}_p^2 + \frac{1}{2}\hat{H}_q\hat{\alpha}_q^2\right)d\eta \quad (3.1)$$

where $p_e = \sqrt{p^2 + \frac{k(1-n)q^2}{3g}}$ is defined as an equivalent stress variable for convenience.

k, g, n are dimensionless material constant calibrated from elastic stress-strain relation at small-strain level. Atmospheric pressure 1 atm (approximately 100 kPa) is usually defined for p_r as reference pressure. α_p and α_q are total isotropic and deviatoric plastic strains respectively. Integration of differential hardening energy is evaluated in terms of internal coordinate η which is limited between 0 to 1. $\eta = 0$ represents the initial hardening stage (the highest hardening response) while $\eta = 1$ represents the final hardening stage (zero hardening response). $\hat{\alpha}_p$ and $\hat{\alpha}_q$ are kinematic internal variable function of η which can be integrated to obtained α_p and α_q by Equations (3.2) and (3.3). Therefore, α_p and α_q can be regarded as a definite integral area of functional variables $\hat{\alpha}_p$ and $\hat{\alpha}_q$ over the domain of η. It is noted that all variables with "^" (hat) throughout this study are referred to internal variable function of η.

$$\alpha_p = \int_0^1 \hat{\alpha}_p d\eta , \quad \alpha_q = \int_0^1 \hat{\alpha}_q d\eta \qquad (3.2),(3.3)$$

$\hat{H}_p, \hat{H}_q$ [in kPa] are non-linear kinematic hardening functions in corresponding to isotropic and deviatoric hardening responses as expressed in Equations (3.4) and (3.6). A hyperbolic function proposed by Puzrin and Houlsby (2001) is adopted to these internal functions. For simplicity, the initial hardening stage of the kinematic hardening functions is made as power function of initial preconsolidation pressure as represented by $\hat{H}_{pi}, \hat{H}_{qi}$ in Equations (3.5) and (3.7).

$$\hat{H}_p = \hat{H}_{pi}(1-\eta)^3 , \text{ where } \hat{H}_{pi} = \frac{kp_0^n p_r^{1-n}}{2(a-1)} \qquad (3.4),(3.5)$$

$$\hat{H}_q = \hat{H}_{qi}(1-\eta)^3 , \text{ where } \hat{H}_{qi} = \frac{3gp_0^n p_r^{1-n}}{2(a-1)} \qquad (3.6),(3.7)$$

where p_0 is an initial preconsolidation pressure at the end of consolidation stage and a is material constant. Plot of the above hardening functions against internal coordinate η

is shown in Figure 3.1. It is clear that $\hat{H}_{pi} \geq \hat{H}_p(\eta) \geq 0$ and $\hat{H}_{qi} \geq \hat{H}_q(\eta) \geq 0$. Therefore, in this study $\hat{H}_p$ and $\hat{H}_q$ are not directly dependent on p and q in energy function.
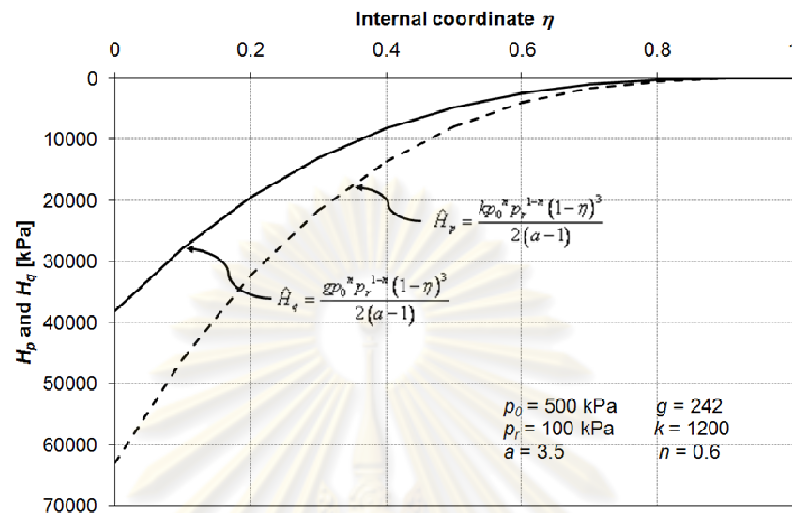
Figure 3.1 Variation of hardening functions against internal coordinate η.

According to the hyperplasticity framework, total strain components are considered as conjugate variables of stresses which are derived from the Gibbs energy function. From Equation (3.1), it follows that the volumetric strain ε_p, deviatoric strain ε_q can be obtained via differentiation with stresses as shown in Equations (3.8) and (3.9).

$$\varepsilon_p = -\frac{\partial E}{\partial p} = \frac{1}{k(1-n)}\left(\frac{p}{p_r^{1-n} p_e^n} - 1\right) + \alpha_p \tag{3.8}$$

$$\varepsilon_q = -\frac{\partial E}{\partial q} = \frac{q}{p_r^{1-n} 3g p_e^n} + \alpha_q \tag{3.9}$$

Because of the total plastic strain components α_p and α_q defined earlier, the dissociation of total elastic and plastic strain components can be clarified.

However, the Gibbs energy function expressed in Equation (3.1) with strain components derived in Equations (3.8) and (3.9) is valid for $0 \leq n < 1$. For $n = 1$ these equations will be particularly replaced by the following Equations (3.10)-(3.12).

$$E = -\frac{p}{k}\left(\ln\left(\frac{p}{p_r}\right) - 1\right) - \frac{q^2}{6gp} - \left(p\alpha_p + q\alpha_q\right) + \int_0^1 \left(\frac{1}{2}\hat{H}_p \hat{\alpha}_p^2 + \frac{1}{2}\hat{H}_q \hat{\alpha}_q^2\right)d\eta \tag{3.10}$$

$$\varepsilon_p = -\frac{\partial E}{\partial p} = \frac{1}{k}\ln\left(\frac{p}{p_r}\right) - \frac{q^2}{6gp^2} + \alpha_p \tag{3.11}$$

$$\varepsilon_q = -\frac{\partial E}{\partial q} = \frac{q}{3gp} + \alpha_q \tag{3.12}$$

According to Equations (3.8), (3.9), (3.11) and (3.12), total strain components are derived as function of p, q and $\alpha_p(\hat{\alpha}_p), \alpha_q(\hat{\alpha}_q)$. By flow rule, rate change of total strain components can be obtained. The second derivatives of Gibbs free energy appeared in the below equations are derived in Box 1.

$$\dot{\varepsilon}_p = \left(-\frac{\partial^2 E}{\partial p^2}\right)\dot{p} + \left(-\frac{\partial^2 E}{\partial q \partial p}\right)\dot{q} + \int_0^1\left(-\frac{\partial^2 E}{\partial \hat{\alpha}_p \partial p}\right)\dot{\hat{\alpha}}_p d\eta + \int_0^1\left(-\frac{\partial^2 E}{\partial \hat{\alpha}_q \partial p}\right)\dot{\hat{\alpha}}_q d\eta \tag{3.13}$$

$$\dot{\varepsilon}_q = \left(-\frac{\partial^2 E}{\partial p \partial q}\right)\dot{p} + \left(-\frac{\partial^2 E}{\partial q^2}\right)\dot{q} + \int_0^1\left(-\frac{\partial^2 E}{\partial \hat{\alpha}_p \partial q}\right)\dot{\hat{\alpha}}_p d\eta + \int_0^1\left(-\frac{\partial^2 E}{\partial \hat{\alpha}_q \partial q}\right)\dot{\hat{\alpha}}_q d\eta \tag{3.14}$$

Rate change of total strain components can be simply written by the following equations. Equation (3.15) is a compacted form of Equations (3.13) and (3.14). Equation (3.16) expresses rate form of plastic strain components while Equation (3.17) expresses rate form of elastic strain components.

$$\left\{\begin{array}{c}\dot{\varepsilon}_p\\\dot{\varepsilon}_q\end{array}\right\} = \begin{bmatrix}-\dfrac{\partial^2 E}{\partial p^2} & -\dfrac{\partial^2 E}{\partial p \partial q}\\ -\dfrac{\partial^2 E}{\partial p \partial q} & -\dfrac{\partial^2 E}{\partial q^2}\end{bmatrix}\cdot\left\{\begin{array}{c}\dot{p}\\\dot{q}\end{array}\right\} + \int_0^1\begin{bmatrix}-\dfrac{\partial^2 E}{\partial \hat{\alpha}_p \partial p} & -\dfrac{\partial^2 E}{\partial \hat{\alpha}_q \partial p}\\ -\dfrac{\partial^2 E}{\partial \hat{\alpha}_p \partial q} & -\dfrac{\partial^2 E}{\partial \hat{\alpha}_q \partial q}\end{bmatrix}\cdot\left\{\begin{array}{c}\dot{\hat{\alpha}}_p\\\dot{\hat{\alpha}}_q\end{array}\right\}d\eta \tag{3.15}$$

$$\left\{\begin{array}{c}\dot{\alpha}_p\\\dot{\alpha}_q\end{array}\right\} = \int_0^1\begin{bmatrix}-\dfrac{\partial^2 E}{\partial \hat{\alpha}_p \partial p} & -\dfrac{\partial^2 E}{\partial \hat{\alpha}_q \partial p}\\ -\dfrac{\partial^2 E}{\partial \hat{\alpha}_p \partial q} & -\dfrac{\partial^2 E}{\partial \hat{\alpha}_q \partial q}\end{bmatrix}\cdot\left\{\begin{array}{c}\dot{\hat{\alpha}}_p\\\dot{\hat{\alpha}}_q\end{array}\right\}d\eta \tag{3.16}$$

$$\left\{\begin{array}{c}\dot{\varepsilon}_p^e\\\dot{\varepsilon}_q^e\end{array}\right\} = \left\{\begin{array}{c}\dot{\varepsilon}_p\\\dot{\varepsilon}_q\end{array}\right\} - \left\{\begin{array}{c}\dot{\alpha}_p\\\dot{\alpha}_q\end{array}\right\} = \begin{bmatrix}-\dfrac{\partial^2 E}{\partial p^2} & -\dfrac{\partial^2 E}{\partial p \partial q}\\ -\dfrac{\partial^2 E}{\partial p \partial q} & -\dfrac{\partial^2 E}{\partial q^2}\end{bmatrix}\cdot\left\{\begin{array}{c}\dot{p}\\\dot{q}\end{array}\right\} \tag{3.17}$$

According to Equation (3.17), the incremental elastic stress-strain relationship can be given as the compliance stiffness matrix.

$$
\left\{ \begin{array}{c} \dot{p} \\ \dot{q} \end{array} \right\} = \left[\begin{array}{cc} -\dfrac{\partial^2 E}{\partial p^2} & -\dfrac{\partial^2 E}{\partial p \partial q} \\ -\dfrac{\partial^2 E}{\partial p \partial q} & -\dfrac{\partial^2 E}{\partial q^2} \end{array} \right]^{-1} \cdot \left\{ \begin{array}{c} \dot{\varepsilon}_p^e \\ \dot{\varepsilon}_q^e \end{array} \right\} = \left[\begin{array}{cc} K & J \\ J & 3G \end{array} \right] \cdot \left\{ \begin{array}{c} \dot{\varepsilon}_p^e \\ \dot{\varepsilon}_q^e \end{array} \right\} \tag{3.18}
$$

where K is non-linear bulk modulus, G is non-linear shear modulus, and J is non-linear coupling modulus. If J is non-zero, the incremental stress-strain response is a stress-induced anisotropic behaviour appeared during loading stages (Houlsby, 1985). J is zero only in the condition of isotropic consolidation.

$$
K = \frac{-\dfrac{\partial^2 E}{\partial q^2}}{\dfrac{\partial^2 E}{\partial p^2}\dfrac{\partial^2 E}{\partial q^2} - \left(\dfrac{\partial^2 E}{\partial p \partial q}\right)^2}, \; G = \frac{1}{3}\frac{-\dfrac{\partial^2 E}{\partial p^2}}{\dfrac{\partial^2 E}{\partial p^2}\dfrac{\partial^2 E}{\partial q^2} - \left(\dfrac{\partial^2 E}{\partial p \partial q}\right)^2},
$$

$$
J = \frac{\dfrac{\partial^2 E}{\partial p \partial q}}{\dfrac{\partial^2 E}{\partial p^2}\dfrac{\partial^2 E}{\partial q^2} - \left(\dfrac{\partial^2 E}{\partial p \partial q}\right)^2}
\tag{3.19}
$$

Box 1: Second derivatives of Gibbs free energy

Gibbs free energy E for $0 \le n < 1$ in Equation (3.1) (after Houlsby and Puzrin, 2006)	Gibbs free energy for $n = 1$ in Equation (3.10) (after Houlsby and Puzrin, 2006)
$-\dfrac{\partial^2 E}{\partial p^2} = \dfrac{1}{k(1-n)p_r^{1-n}p_e^n}\left(1 - \dfrac{np^2}{p_e^2}\right)$	$-\dfrac{\partial^2 E}{\partial p^2} = \dfrac{1}{kp}\left(1 + \dfrac{kq^2}{3gp^2}\right)$
$-\dfrac{\partial^2 E}{\partial q^2} = \dfrac{1}{3gp_r^{1-n}p_e^n}\left(1 - \dfrac{nk(1-n)q^2}{3gp_e^2}\right)$	$-\dfrac{\partial^2 E}{\partial q^2} = \dfrac{1}{3gp}$
$-\dfrac{\partial^2 E}{\partial p \partial q} = -\dfrac{npq}{3gp_r^{1-n}p_e^{n+2}}$	$-\dfrac{\partial^2 E}{\partial p \partial q} = -\dfrac{q}{3gp^2}$

Gibbs free energy E for $0 \le n \le 1$		
$-\dfrac{\partial^2 E}{\partial \hat{\alpha}_p \partial p} = 1$		$-\dfrac{\partial^2 E}{\partial \hat{\alpha}_p \partial q} = 0$
$-\dfrac{\partial^2 E}{\partial \hat{\alpha}_q \partial p} = 0$		$-\dfrac{\partial^2 E}{\partial \hat{\alpha}_q \partial q} = 1$

The relation between among stress variables is not existed in the previous description based on energy function. This relation is described in yield function which

contains stress variables to couple with energy function. In the non-linear KHMCC model (see Likitlersuang, 2003; Likitlersuang and Houlsby, 2006 for details), the yield function $\hat{y}$ in term of triaxial stress parameters is defined:

$$\hat{y} = \sqrt{\hat{\chi}_p{}^2 + \hat{\chi}_q{}^2 / M^2} - \hat{c} = 0 \qquad (3.20)$$

where *M* is a frictional critical state parameter (Roscoe and Burland, 1968) which is the value that stress ratio q/p' attains at critical state, $\hat{c} = \hat{H}_p \alpha_p \eta$ is a yield stress which represents the size of yield surface function, $\hat{\chi}_p$ and $\hat{\chi}_q$ are generalised stresses in term of volumetric and deviatoric stresses. Materials behave plastically when the yield surface is active ($\hat{y} \geq 0$). Materials behave elastically when the stress is inside the yield surface ($\hat{y} < 0$). The generalised stresses are defined as changing of free energy functional with respect to the internal kinematic variables. Gibb's free energy functional $\hat{E}$ can be defined as the internal energy with respect to η . So the integration of $\hat{E}$ throughout the domain of η is Gibb's free energy as shown in Equation (3.21).

$$E = \int\limits_0^1 \hat{E} d\eta \qquad (3.21)$$

According to Equations (3.1)-(3.3) and (3.21), Gibb's free energy functional $\hat{E}$ is obtained by the following equation.

$$\hat{E} = -\frac{p_e{}^{2-n}}{p_r{}^{1-n} k (1-n)(2-n)} + \frac{p}{k(1-n)} - \left(p \hat{\alpha}_p + q \hat{\alpha}_q \right) + \left(\frac{1}{2} \hat{H}_p \hat{\alpha}_p{}^2 + \frac{1}{2} \hat{H}_q \hat{\alpha}_q{}^2 \right) \qquad (3.22)$$

Therefore, $\hat{\chi}_p$ and $\hat{\chi}_q$ are referred in Equations (3.23) and (3.24) as the derivatives of $\hat{E}$ with respect to $\hat{\alpha}_p$ and $\hat{\alpha}_q$ respectively. It is found that $\hat{\chi}_p$ and $\hat{\chi}_q$ can be considered as the difference between stress variables and yield stresses which is associated with kinematic hardening variables. In this study, the derivation of Equations (3.23) and (3.24) is simplified because the definitions of α_p and α_q are initially adopted in Equations (3.2) and (3.3). If α_p , α_q and $\hat{\alpha}_p$ and $\hat{\alpha}_q$ are considered as independent variables in Gibb's free energy, the constraint function using Lagrangian multiplier and Ziegler's orthogonality condition (Ziegler, 1983) must be employed. This detailed proof can be found in Houlsby and Puzrin (2006).

$$\hat{\chi}_p = \frac{\partial \hat{E}}{\partial \hat{\alpha}_p} = p - \hat{H}_p \hat{\alpha}_p \qquad (3.23)$$

$$\hat{\chi}_q = \frac{\partial \hat{E}}{\partial \hat{\alpha}_q} = q - \hat{H}_q \hat{\alpha}_q \qquad (3.24)$$

According to Houlsby and Puzrin (2006), the evolution rule of kinematic internal variable function $\hat{\alpha}_p$ and $\hat{\alpha}_q$ are followed Equations (3.25) and (3.26) respectively as the derivatives of flow potential w with respect to generalised stress variables. One may associate this kind of evolution rule to flow rule used in classical plasticity. The flow potential w is defined in relevant to yield function $\hat{y}$ as shown in Equation (3.27).

$$\dot{\hat{\alpha}}_p = \frac{\partial w}{\partial \hat{\chi}_p}, \quad \dot{\hat{\alpha}}_q = \frac{\partial w}{\partial \hat{\chi}_q} \qquad (3.25),(3.26)$$

$$w = \frac{\langle \hat{y} \rangle^2}{2\mu} = \frac{\left\langle \sqrt{\hat{\chi}_p^{\,2} + \hat{\chi}_q^{\,2}/M^2} - \hat{c} \right\rangle^2}{2\mu} \qquad (3.27)$$

where μ is viscosity coefficient which is in rate-dependent algorithm plays the role as an "artificial" viscosity that imposed to unity. However, we can actually define μ as a "true" viscosity coefficient such in modelling creep behaviour. The operator $\langle\ \rangle$ is Macaulay brackets which defines $\langle \bullet \rangle = \begin{cases} 0; & \bullet < 0 \\ \bullet; & \bullet \geq 0 \end{cases}$

As a consequence of Equations (3.25)-(3.27), the rate form of stress-strain relationship obtained in Equation (3.15) can be expressed. The derivatives of flow potential w in Equations (3.25) and (3.26) are shown in Box 2.

$$\begin{bmatrix} -\dfrac{\partial^2 E}{\partial p^2} & -\dfrac{\partial^2 E}{\partial p \partial q} \\ -\dfrac{\partial^2 E}{\partial p \partial q} & -\dfrac{\partial^2 E}{\partial q^2} \end{bmatrix} \cdot \begin{Bmatrix} \dot{p} \\ \dot{q} \end{Bmatrix} = \begin{Bmatrix} \dot{\varepsilon}_p \\ \dot{\varepsilon}_q \end{Bmatrix} - \int_0^1 \begin{bmatrix} -\dfrac{\partial^2 E}{\partial \hat{\alpha}_p \partial p} & -\dfrac{\partial^2 E}{\partial \hat{\alpha}_q \partial p} \\ -\dfrac{\partial^2 E}{\partial \hat{\alpha}_p \partial q} & -\dfrac{\partial^2 E}{\partial \hat{\alpha}_q \partial q} \end{bmatrix} \cdot \begin{Bmatrix} \dfrac{\partial w}{\partial \hat{\chi}_p} \\ \dfrac{\partial w}{\partial \hat{\chi}_q} \end{Bmatrix} d\eta \qquad (3.28)$$

Box 2: Derivatives of flow potential with respect to generalised stress variables

$$\frac{\partial w}{\partial \hat{\chi}_p} = \frac{\sqrt{\hat{\chi}_p^2 + \dfrac{\hat{\chi}_q^2}{M^2}} - \hat{c} + \left| \sqrt{\hat{\chi}_p^2 + \dfrac{\hat{\chi}_q^2}{M^2}} - \hat{c} \right|}{2\mu} \cdot \left(\frac{\hat{\chi}_p^2}{2\sqrt{\hat{\chi}_p^2 + \dfrac{\hat{\chi}_q^2}{M^2}}} + \frac{\hat{\chi}_p^2 \cdot \left| \sqrt{\hat{\chi}_p^2 + \dfrac{\hat{\chi}_q^2}{M^2}} - \hat{c} \right|}{\sqrt{\hat{\chi}_p^2 + \dfrac{\hat{\chi}_q^2}{M^2}}} \right)$$

$$\frac{\partial w}{\partial \hat{\chi}_q} = \frac{\sqrt{\hat{\chi}_p^2 + \dfrac{\hat{\chi}_q^2}{M^2}} - \hat{c} + \left| \sqrt{\hat{\chi}_p^2 + \dfrac{\hat{\chi}_q^2}{M^2}} - \hat{c} \right|}{2\mu} \cdot \left(\frac{\dfrac{\hat{\chi}_q^2}{M^2}}{2\sqrt{\hat{\chi}_p^2 + \dfrac{\hat{\chi}_q^2}{M^2}}} + \frac{\dfrac{\hat{\chi}_q^2}{M^2} \cdot \left| \sqrt{\hat{\chi}_p^2 + \dfrac{\hat{\chi}_q^2}{M^2}} - \hat{c} \right|}{\sqrt{\hat{\chi}_p^2 + \dfrac{\hat{\chi}_q^2}{M^2}}} \right)$$

3.2.3 General Stress Formulation

In order to implement in a finite element program a non-linear KHMCC model should be formulated in general stress. Then, the Gibbs free energy is expressed in the form $E = E\left(\sigma_{ij}, \alpha_{ij}, \hat{\alpha}_{ij}\right)$:

$$E = -\frac{p_e^{2-n}}{p_r^{1-n}k(1-n)(2-n)} - \frac{\sigma_{kk}}{3k(1-n)} - \sigma_{ij}\alpha_{ij} + \int_0^1 \left(\frac{\hat{H}_p \hat{\alpha}_{kk}^2}{2} + \frac{\hat{H}_q \hat{\alpha}_{ij}' \hat{\alpha}_{ij}'}{3}\right)d\eta \qquad (3.29)$$

where $p_e = \sqrt{\dfrac{\sigma_{ii}\sigma_{jj}}{9} + \dfrac{k(1-n)\sigma_{ij}'\sigma_{ij}'}{2g}}$ is defined as equivalent stress for convenience. Other variables are similar definition with the triaxial formulation, but now in term of tensorial form. The formulation in Equation (3.29) is employed for $n \neq 1$. Whereas, the Gibbs free energy for $n = 1$ is:

$$E = -\frac{\sigma_{ii}}{3k}\left(\ln\left(\frac{\sigma_{jj}}{3p_r}\right) - 1\right) - \frac{\sigma_{ij}'\sigma_{ij}'}{4g\sigma_{kk}} - \sigma_{ij}\alpha_{ij} + \int_0^1 \left(\frac{\hat{H}_p \hat{\alpha}_{kk}^2}{2} + \frac{\hat{H}_q \hat{\alpha}_{ij}' \hat{\alpha}_{ij}'}{3}\right)d\eta \qquad (3.30)$$

$\hat{H}_p, \hat{H}_q$ [in kPa] are non-linear kinematic hardening functions in corresponding to isotropic and deviatoric hardening responses as similar expression with Equations (3.4) and (3.6), except $p_0 = \sigma_{0kk}/3$. From Equation (3.30), it follows that the strains ε_{ij} can be obtained via differentiation with stresses σ_{ij} as shown in Equation (3.31).

$$\varepsilon_{ij} = -\frac{\partial E}{\partial \sigma_{ij}} = \frac{1}{3k(1-n)}\left[\frac{\sigma_{kk}}{3p_r^{1-n}p_e^n} - 1\right]\delta_{ij} + \frac{\sigma_{ij}'}{2gp_r^{1-n}p_e^n} + \alpha_{ij} \qquad (3.31)$$

However, the Gibbs energy function expressed in Equation (3.30) with strain components derived in Equations (3.31) can only produce a constant modulus ($n = 0$) or power function of pressure dependent modulus ($0 < n < 1$). For linear pressure dependent modulus ($n = 1$) these equations will be particularly replaced by Equations (3.32) and (3.33).

$$E = -\frac{\sigma_{ii}}{3k}\left(\ln\left(\frac{\sigma_{jj}}{3p_r}\right) - 1\right) - \frac{3\sigma_{ij}'\sigma_{ij}'}{4g\sigma_{kk}} - \sigma_{ij}\alpha_{ij} + \int_0^1 \left(\frac{\hat{H}_p \hat{\alpha}_{kk}^2}{2} + \frac{\hat{H}_q \hat{\alpha}_{ij}' \hat{\alpha}_{ij}'}{3}\right)d\eta \qquad (3.32)$$

$$\varepsilon_{ij} = -\frac{\partial E}{\partial \sigma_{ij}} = \left(\frac{1}{3k}\ln\left[\frac{\sigma_{kk}}{3p_r}\right] - \frac{3\sigma_{ij}' \cdot \sigma_{ij}'}{4g\sigma_{ii}\sigma_{jj}}\right)\cdot\delta_{ij} + \frac{1}{2g}\cdot\frac{\sigma_{ij}'}{p_r^{1-n}p_e^n} + \alpha_{ij} \qquad (3.33)$$

Rate change of total strain components can be written by the following equations.

$$\{\dot{\varepsilon}_{ij}\} = \left[-\frac{\partial^2 E}{\partial \sigma_{ij}\partial \sigma_{kl}}\right]\{\dot{\sigma}_{kl}\} + \int_0^1 \left[-\frac{\partial^2 E}{\partial \sigma_{ij}\partial \hat{\alpha}_{kl}}\right]\{\dot{\hat{\alpha}}_{kl}\}d\eta \qquad (3.34)$$

The second derivatives of Gibbs free energy are derived in Box 3. This form is applicable for $0 \leq n \leq 1$.

Box 3: Second derivatives of Gibbs free energy (after Houlsby and Puzrin, 2006)

$$-\frac{\partial^2 E}{\partial \sigma_{ij} \partial \sigma_{kl}} = \frac{1}{p_a}\left(\frac{p_a}{p_0}\right)^n \left\{ \begin{bmatrix} \left[\left(\frac{1}{k} + \frac{n\sigma_{ij}'\sigma_{ij}'}{2gp_e^2}\right)\frac{\delta_{ij}\delta_{kl}}{9} - \frac{n\sigma_{mm}}{18gp_e^2}\left(\sigma_{ij}'\delta_{kl} + \delta_{ij}\sigma_{kl}'\right) + \frac{1}{2g}\left(\delta_{ik}\delta_{jl} - \frac{\delta_{kl}\delta_{ij}}{3}\right) \right] \\ -\frac{nk(1-n)}{4g^2 p_e^2}\sigma_{ij}'\sigma_{kl}' \end{bmatrix} \right\}$$

$$-\frac{\partial^2 E}{\partial \hat{\alpha}_{ij} \partial \sigma_{kl}} = \delta_{ij}\delta_{kl} = \text{identity matrix}$$

The generalised stresses $\hat{\chi}_{ij}$ are referred in Equation (3.35) as the derivatives of $\hat{E}$ with respect to $\hat{\alpha}_{ij}$.

$$\hat{\chi}_{ij} = \frac{\partial \hat{E}}{\partial \hat{\alpha}_{ij}} = \sigma_{ij} - \hat{H}_p \hat{\alpha}_{kk} \delta_{ij} - \frac{2}{3} \cdot \hat{H}_q \hat{\alpha}_{ij}' \tag{3.35}$$

Further, the yield function in term of generalised stress variables is defined:

$$\hat{y} = \sqrt{\frac{\hat{\chi}_{kk}^2}{9} + \frac{3}{2} \cdot \frac{\hat{\chi}_{ij}'\hat{\chi}_{ij}'}{M^2}} - \hat{c} = 0 \tag{3.36}$$

where $\hat{c} = \hat{H}_p \alpha_{kk} \eta$ and M is critical state parameter. Then the flow potential w can be defined in relevant to yield function $\hat{y}$ as shown in Equation (3.37).

$$w = \frac{\langle \hat{y} \rangle^2}{2\mu} = \frac{\left\langle \sqrt{\frac{\hat{\chi}_{kk}^2}{9} + \frac{3}{2} \cdot \frac{\hat{\chi}_{ij}'\hat{\chi}_{ij}'}{M^2}} - \hat{c} \right\rangle^2}{2\mu} \tag{3.37}$$

Finally, the rate form of stress-strain relationship can be expressed.

$$\left[-\frac{\partial^2 E}{\partial \sigma_{ij} \partial \sigma_{kl}}\right] \cdot \{\dot{\sigma}_{kl}\} = \{\dot{\varepsilon}_{ij}\} - \int_0^1 \left[-\frac{\partial^2 E}{\partial \sigma_{ij} \partial \hat{\alpha}_{kl}}\right] \cdot \left\{\frac{\partial w}{\partial \hat{\chi}_{ij}}\right\} d\eta \tag{3.38}$$

The derivative of flow potential w in Equation (3.37) is shown in Equation (3.39).

$$\frac{\partial w}{\partial \hat{\chi}_{ij}} = \frac{\left\langle \sqrt{\frac{\hat{\chi}_{kk}^2}{9} + \frac{3}{2} \cdot \frac{\hat{\chi}_{ij}'\hat{\chi}_{ij}'}{M^2}} - \hat{H}_p \alpha_{kk} \eta \right\rangle}{\mu} \cdot \frac{\frac{2}{9}\hat{\chi}_{kk}\delta_{ij} + \frac{3}{M^2}\hat{\chi}_{ij}'}{2 \cdot \sqrt{\frac{\hat{\chi}_{kk}^2}{9} + \frac{3}{2} \cdot \frac{\hat{\chi}_{ij}'\hat{\chi}_{ij}'}{M^2}}} \tag{3.39}$$

3.2.4 Model Parameter Determination

The non-linear KHMCC model has five parameters, which is composed of three dimensionless material constant parameters (g, k, and n), one parameter for critical state (M), and the last one for kinematic hardening parameter (a). These parameters are obtained through processes of parameter calibration from the experiment results. The dimensionless material constant g, k, and n are related to elastic stiffness which can be determined from experimental measurement of small-strain stiffness such as bender element test or for preliminary analysis can be determined from empirical equation as summarised in Table 3.1. These elastic stiffness parameters should be determined at the initial loading stage in order to minimize the effect from hardening responses. Critical state frictional parameter M is determined at the stage of failure condition. It can be approximated by relationship with internal friction angle ϕ in Equation (3.40).

$$M = \frac{6\sin\phi}{3-\sin\phi} \qquad (3.40)$$

Table 3.1 Small-strain stiffness empirical equations $G = AF(e)(p)^n$ (After Soga and Yimsiri, 2001)

Soil type	A	$F(e)$	n	Void ratio e	Test method	references
Reconstituted NC kaolin	3,270	$\dfrac{(2.973-e)^2}{1+e}$	0.5	0.5-1.5	Resonant Column	Hardin and Black (1968)
Several undisturbed NC clays	3,270	$\dfrac{(2.973-e)^2}{1+e}$	0.5	0.5-1.7	Resonant Column	Hardin and Black (1968)
Several undisturbed silts and clays	1,726	$\dfrac{(2.973-e)^2}{1+e}$	0.46-0.61	0.4-1.1	Resonant Column	Kim and Novak (1981)
Undisturbed NC clays	90	$\dfrac{(7.32-e)^2}{1+e}$	0.6	1.7-3.8	Cyclic Triaxial	Kokusho et al. (1982)
Undisturbed Italians clays	4,400-8,100	e^{-x} $(x = 1.11-1.43)$	0.4-0.58	0.6-1.8	Resonant Column and Bender Element	Jamiolkowsky et al. (1995)

Once parameters which relate to elastic responses and failure conditions are determined, the kinematic hardening parameter is calibrated. In this study, the scope of application is restricted to isotropic consolidated materials. Therefore, the initial stiffness after the completion of isotropic consolidation is calibrated. To match with this condition, stress-

strain responses during isotropic loading is imposed to Equation (3.19) so that moduli expression of G and K can be obtained while $J = 0$. It can be shown that the initial stiffness G and K after completion of isotropic consolidation are given by:

$$G(p, q = 0) = gp^n p_r^{1-n} \tag{3.41}$$

$$K(p, q = 0) = kp^n p_r^{1-n} \tag{3.42}$$

According to Equations (3.41) and (3.42), it is found that during isotropic consolidation, the ratio of K/G is constant regardless of consolidation pressure. Therefore, Poisson's ratio v for isotropic materials can be conveniently obtained by Equation (3.44).

$$\frac{K(p, q = 0)}{G(p, q = 0)} = \frac{-\dfrac{\partial^2 E}{\partial q^2}\bigg|}{-\dfrac{\partial^2 E}{\partial p^2}\bigg|_{q=0}} = \frac{k}{g} \tag{3.43}$$

$$\frac{K}{G} = \frac{k}{g} = \frac{2(1+v)}{3(1-2v)} \tag{3.44}$$

From the experimental observations using bender element test, the elastic modulus at small-strain is generally expressed as a power function of the mean effective stresses such as in the following forms for isotropically consolidated samples (Tanizawa et. al. (1994), Kohata et. al. (1997), Pennington et. al. (1997), Techavorasinskun et. al. (2002)):

$$G = Cp^n \tag{3.45}$$

where C and n are constants. This equation is identical with Equation (3.41) which is derived from constitutive model. This equation can be normalised into the form suggested by Houlsby et al. (2005) is shown in Equation (3.46), to obtain the dimensionless material constant g and n. Another dimensional material constant k can be determined using the elastic relationship as presented in Equation (3.44). Value of poisson ratio v is ranged in a certain limit and can be related to the coefficient of earth pressure at-rest K_0 as shown in Equation (3.47).

$$\frac{G}{p_r} = g\left(\frac{p}{p_r}\right)^n \tag{3.46}$$

$$v = \frac{K_0}{1 + K_0} \tag{3.47}$$

According to Houlsby and Puzrin (2006), the kinematic hardening parameter a is calibrated to fit the stress-strain curve for specific test data (such as triaxial undrained

or drained tests) as shown in Figure 3.2 for an example This parameter characterises first loading curve (also referred by many as backbone curve) of the stress-strain response with hyperbolic curve . Followings are general step by step procedures to determine parameter *a*:

(1) Normalise undrained or drained stress at vertical axis by undrained or drained strength *c*.

(2) Multiply the strain response at horizontal axis by appropriate initial stiffness and divided by *c*.

(3) Find *a* as inversion slope (1/secant stiffness) of a point at 50% of normalised stress.

However, procedures (1)-(3) are applicable if the laboratory stress-strain curve can be approached with a simple hyperbolic stress-strain curve. In many practical scenarios, kinematic hardening parameter a can be directly obtained from a small parametric study to match the stress-strain curve of specific test as shown in Figure 3.3.
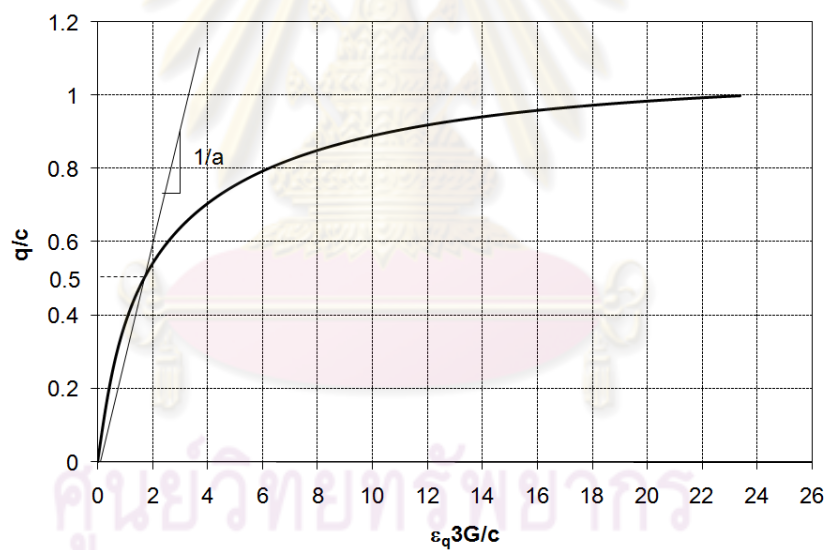
Figure 3.2 Determination of parameter *a* using procedures (1)-(3)
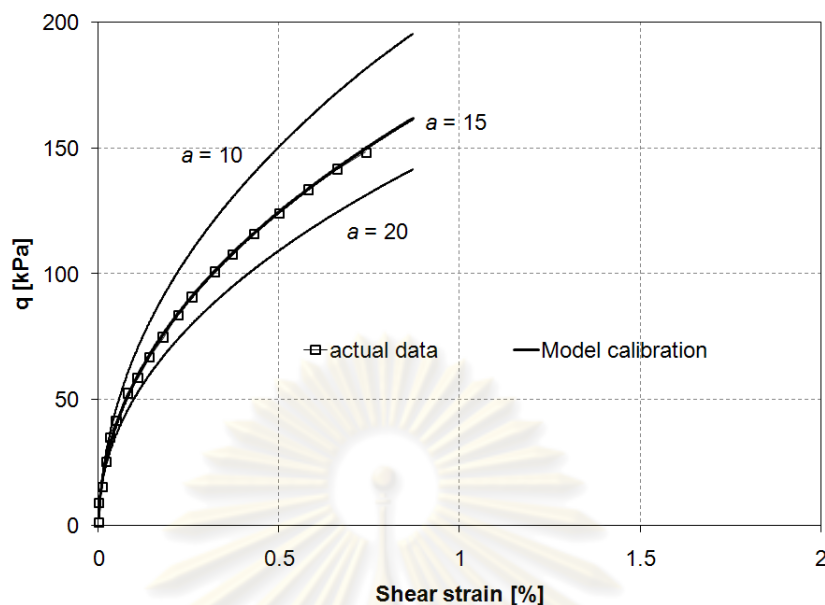
Figure 3.3 Determination of parameter *a* using small parametric study

3.3   Numerical Implementation

3.3.1   Incremental Stress-Strain Response

From the previous formulation, rate form of the stress-strain relationship based on the continuous hyperplasticity is described. However, the continuous hyperplasticity is suitable for stiff calculation with simple hardening function. Due to this limitation to handle complicated loading conditions, the multisurface hyperplasticity is generally employed in numerical implementation. Non-linearity is expressed by multiple piece-wise responses (see also Mroz & Norris, 1982). Therefore, multiple internal variables play a role as discrete memories of materials and the smooth transition between piece-wise responses depends on the finite number of internal variables. For KHMCC model, continuous yield surface is discretised to a finite number of yield surfaces (Likitlersuang (2003), Likitlersuang and Houlsby (2006)). Integration operator simply turns to summation operator without losing general meaning. Each yield surfaces have their own state variables which are generalised stresses and yield stress. A finite number of yield stress can be considered as multiple material memories which are updated when the multiple yield surfaces are active. The illustration of multiple yield surfaces in principal stress space can be depicted in Figure 3.4.

In this study, 10 number of multiple yield functions are demonstrated. Plot of 10 number of yield surfaces in p-q plane under generalised stress space and true stress space are envisaged in Figure 3.5 and Figure 3.6, respectively. The rate-dependent incremental response of a single element calculation is obtained by integrating the

incremental stress-strain relation using strain driven forward-Euler integration scheme. This means an increment of variable based on rate form $\dot{x} = f(x)$ can be typically written in the manner $x_{i+1} - x_i = f(x_i)\Delta t$ where $\Delta t = t_{i+1} - t_i$ and $i+1$ represents the current step number. Equation (3.28) combined with (3.27) are used to update stress components in any increment of strain, and then it can be used to update the generalised stress components by Equations (3.23) and (3.24) after internal variable is updated from the evolution rule given by Equations (3.25) and (3.26). The algorithms of the rate-dependent numerical implementation in triaxial and general stress are explained in Box 3 and Box 4. The subscript m and t are a positive integer representing the index of the yield surfaces and incremental of specific variables, respectively. A parentheses ( ) enclosed a subscript index is used to distinguish between tensor expression index. For an arbitrary variable tensor •, component of tensor in according to the yield surface-m^{th} at increment-i^{th} is represented by $\bullet_{ij(m,t)}$, where N is a number of yield surfaces.
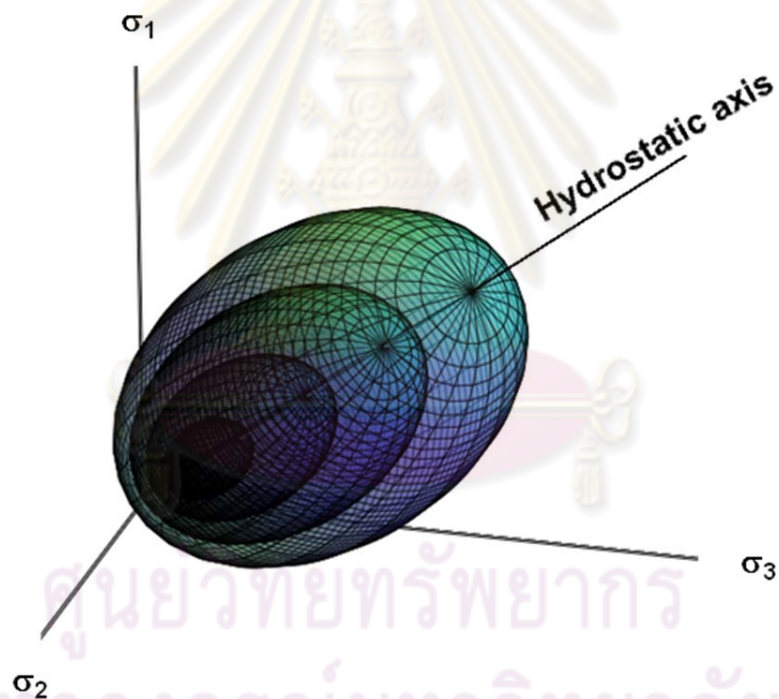
Figure 3.4 Non-linear KHMCC yield surfaces in three-dimensional stress space.
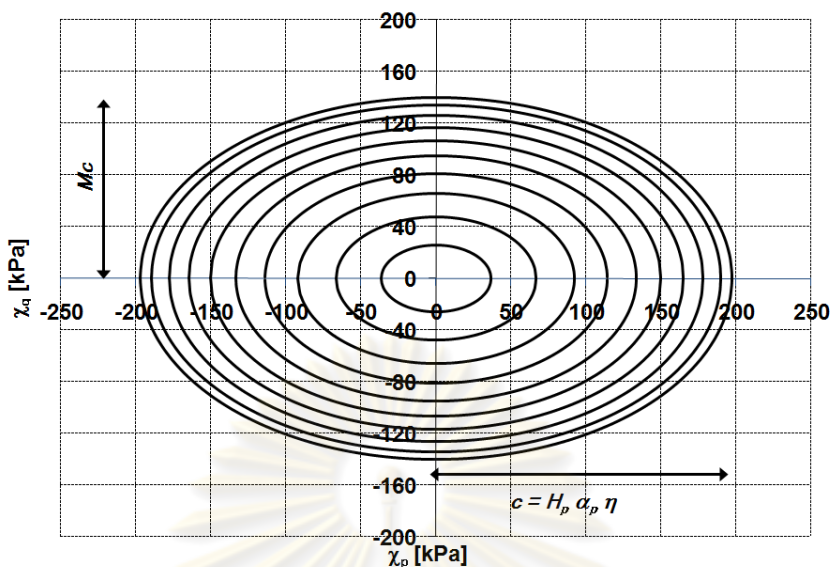
Figure 3.5 Non-linear KHMCC yield surfaces in the generalised stress.

It is noted that when rate-independence is described as the particular case of rate-dependent behaviour, significant simplifications in calculations can be achieved. A significant advantage of the rate-dependent calculation is that, it is not necessary to attach with the consistency condition during the calculation of plastic strains. Therefore, the higher complexity of numerical calculation such as special procedure for error controlling is not required like that of the rate-independent (see Houlsby and Puzrin, 2006).
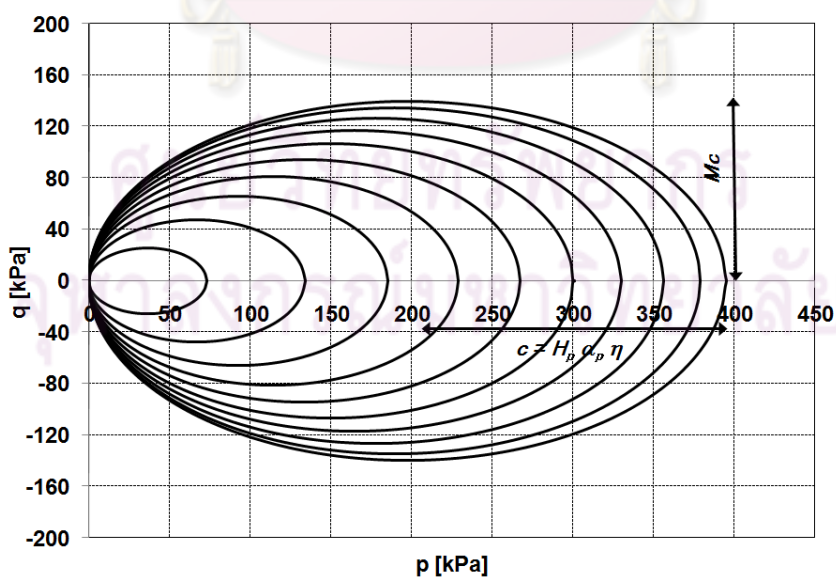
Figure 3.6 Non-linear KHMCC yield surfaces in the true stress.

Box 3: Strain-driven forward-Euler integration scheme (Triaxial stress)

For given Gibbs free-energy E, $\dot{\varepsilon}_p$, $\dot{\varepsilon}_q$, Δt, $\varepsilon_{p(i)}$, $\varepsilon_{q(i)}$, $p_{(i)}$, $q_{(i)}$, $\alpha_{p(m,i)}$, $\alpha_{q(m,i)}$,

for $m \in \{1,2,..,N\}$

1. Initialise

$$\varepsilon_{p(i+1)} = \varepsilon_{p(i)} + \dot{\varepsilon}_p \, \Delta t \, , \; \varepsilon_{q(i+1)} = \varepsilon_{q(i)} + \dot{\varepsilon}_q \, \Delta t \, , \; \alpha_{p(i)} = \sum_{n=1}^{N} \alpha_{p(n,i)} \, , \; \alpha_{q(i)} = \sum_{n=1}^{N} \alpha_{q(n,i)}$$

for $m \in \{1,2,..,N\}$

$$\chi_{p(m,i)} = p_{(i)} - H_{p(m,i)}\alpha_{p(m,i)} \, , \; \chi_{q(m,i)} = q_{(i)} - H_{q(m,i)}\alpha_{q(m,i)}$$

$$c_{(m,i)} = H_{p(m,i)}\alpha_{p(m,i)} \, , \; y_{(m,i)} = \sqrt{\chi^2_{p(m,i)} + \chi^2_{q(m,i)} / M^2} - c_{(m,i)} \, , \; \mu = 1$$

$$w_{(m,i)} = \frac{\left\langle y_{(m,i)} \right\rangle^2}{2\mu}$$

2. Determine plastic parameters

for $m \in \{1,2,..,N\}$

if $y_{(m,i)} \leq 0$ then $\dot{\alpha}_{p(m,i)} = 0$ and $\dot{\alpha}_{q(m,i)} = 0$

else $\dot{\alpha}_{p(m,i)} = \dfrac{\partial w_{(m,i)}}{\partial \chi_{p(m,i)}}$, $\dot{\alpha}_{q(m,i)} = \dfrac{\partial w_{(m,i)}}{\partial \chi_{q(m,i)}}$

3. Compute incremental variables

$$\begin{bmatrix} \Delta p \\ \Delta q \end{bmatrix} = \begin{bmatrix} -\dfrac{\partial^2 E}{\partial p^2} & -\dfrac{\partial^2 E}{\partial q \partial p} \\ -\dfrac{\partial^2 E}{\partial q \partial p} & -\dfrac{\partial^2 E}{\partial q^2} \end{bmatrix}^{-1} \left[\begin{Bmatrix} \dot{\varepsilon}_p \\ \dot{\varepsilon}_q \end{Bmatrix} - \frac{1}{N}\sum_{m=1}^{N} \left(\begin{bmatrix} -\dfrac{\partial^2 E}{\partial \alpha_p \partial p} & -\dfrac{\partial^2 E}{\partial \alpha_q \partial p} \\ -\dfrac{\partial^2 E}{\partial \alpha_p \partial q} & -\dfrac{\partial^2 E}{\partial \alpha_q \partial q} \end{bmatrix} \begin{bmatrix} \dot{\alpha}_{p(m,i)} \\ \dot{\alpha}_{q(m,i)} \end{bmatrix} \right) \right] \Delta t$$

4. Update state variables

$p_{(i+1)} = p_{(i)} + \Delta p$, $q_{(i+1)} = q_{(i)} + \Delta q$

for $m \in \{1,2,..,N\}$

$$\alpha_{p(m,i+1)} = \alpha_{p(m,i)} + \dot{\alpha}_{p(m,i)}\Delta t \, , \; \alpha_{q(m,i+1)} = \alpha_{q(m,i)} + \dot{\alpha}_{q(m,i)}\Delta t$$

$$\chi_{p(m,i+1)} = p_{(i+1)} - H_{p(m,i+1)}\alpha_{p(m,i+1)} \, , \; \chi_{q(m,i+1)} = q_{(i+1)} - H_{q(m,i+1)}\alpha_{q(m,i+1)}$$

5. Go to next incremental step

Box 4: Strain-driven forward-Euler integration scheme (General stress)

For given Gibbs free-energy E, $\dot{\varepsilon}_{ij}$, Δt, $\varepsilon_{ij(t)}$, $\sigma_{ij(t)}$, $\alpha_{ij(t)}^{(m)}$

for $m \in \{1,2,..,N\}$

1. Initialise

$$\varepsilon_{ij(t+1)} = \varepsilon_{ij(t)} + \dot{\varepsilon}_{ij}\,\Delta t \;,\; \alpha_{ij(t)} = \sum_{n=1}^{N} \alpha_{ij(n,t)}$$

for $m \in \{1,2,..,N\}$

$$\chi_{ij(m,t)} = \sigma_{ij(t)} - H_{p(m,t)}\alpha_{kk(m,t)}\delta_{ij} - \frac{2}{3}H_{q(m,t)}\alpha'_{ij(m,t)}$$

$$c_{(m,t)} = H_{p(m,t)}\alpha_{kk(m,t)}\;,\; y_{(m,t)} = \sqrt{\frac{\chi_{kk(m,t)}^2}{9} + \frac{3}{2}\frac{\chi'_{ij(m,t)}\chi'_{ij(m,t)}}{M^2}} - c_{(m,t)} = 0\;,\; \mu = 1$$

$$w_{(m,t)} = \frac{\langle y_{(m,t)} \rangle^2}{2\mu}$$

2. Determine plastic parameters

for $m \in \{1,2,..,N\}$

if $y_{(m,t)} \leq 0$ then $\dot{\alpha}_{ij(m,t)} = 0$

else $\dot{\alpha}_{ij(m,t)} = \dfrac{\partial w_{(m,t)}}{\partial \chi_{ij(m,t)}}$

3. Compute incremental variables

$$\Delta\sigma_{kl} = \left[\frac{\partial^2 E}{\partial\sigma_{ij}\partial\sigma_{kl}}\right]^{-1}\left[\dot{\varepsilon}_{ij} - \frac{1}{N}\sum_{m=1}^{N}\left(\left[-\frac{\partial^2 E}{\partial\alpha_{kl(m,t)}\partial\sigma_{ij}}\right]\dot{\alpha}_{ij(m,t)}\right)\right]\Delta t$$

4. Update state variables

$$\sigma_{ij(t+1)} = \sigma_{ij(t)} + \Delta\sigma_{ij}$$

for $m \in \{1,2,..,N\}$

$$\alpha_{ij(m,t+1)} = \alpha_{ij(m,t)} + \dot{\alpha}_{ij(m,t)}\Delta t$$

$$\chi_{ij(m,t+1)} = \sigma_{ij(t+1)} - H_{p(m,t+1)}\alpha_{kk(m,t+1)}\delta_{ij} - \frac{2}{3}H_{q(m,t+1)}\alpha_{ij(m,t+1)}$$

5. Go to next incremental step

3.3.2 *Numerical Integration of Hardening Function*

In equation (3.1) or (3.10), Gibbs free energy is completely described with the integration of hardening function $\hat{H}$ and kinematic hardening variables $\hat{\alpha}$ in terms of internal coordinate η. For instance, a hyperbolic function $f(\eta)$ expressed in Equation (3.48) is supposed to integrate numerically. The numerical integration techniques can be employed and verified by the closed-form solution. The definite integration of $f(\eta)$ can be algebraically obtained by F_1 as shown in Equation (3.49).

$$f(\eta) = \hat{H}/\hat{H}_i = (1-\eta)^3 \tag{3.48}$$

$$F_1 = \int_o^1 f(\eta)\,d\eta = -\frac{1}{4}(1-\eta)^4 \Big|_0^1 = \frac{1}{4} \tag{3.49}$$

Various quadrature rules emanated from the method of differential slices are employed in this study. As shown in Equation (3.50), three general integrators which are equivalent to forward-quadrature F_2 , backward-quadrature F_3 and midpoint quadrature F_4 are expressed. The continuous function of $f(\eta)$ is discretised to N slices with equal width $1/N$ where N is number of yield surfaces. Therefore, integration of $f(\eta)$ is the area summation of each slices. It can be seen that η is replaced by i/N in F_2, $(i-1)/N$ in F_3 and $(i-0.5)/N$ in F_4 where i is i-th active yield surface. To obtain zero hardening response from the last N-th yield surface, F_2 should be the best candidate because $f\left(\dfrac{i}{N}\right) = 0$ when $i = N$. However, it causes the singularity problem due to division by zero at initialisation of internal state variables (yield surface location) like $\hat{\alpha}_p = p_0/\hat{H}_p$.

$$F_2 = \frac{1}{N}\sum_{i=1}^{N} f\left(\frac{i}{N}\right), \; F_3 = \frac{1}{N}\sum_{i=1}^{N} f\left(\frac{i-1}{N}\right), \; F_4 = \frac{1}{N}\sum_{i=1}^{N} f\left(\frac{i-0.5}{N}\right) \tag{3.50}$$
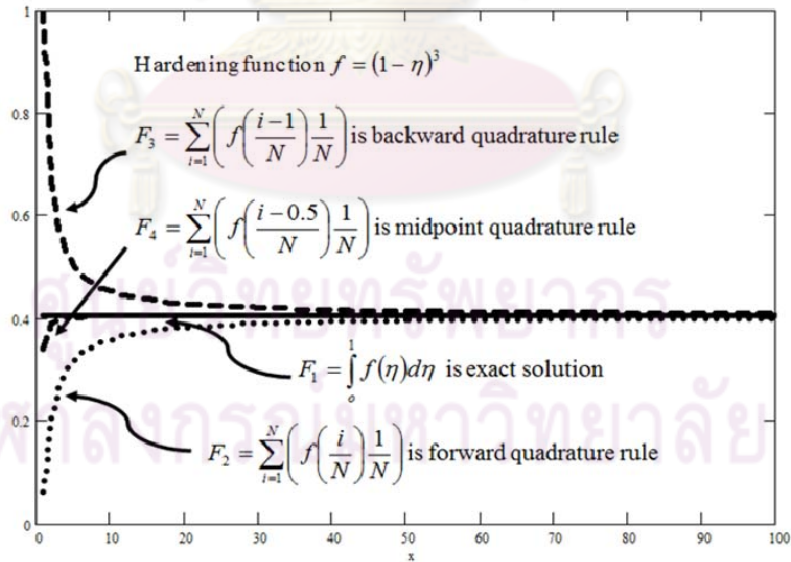
Figure 3.7 Numerical study result of some integration schemes.

To prevent this singularity problem, then the hyperbolic function $f(\eta)$ expressed in Equation (3.48) is modified in to $f(\eta) = \hat{H}/\hat{H}_i = (1-r\eta)^3$ where r is ranged between 0 and 1. Equation (3.48) can be numerically integrated without singularity problem by

using F_3 and F_4 though zero hardening response from the last N-th yield surface cannot be exactly attained. Furthermore, a numerical study is performed in according to investigate the computational effect of these integration rules. Figure 3.7 shows that F_4 need less number of yield surfaces N compared to F_2 and F_3 in according to obtain the definite integration of hardening function (marked by solid line).

Figure 3.8 shows the stress-strain response using F_2, F_3, and F_4 for several N number of yield surfaces. It also shows that F_4 need less number of yield surfaces N compared to F_2 in according to integrate the specified hardening functions in this model.
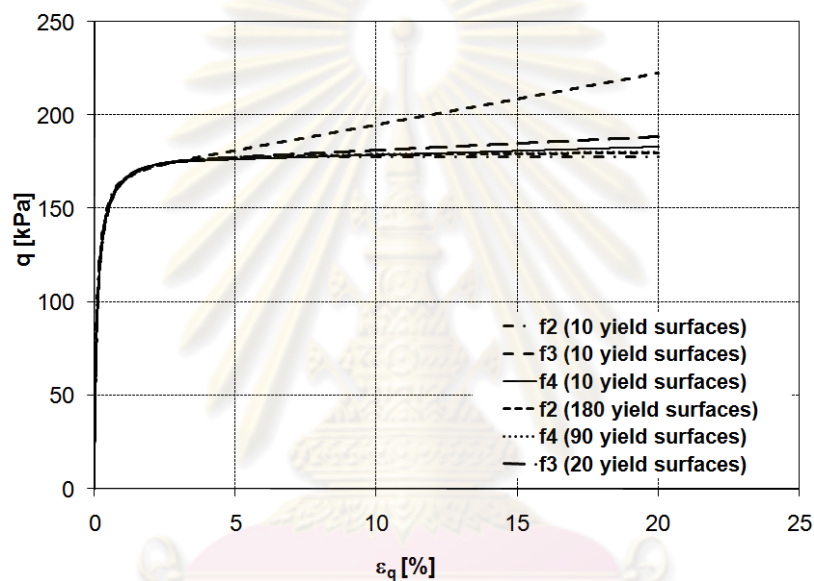
Figure 3.8 Comparison of several numerical integration schemes.

3.3.3 Effect of Time Step and Number of Yield Surfaces

Effect of time step on the accuracy and numerical stability of pseudo rate-dependent algorithm have been reported by several researchers (Cormeau, 1975; Potts, 2003). In these cases, the rate-dependent algorithm was implemented on elasto-perfectly plastic and isotropic hardening model. Due to the limitations, pseudo rate-dependent algorithm approaches a rate-independent calculation by assuming a sufficient small value of time step and pseudo viscosity coefficient (μ). However, the advantage of rate-dependent algorithm is that these parameters have actual physical meaning and it can be directly used for modelling real time response in soil mechanics.

On the implementation of the hyperplasticity non-linear KHMCC with multiple kinematic hardening surfaces, this effect also apparent as shown in Figure 3.9 and 3.10,

with constant number of yield surfaces *N* and different time steps *dt*. It can be concluded that the numerical stability is affected by increasing time step.
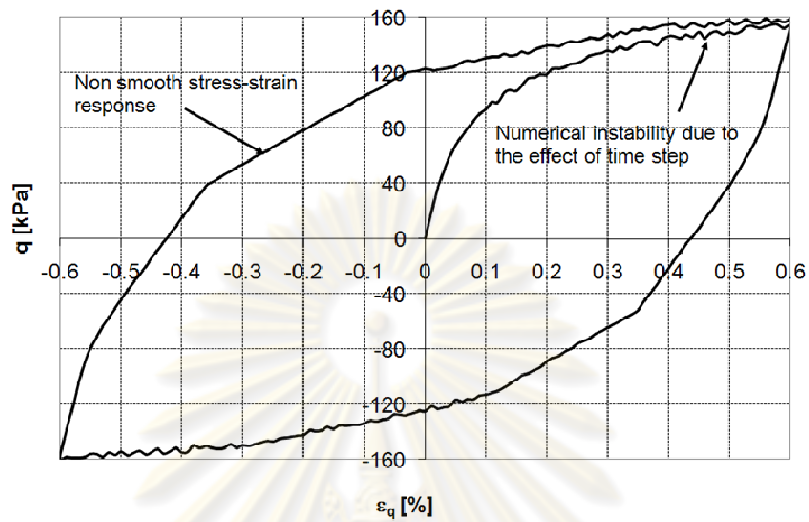
Figure 3.9 Effect of time step and number of yield surfaces with
$dt = 1 \times 10^{-5}$, $\mu = 1$ and $N = 5$.
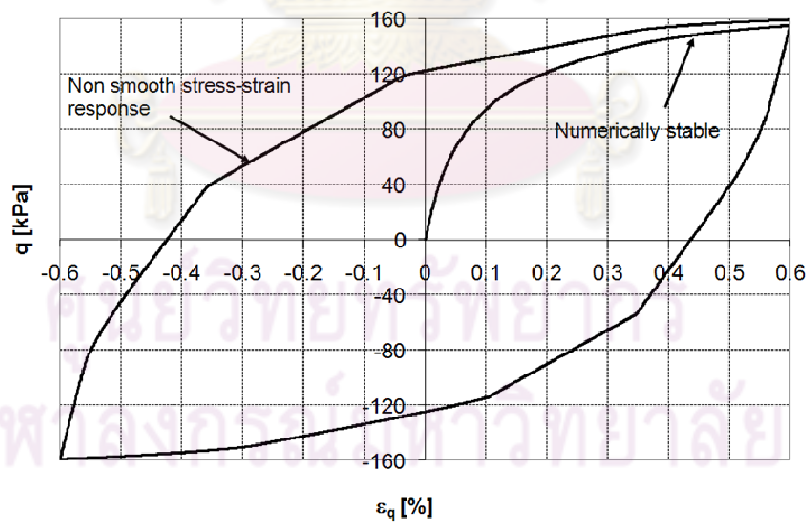
Figure 3.10 Effect of time step and number of yield surfaces with
$dt = 1 \times 10^{-6}$, $\mu = 1$ and $N = 5$.
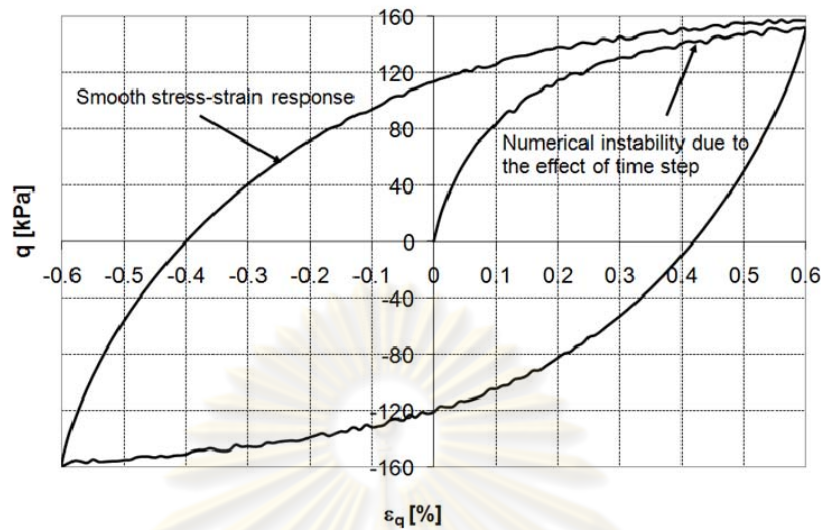
Figure 3.11 Effect of time step and number of yield surfaces with
$dt = 1 \times 10^{-5}$, $\mu = 1$ and $N = 50$.
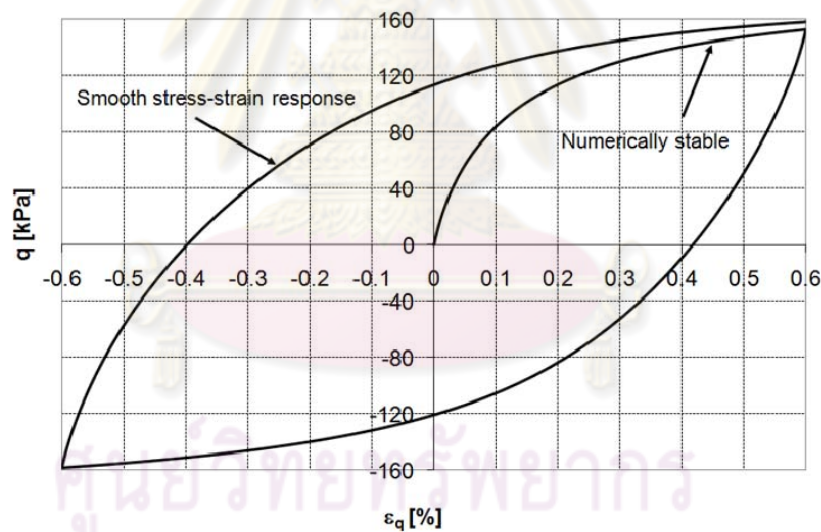
Figure 3.12 Effect of time step and number of yield surfaces with
$dt = 1 \times 10^{-6}$, $\mu = 1$ and $N = 50$.

It is observed that the stress-strain response smoother when the number of yield surfaces is increased as shown in Figures 3.11 and 3.12. Figure 3.13 shows more clearly effect of number of yield surfaces to the stress-strain characteristic. Figure 3.14 indicates that calculation running time increases linearly against increasing number of yield surfaces. This simple computation was running by Intel®Core™ 2 T7250 2.0 GHz. However, as faster computers become available, the computation time will be significantly reduced.
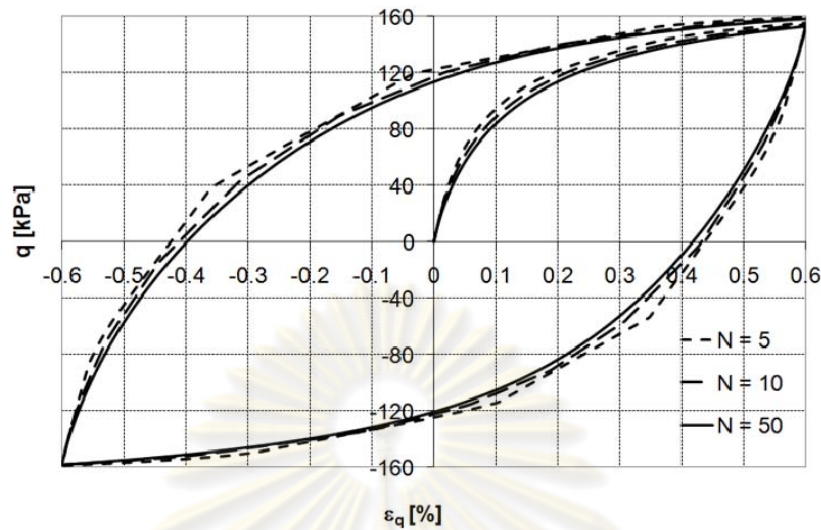
Figure 3.13 Demonstration with different number of yield surfaces.
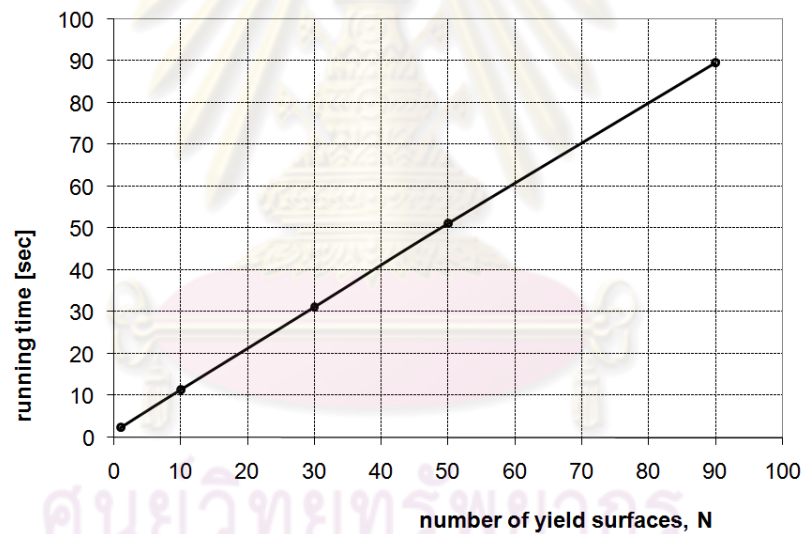
Figure 3.14 Plot of running time against *N*.

3.3.4 General Stress-Strain Implementation

For general stress and strain, as a result of moment equilibrium demands there are still six independent stress components: three normal stresses (σ_{xx}, σ_{yy}, σ_{zz}) and three shear stresses (τ_{xy}, τ_{yz}, τ_{zx}), are called the components of the stress tensor σ_{ij} as shown in Equation (3.51) .

$$\sigma_{ij} = \begin{bmatrix} \sigma_{11} & \sigma_{12} & \sigma_{13} \\ \sigma_{21} & \sigma_{22} & \sigma_{23} \\ \sigma_{31} & \sigma_{32} & \sigma_{33} \end{bmatrix} = \begin{bmatrix} \sigma_x & \tau_{xy} & \tau_{xz} \\ \tau_{yx} & \sigma_y & \tau_{yz} \\ \tau_{zx} & \tau_{zy} & \sigma_z \end{bmatrix} \tag{3.51}$$

Based on Equation (3.38), it can be shown that the incremental of stress-strain relationships of rate dependent strain-driven forward-Euler integration scheme in general stress is:

$$\begin{bmatrix} C_{1111} & C_{1122} & C_{1133} & C_{1112} & C_{1123} & C_{1131} \\ C_{2211} & C_{2222} & C_{2233} & C_{2212} & C_{2223} & C_{2231} \\ C_{3311} & C_{3322} & C_{3333} & C_{3312} & C_{3323} & C_{3331} \\ C_{1211} & C_{1222} & C_{1233} & C_{1212} & C_{1223} & C_{1231} \\ C_{2311} & C_{2322} & C_{2333} & C_{2312} & C_{2323} & C_{2331} \\ C_{3111} & C_{3122} & C_{3133} & C_{3112} & C_{3123} & C_{3131} \end{bmatrix} \begin{Bmatrix} \Delta\sigma_{11} \\ \Delta\sigma_{22} \\ \Delta\sigma_{33} \\ \Delta\tau_{12} \\ \Delta\tau_{23} \\ \Delta\tau_{31} \end{Bmatrix} = \left(\begin{Bmatrix} \Delta\varepsilon_{11} \\ \Delta\varepsilon_{22} \\ \Delta\varepsilon_{33} \\ \Delta\gamma_{12} \\ \Delta\gamma_{23} \\ \Delta\gamma_{31} \end{Bmatrix} - \frac{1}{N}\sum_{m=1}^{N} \begin{bmatrix} 1 & 0 & 0 & 0 & 0 & 0 \\ 0 & 1 & 0 & 0 & 0 & 0 \\ 0 & 0 & 1 & 0 & 0 & 0 \\ 0 & 0 & 0 & 1 & 0 & 0 \\ 0 & 0 & 0 & 0 & 1 & 0 \\ 0 & 0 & 0 & 0 & 0 & 1 \end{bmatrix} \begin{Bmatrix} \dot{\alpha}_{11(m,t)} \\ \dot{\alpha}_{22(m,t)} \\ \dot{\alpha}_{33(m,t)} \\ \dot{\alpha}_{12(m,t)} \\ \dot{\alpha}_{23(m,t)} \\ \dot{\alpha}_{31(m,t)} \end{Bmatrix} \right) \Delta t$$

$$(3.52)$$

In the Equation (3.52), the evolution rule of kinematic internal variable functions tensor $\hat{\alpha}_{ij}$ is determined using Equation (3.39). However, for computer programming purposes, the component of tangent compliance matrix C_{ijkl} in Equation (3.52) can be easier determined when we re-write the tangent compliance matrix in Box 1 (second derivatives of Gibbs free energy in respect to stresses) in expanded form as shown in Box 3.

Box 3: Tangent compliance matrix in expanded form for general stress implementation

$$C_{ijkl} = \begin{cases} \frac{1}{p_r}\left(\frac{p_r}{p_e}\right)^n \left\{ \left(\frac{1}{k} + \frac{n\sigma'_{ij}\sigma'_{ij}}{2gp_e^2}\right)\frac{1}{9} - \frac{np\sigma'_{ij}}{3gp_e^2} + \frac{1}{3g} - \frac{nk(1-n)}{4g^2p_e^2}\sigma'_{ij}\sigma'_{ij} \right\}, & i=j=k=l \in \{1,2,3\} \\[4mm] \frac{1}{p_r}\left(\frac{p_r}{p_e}\right)^n \left\{ \left(\frac{1}{k} + \frac{n\sigma'_{ij}\sigma'_{ij}}{2gp_e^2}\right)\frac{1}{9} - \frac{np\left(\sigma'_{ij}+\sigma'_{kl}\right)}{6gp_e^2} - \frac{1}{6g} - \frac{nk(1-n)}{4g^2p_e^2}\sigma'_{ij}\sigma'_{kl} \right\}, & i=j \neq k=l \in \{1,2,3\} \\[4mm] \frac{1}{p_r}\left(\frac{p_r}{p_e}\right)^n \left\{ -\frac{np\left(\sigma'_{ij}+\sigma'_{kl}\right)}{6gp_e^2} - \frac{nk(1-n)}{4g^2p_e^2}\sigma'_{ij}\sigma'_{kl} \right\}, & i \neq j \text{ xor } k \neq l \in \{1,2,3\} \\[4mm] \frac{1}{p_r}\left(\frac{p_r}{p_e}\right)^n \left\{ \frac{1}{g} - \frac{nk(1-n)}{4g^2p_e^2}\sigma'_{ij}\sigma'_{kl} \right\}, & i \neq j \text{ and } k \neq l \in \{1,2,3\} \end{cases}$$

where

$$p_e^2 = \frac{\sigma_{ii}\sigma_{jj}}{9} + \frac{k(1-n)\sigma'_{ij}\sigma'_{ij}}{2g} = p^2 + \frac{k(1-n)\sigma'_{ij}\sigma'_{ij}}{2g}$$

note :

• $i=j=k=l \in \{1,2,3\} \Rightarrow C_{1111}, C_{2222}, C_{3333}$

• $i=j \neq k=l \in \{1,2,3\} \Rightarrow C_{1122}, C_{1133}, C_{2211}, C_{2233}, C_{3311}, C_{3322}$

• $i \neq j$ xor $k \neq l \in \{1,2,3\} \Rightarrow C_{1211}, C_{1222}, C_{1233}, C_{1112}, C_{2212}, C_{3312}, C_{2311}, C_{2322}, C_{2333}, C_{1123}, C_{2223}, C_{3323}, C_{3111},$
$\qquad\qquad C_{3122}, C_{3133}, C_{1131}, C_{2231}, C_{3331}$

• $i \neq j$ and $k \neq l \in \{1,2,3\} \Rightarrow C_{1212}, C_{1223}, C_{1231}, C_{2312}, C_{3112}, C_{2323}, C_{2331}, C_{3123}, C_{3131}$

3.3.5 Two -dimensional stress-strain implementation

In two-dimensional case, there are usually four stresses tensor component involved: three normal stresses (σ_{xx}, σ_{yy}, σ_{zz}) and one shear stress (τ_{xy}) as shown in Equation (3.53).

$$\sigma_{ij} = \begin{bmatrix} \sigma_{11} & \sigma_{12} & 0 \\ \sigma_{21} & \sigma_{22} & 0 \\ 0 & 0 & \sigma_{33} \end{bmatrix} = \begin{bmatrix} \sigma_x & \tau_{xy} & 0 \\ \tau_{yx} & \sigma_y & 0 \\ 0 & 0 & \sigma_z \end{bmatrix} \tag{3.53}$$

Then, the incremental of stress-strain relationships of rate dependent strain-driven forward-Euler integration scheme in Equation (3.52) can simply defined as shown in Equation (3.54).

$$\begin{bmatrix} C_{1111} & C_{1122} & C_{1133} & C_{1112} \\ C_{2211} & C_{2222} & C_{2233} & C_{2212} \\ C_{3311} & C_{3322} & C_{3333} & C_{3312} \\ C_{1211} & C_{1222} & C_{1233} & C_{1212} \end{bmatrix} \begin{Bmatrix} \Delta\sigma_{11} \\ \Delta\sigma_{22} \\ \Delta\sigma_{33} \\ \Delta\tau_{12} \end{Bmatrix} = \begin{Bmatrix} \Delta\varepsilon_{11} \\ \Delta\varepsilon_{22} \\ \Delta\varepsilon_{33} \\ \Delta\gamma_{12} \end{Bmatrix} - \frac{1}{N}\sum_{m=1}^{N} \left(\begin{bmatrix} 1 & 0 & 0 & 0 \\ 0 & 1 & 0 & 0 \\ 0 & 0 & 1 & 0 \\ 0 & 0 & 0 & 1 \end{bmatrix} \begin{Bmatrix} \dot{\alpha}_{11(m,t)} \\ \dot{\alpha}_{22(m,t)} \\ \dot{\alpha}_{33(m,t)} \\ \dot{\alpha}_{12(m,t)} \end{Bmatrix} \right) \Delta t$$

$$\tag{3.54}$$

The component of tangent compliance matrix C_{ijkl} and the in Equation (3.54) can be also easier determined using expanded form in Box 3. Also, the evolution rule of kinematic internal variable functions tensor $\alpha_{ij(m,t)}$ is determined using Equation (3.39).

For computer programming purposes, it can be simpler if we define index notation $\sigma_1, \sigma_2, \sigma_3, \sigma_4$ are equivalent to $\sigma_{11}, \sigma_{22}, \sigma_{33}, \sigma_{12}$ and $\varepsilon_1, \varepsilon_2, \varepsilon_3, \varepsilon_4$ are equivalent to $\varepsilon_{11}, \varepsilon_{22}, \varepsilon_{33}, 2\varepsilon_{12}$. Similar definition also applied for $\chi_1, \chi_2, \chi_3, \chi_4$ which are equivalent to $\chi_{11}, \chi_{22}, \chi_{33}, \chi_{12}$ and $\alpha_1, \alpha_2, \alpha_3, \alpha_4$ are equivalent to $\alpha_{11}, \alpha_{22}, \alpha_{33}, 2\alpha_{12}$. The Gibbs free energy and yield function can be re-written as shown in Box 4. Then, the incremental stress-strain relationships in Equation (3.54) can be re-written as in the following:

$$\begin{bmatrix} C_{11} & C_{12} & C_{13} & C_{14} \\ C_{21} & C_{22} & C_{23} & C_{24} \\ C_{31} & C_{32} & C_{33} & C_{34} \\ C_{41} & C_{42} & C_{43} & C_{44} \end{bmatrix} \begin{Bmatrix} \Delta\sigma_1 \\ \Delta\sigma_2 \\ \Delta\sigma_3 \\ \Delta\sigma_4 \end{Bmatrix} = \begin{Bmatrix} \Delta\varepsilon_1 \\ \Delta\varepsilon_2 \\ \Delta\varepsilon_3 \\ \Delta\varepsilon_4 \end{Bmatrix} - \frac{1}{N}\sum_{m=1}^{N} \left(\begin{bmatrix} 1 & 0 & 0 & 0 \\ 0 & 1 & 0 & 0 \\ 0 & 0 & 1 & 0 \\ 0 & 0 & 0 & 1 \end{bmatrix} \begin{Bmatrix} \dot{\alpha}_{1(m,t)} \\ \dot{\alpha}_{2(m,t)} \\ \dot{\alpha}_{3(m,t)} \\ \dot{\alpha}_{4(m,t)} \end{Bmatrix} \right) \Delta t \tag{3.55}$$

The component of tangent compliance matrix C_{ij} in Equation (3.55) can be simply defined in expanded form as shown in Box 5. The effective generalised stress tensor $\chi_{ij(m,t)}$ is calculated using Equations (3.56) and (3.57). And the kinematic internal variable function tensor $\alpha_{ij(m,t)}$ is calculated using Equations (3.58) and (3.59).

$$\chi_{i(m,t)} = -\frac{\partial E}{\partial \alpha_{i(m,t)}} = \sigma_{i(t)} - H_{p(m,t)}\alpha_{p(m,t)} - \frac{2}{3}H_{q(m,t)}\alpha'_{i(m,t)} \quad ; \ i=1...3 \tag{3.56}$$

$$\chi_{4(m,t)} = -\frac{\partial E}{\partial \alpha_{4(m,t)}} = \sigma_{4(t)} - \frac{1}{3}H_{q(m,t)}\alpha'_{4(m,t)} \tag{3.57}$$

$$\dot{\alpha}_{i(m,t)} = \frac{\partial w_{(m,t)}}{\partial \chi_{i(m,t)}} = \frac{\langle y_{(m,t)}\rangle}{\mu} \frac{\frac{2}{3}\chi_{p(m,t)} + \frac{3}{M^2}\chi'_{i(m,t)}}{2\cdot\sqrt{\dfrac{\left(\sum\limits_{i=1}^{3}\chi_{i(m,t)}\right)^2}{9} + \dfrac{3}{2}\dfrac{\left(\sum\limits_{i=1}^{3}\left(\chi'^2_{i(m,t)}\right) + 2\chi'^2_{4(m,t)}\right)}{M^2}}} \quad ; \ i=1...3$$

$$\tag{3.58}$$

$$\dot{\alpha}_{4(m,t)} = \frac{\partial w_{(m,t)}}{\partial \chi_{4(m,t)}} = \frac{\langle y_{(m,t)}\rangle}{\mu} \frac{\frac{3}{M^2}\chi'_{4(m,t)}}{2\cdot\sqrt{\dfrac{\left(\sum\limits_{i=1}^{3}\chi_{i(m,t)}\right)^2}{9} + \dfrac{3}{2}\dfrac{\left(\sum\limits_{i=1}^{3}\left(\chi'^2_{i(m,t)}\right) + 2\chi'^2_{4(m,t)}\right)}{M^2}}} \tag{3.59}$$

Box 4: Gibbs free energy and yield function for two-dimensional implementation

Gibbs free energy for $n \neq 1$:

$$E = \frac{p_e^{2-n}}{p_r^{1-n}k(1-n)(2-n)} - \frac{\sum\limits_{i=1}^{3}\sigma_{i(t)}}{3k(1-n)} - \left(\sum\limits_{i=1}^{3}\left(\sigma_{i(t)}\cdot\alpha_{i(t)}\right) + 2\sigma_{4(t)}\cdot\frac{\alpha_{4(m,t)}}{2}\right)$$

$$+ \frac{1}{N}\sum\limits_{m=1}^{N}\left(\frac{H_{p(m,t)}\left(\sum\limits_{i=1}^{3}\alpha_{i(m,t)}\right)^2}{2} + \frac{H_{q(m,t)}\left(\sum\limits_{i=1}^{3}\left(\alpha'^2_{i(m,t)}\right) + 2\left(\frac{\alpha'_{4(m,t)}}{2}\right)^2\right)}{3}\right)$$

Gibbs free energy for $n \neq 1$:

$$E = -\frac{\sum\limits_{i=1}^{3}\sigma_{i(t)}}{3k}\left(\ln\left(\frac{\sum\limits_{i=1}^{3}\sigma_{i(t)}}{3p_r}\right) - 1\right) - \frac{3\sum\limits_{i=1}^{3}\left(\sigma'^2_{i(t)}\right) + 2\sigma'^2_{4(t)}}{4g\sum\limits_{i=1}^{3}\sigma_{i(t)}} - \left(\sum\limits_{i=1}^{3}\left(\sigma_{i(t)}\cdot\alpha_{i(t)}\right) + 2\sigma_{4(t)}\cdot\frac{\alpha_{4(t)}}{2}\right)$$

$$+ \frac{1}{N}\sum\limits_{m=1}^{N}\left(\frac{H_{p(m,t)}\left(\sum\limits_{i=1}^{3}\alpha_{i(m,t)}\right)^2}{2} + \frac{H_{q(m,t)}\left(\sum\limits_{i=1}^{3}\left(\alpha'^2_{i(m,t)}\right) + 2\left(\frac{\alpha'_{4(m,t)}}{2}\right)^2\right)}{3}\right)$$

where

$$p_e^2 = \frac{\left(\sum\limits_{i=1}^{3}\sigma_{i(t)}\right)^2}{9} + \frac{k(1-n)\sum\limits_{i=1}^{3}\left(\sigma'^2_{i(t)}\right) + 2\sigma'^2_{4(t)}}{2g}$$

Yield function:

$$y_{(m,t)} = \sqrt{\frac{\left(\sum_{i=1}^{3} \chi_{i(m,t)}\right)^2}{9} + \frac{3}{2}\frac{\left(\sum_{i=1}^{3}\left(\chi'^2_{i(m,t)}\right) + 2\chi'^2_{4(m,t)}\right)}{M^2}} - H_{p(m,t)}\left(\sum_{i=1}^{3} \alpha_{i(m,t)}\right)$$

Box 5: Tangent compliance matrix in expanded form for two-dimensional implementation

$$C_{ij} = \begin{cases} \dfrac{1}{p_r}\left(\dfrac{p_r}{p_e}\right)^n \left\{ \left[\dfrac{1}{k} + \dfrac{n\left(\sum_{i=1}^{3}\left(\sigma_i'^2\right) + 2\sigma_4'^2\right)}{2gp_e^2}\right]\dfrac{1}{9} - \dfrac{np\sigma_i'}{3gp_e^2} + \dfrac{1}{3g} - \dfrac{nk(1-n)}{4g^2p_e^2}\left(\sum_{i=1}^{3}\left(\sigma_i'^2\right) + 2\sigma_4'^2\right) \right\}, \ i = j \in \{1,2,3\} \\[4mm] \dfrac{1}{p_r}\left(\dfrac{p_r}{p_e}\right)^n \left\{ \left[\dfrac{1}{k} + \dfrac{n\left(\sum_{i=1}^{3}\left(\sigma_i'^2\right) + 2\sigma_4'^2\right)}{2gp_e^2}\right]\dfrac{1}{9} - \dfrac{np\left(\sigma_i' + \sigma_j'\right)}{6gp_e^2} - \dfrac{1}{6g} - \dfrac{nk(1-n)}{4g^2p_e^2}\left(\sum_{i=1}^{3}\left(\sigma_i'^2\right) + 2\sigma_4'^2\right) \right\}, \ i \neq j \in \{1,2,3\} \\[4mm] \dfrac{1}{p_r}\left(\dfrac{p_r}{p_e}\right)^n \left\{ -\dfrac{np\left(\sigma_i' + \sigma_j'\right)}{6gp_e^2} - \dfrac{nk(1-n)}{4g^2p_e^2}\sigma_i'\sigma_j' \right\}, \ i = 4 \text{ xor } j = 4 \\[4mm] \dfrac{1}{p_r}\left(\dfrac{p_r}{p_e}\right)^n \left\{ \dfrac{1}{g} - \dfrac{nk(1-n)}{4g^2p_e^2}\sigma_4'^2 \right\}, \ i = j = 4 \end{cases}$$

where

$$p_e^2 = \frac{\sigma_{ii}\sigma_{jj}}{9} + \frac{k(1-n)\sigma_{ij}'\sigma_{ij}'}{2g} = p^2 + \frac{k(1-n)\sigma_{ij}'\sigma_{ij}'}{2g}$$

note:
- $i = j \in \{1,2,3\} \Rightarrow C_{11}, C_{22}, C_{33}$
- $i \neq j \in \{1,2,3\} \Rightarrow C_{12}, C_{13}, C_{21}, C_{23}, C_{31}, C_{32}$
- $i = 4 \text{ xor } j = 4 \Rightarrow C_{41}, C_{42}, C_{43}, C_{14}, C_{24}, C_{34}$
- $i = j = 4 \Rightarrow C_{44}$

3.3.6 Geometric Idealisation

Due to the special geometric characteristic in the real geotechnical problems, certain idealisations should be made. There are two kinds of geometric idealisation usually applied in geotechnical problems i.e.: plane strain and axi-symmetry.

For plane strain problems the thickness dimension normal to a certain plane (say the *xy* plane) is large compared with the typical dimensions in *xy* plane and the body is subjected to loads in the *xy* plane only. It may be assumed that the displacements in the *z* direction are negligible and the displacements *u* and *v* are independent of the *z* coordinate, it means that:

$$\varepsilon_z = 0; \gamma_{yz} = 0; \gamma_{zx} = 0 \tag{3.60}$$

Then the constitutive relationship in Equation (3.54) reduces to:

$$
\begin{bmatrix} C_{1111} & C_{1122} & C_{1112} \\ C_{2211} & C_{2222} & C_{2212} \\ C_{1211} & C_{1222} & C_{1212} \end{bmatrix} \begin{Bmatrix} \Delta\sigma_{11} \\ \Delta\sigma_{22} \\ \Delta\tau_{12} \end{Bmatrix} = \begin{Bmatrix} \Delta\varepsilon_{11} \\ \Delta\varepsilon_{22} \\ \Delta\gamma_{12} \end{Bmatrix} - \frac{1}{N} \sum_{m=1}^{N} \left(\begin{bmatrix} 1 & 0 & 0 \\ 0 & 1 & 0 \\ 0 & 0 & 1 \end{bmatrix} \begin{Bmatrix} \dot{\alpha}_{11(m,t)} \\ \dot{\alpha}_{22(m,t)} \\ \dot{\alpha}_{12(m,t)} \end{Bmatrix} \right) \Delta t
\tag{3.61}
$$

where $\Delta\sigma_{22} = \Delta\sigma_{33}$

Some problems in geotechnical engineering are categorised as axi-symmetry. In this problem it is usually to perform analysis using cylindrical coordinates r (radial direction), z (vertical direction) and θ (circumferential direction). Due to the symmetry condition, there is no displacement in the θ direction and the displacement in the r and z directions are independent of θ, it means that:

$$
\gamma_{r\theta} = 0 \text{ and } \gamma_{z\theta} = 0
\tag{3.62}
$$

therefore the strains reduce to (Timoshenko and Goodier, 1951):

$$
\begin{bmatrix} C_{1111} & C_{1122} & C_{1133} & C_{1112} \\ C_{2211} & C_{2222} & C_{2233} & C_{2212} \\ C_{3311} & C_{3322} & C_{3333} & C_{3312} \\ C_{1211} & C_{1222} & C_{1233} & C_{1212} \end{bmatrix} \begin{Bmatrix} \Delta\sigma_z \\ \Delta\sigma_r \\ \Delta\sigma_\theta \\ \Delta\tau_{rz} \end{Bmatrix} = \begin{Bmatrix} \Delta\varepsilon_z \\ \Delta\varepsilon_r \\ \Delta\varepsilon_\theta \\ \Delta\gamma_{rz} \end{Bmatrix} - \frac{1}{N} \sum_{m=1}^{N} \left(\begin{bmatrix} 1 & 0 & 0 & 0 \\ 0 & 1 & 0 & 0 \\ 0 & 0 & 1 & 0 \\ 0 & 0 & 0 & 1 \end{bmatrix} \begin{Bmatrix} \dot{\alpha}_{z(m,t)} \\ \dot{\alpha}_{r(m,t)} \\ \dot{\alpha}_{\theta(m,t)} \\ \dot{\alpha}_{rz(m,t)} \end{Bmatrix} \right) \Delta t
\tag{3.63}
$$

Figure 3.15 shows some examples of these problems in geotechnical engineering.
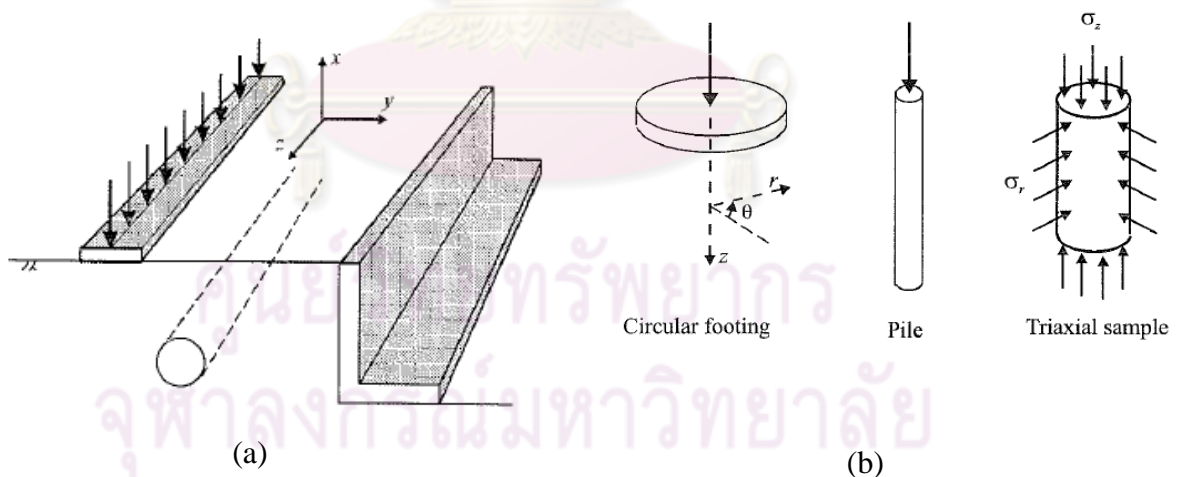
Figure 3.15 Examples of (a) plane strain and (b) axy-symmetry problems (Potts and Zdravkovic, 1999).

3.4 Verification of Numerical Model Implementation with Analytical Solution

To verify the performance of the numerical model implementation, the analytical solution of simple idealised undrained triaxial test on normally consolidated

clay has been considered. This solution has been obtained by theoretically integrating the MCC constitutive equation over the imposed stress or strain path (Roscoe and Burland, 1968; Potts, 1994). These solutions are given in the following equation:

$$q = pM \sqrt{\left(\frac{p_0}{p} \right)^{1/\Lambda} - 1} \qquad (3.64)$$

where p_0 is mean effective stress on the isotropic virgin consolidation line and $\Lambda = 1 - \dfrac{\kappa}{\lambda}$. The above equation provides the stress path in $q - p$ space, since p_0 remain constant in an undrained test. The material properties assumed in this validation are given in Table 3.2.

Table 3.2 Material properties for simple idealised undrained triaxial test

Slope of virgin consolidation line in v-$ln\ p'$ space	λ	0.066
Slope of swelling line v-$ln\ p'$ space	κ	0.0077
Slope of critical state line in $q - p$ space	M	1.2
p_0		200 kPa
Material constant	g	100
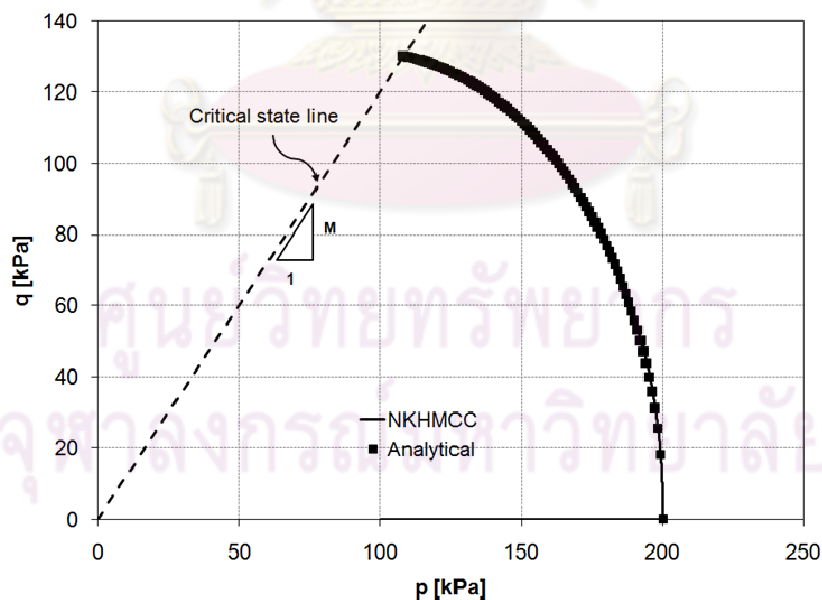
Figure 3.16 Stress path response of idealised undrained triaxial test on normally consolidated clay.

In this validation, full pressure-dependent is considered for non-linear KHMCC model under single yield surface using $n = 1$, and other parameters are $k = 232$, $a = 1.1$.

Result for this validation is shown in Figure 3.16. It is shown that the numerical prediction of non-linear KHMCC model is in good agreement with analytical solution.

3.5 Numerical Demonstration

This part shows several numerical demonstrations of the non-linear KHMCC model. All attempts of demonstration are to emphasize the performance of hyperplasticity framework which can contain several complicated characteristics of constitutive models under the unified framework. All the following demonstrations use the parameter $g = 242$, $k = 1200$, $n = 0.6$, $M = 0.71$, and $a = 3.5$ for non-linear KHMCC then $M = 0.71$, $\kappa = 0.2$ and $\lambda = 0.6$ for MCC model.

3.5.1 Smooth Transition from Elastic to Plastic Behaviour

Figures 3.17 and 3.18 show the stress path and stress-strain curve of undrained triaxial test of lightly-overconsolidated clay. The sample is consolidated with isotropic consolidation pressure $p = 500$ kPa then unloaded to $p = 300$ kPa (OCR = 1.67) and after that the sample is sheared under undrained condition. It is clearly shown that non-linear KHMCC model can simulate smooth transition from elastic to plastic behaviour comparing with the MCC prediction. The characteristic S-shaped curve for the variation of stiffness with log of strain clearly present in Figure 3.19.
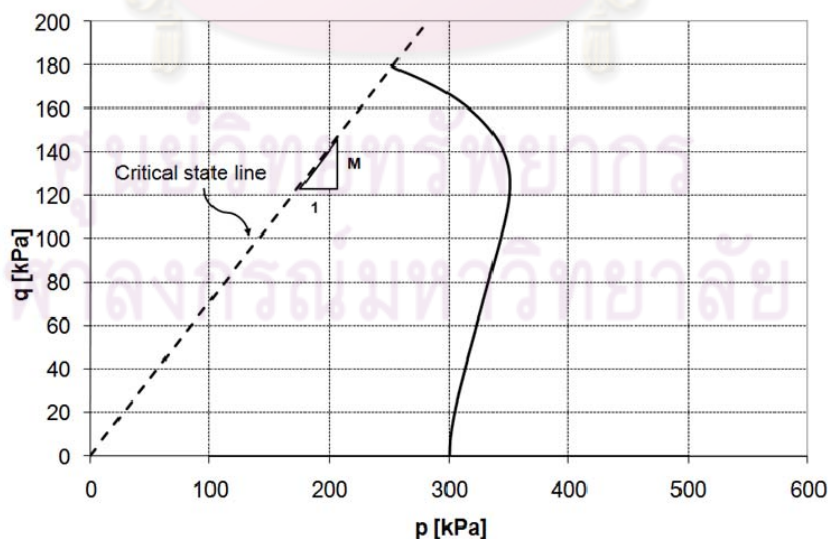
Figure 3.17 Undrained stress path of overconsolidated clay.
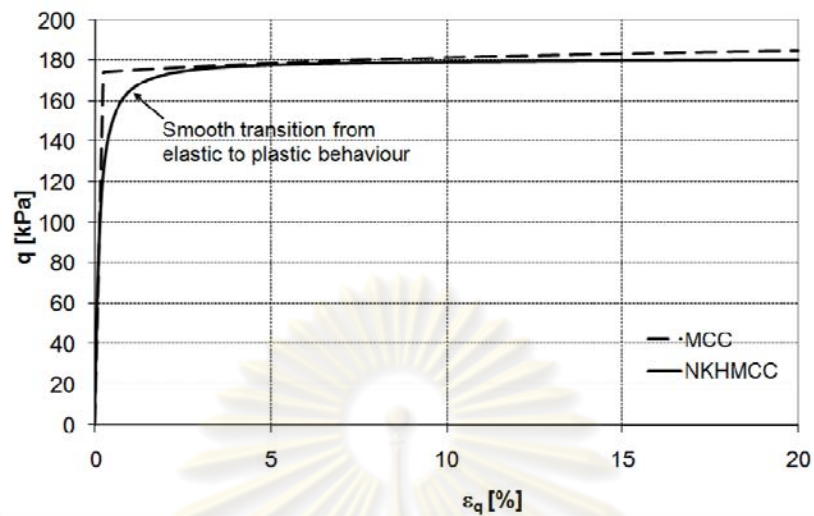
Figure 3.18 Undrained stress-strain response of overconsolidated clay.
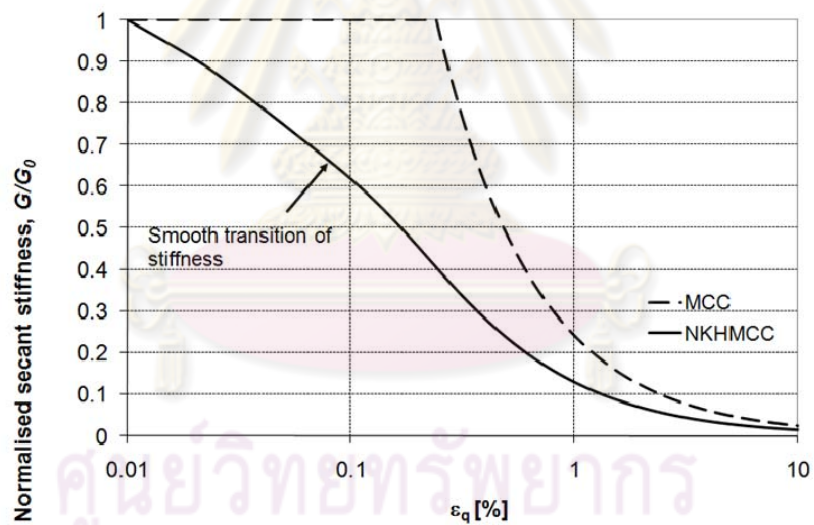
Figure 3.19 Normalised secant stiffness against log of strain of overcosolidated clay.

3.5.2 *Effect of Immediate Past Stress History*

Atkinson (1990) and Houlsby (1999) observed an additional influence on the stress-strain behaviour that is the immediate or recent stress history of soil described by the most recent loading, which may take the form of an extended period of rest or a sudden change in the direction of the stress path. Figure 3.20 shows a given series of stress points (A, B and C). Two cases of consolidated stress path are given i.e. ACB and ACAB. To demonstrate the effect of immediate past stress, we shall consider two

undrained tests from point B, which have OCR of 1.5. Wherein, point B has been approached by two sets of drained loading from the direction of point A and C. Also shown in Figure 3.20, all stress histories located within the MCC surface.

Figure 3.21 shows the demonstration results of undrained stress-strain curves when sample is sheared from point B. For MCC model, because all stress points lie within this surface, the model gives the same purely elastic response for both two cases.
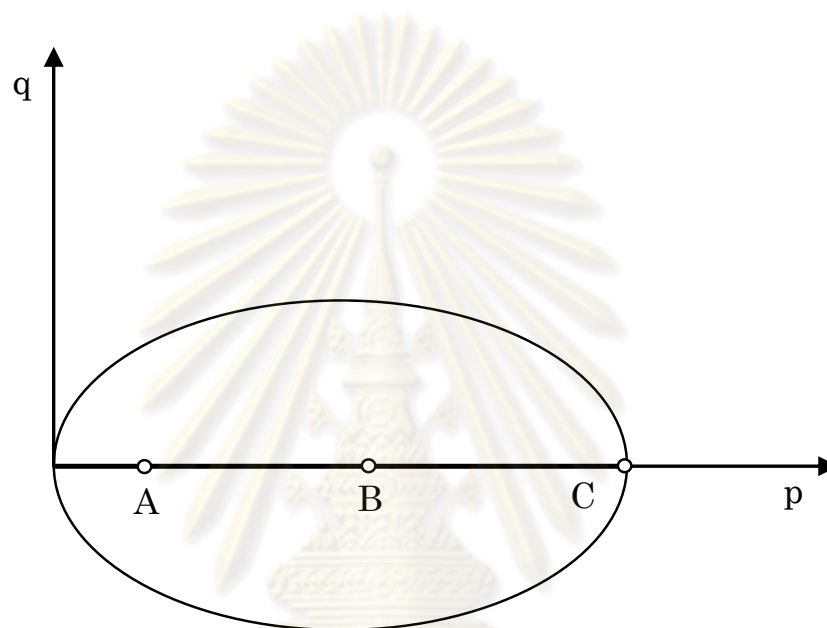
Figure 3.20 Series of stress point with different stress paths for over consolidated clay.
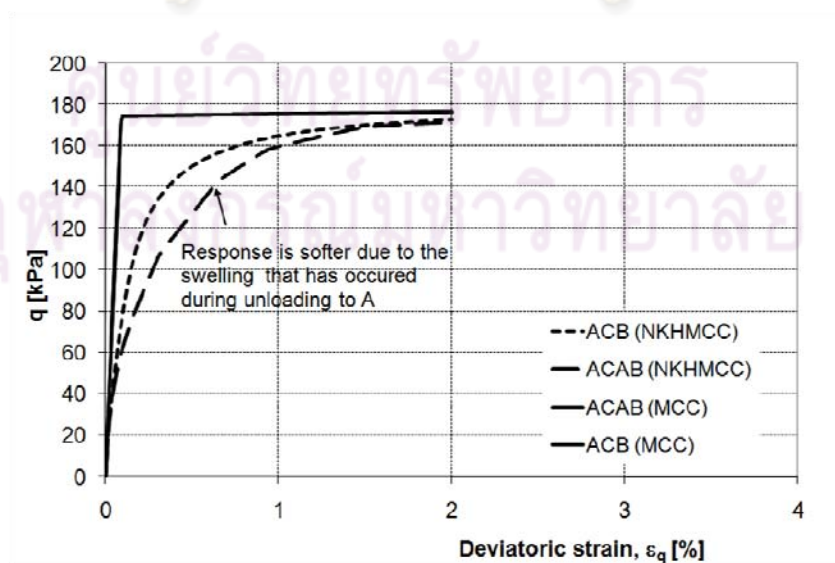
Figure 3.21 Stress-strain response after different recent stress histories.

It is clearly shown one of the drawbacks of the MCC model. On the other hand, the two responses from the non-linear KHMCC model are quite different. Response of ACAB is softer rather than ACB, because of the swelling effect that occurred during unloading to point A. The effect of recent stress history on the stiffness is more clearly shown in Figure 3.22, which shows plot of normalised secant stiffness G/G_0 against the deviatoric strain.
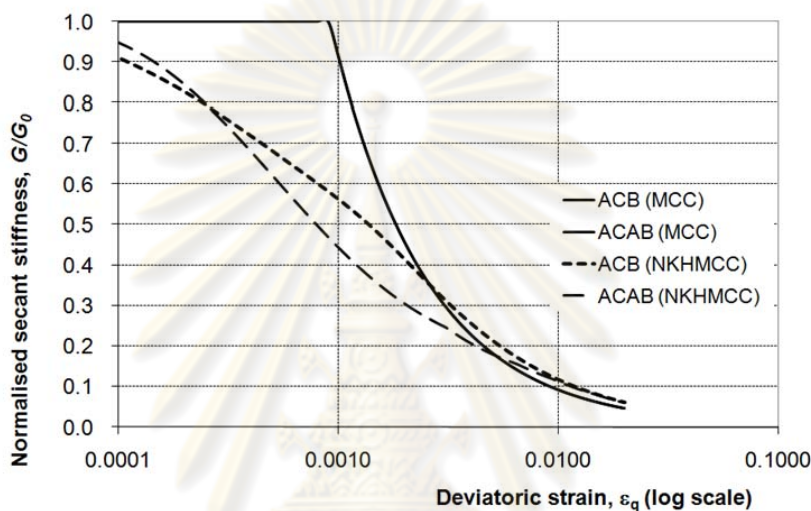
Figure 3.22 Effect of immediate stress history on the stiffness.

Figure 3.23 shows two undrained stress paths response from non-linear KHMCC and MCC model. It is obvious that the non-linear KHMCC model can predict the dependence of effective stress path on the immediate stress history during undrained shear as observed by Stallebrass and Taylor (1997) comparing with the MCC model.

3.5.3 Unloading-Reloading Cycles

Figures 3.24 and 3.25 show cyclic load response of non-linear KHMCC and MCC model, respectively. The non-linear KHMCC model demonstration shows a hysteresis loop and smooth transition of stiffness during unloading-reloading compared to MCC model. The non-linear KHMCC model can explains the fact that the openness of the hysteresis loop increases with strain amplitude.
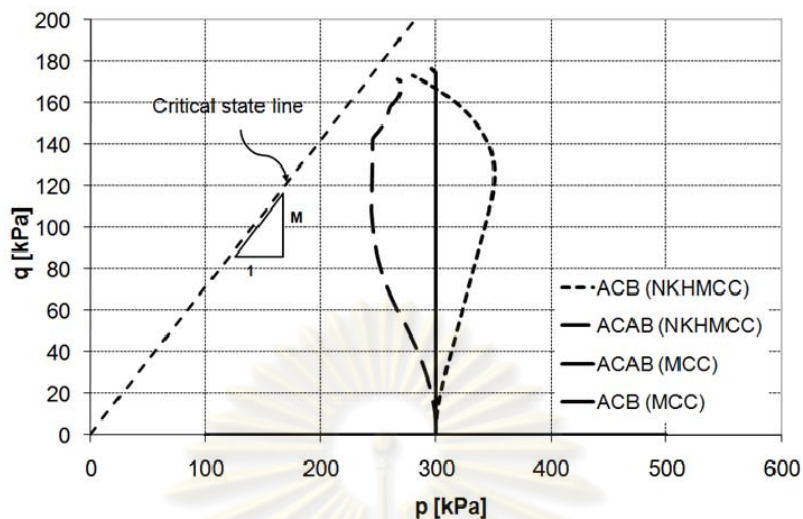
Figure 3.23 Stress paths response after different immediate stress histories.

Figures 3.26 and 3.27 show the demonstration results from five cycles of unloading-reloading undrained stress-strain curve with confining pressures of 500 kPa using non-linear KHMCC and MCC model, respectively. It is shown that the non-linear KHMCC model can describe the stress-strain response of the repetitive unloading-reloading undrained shear.
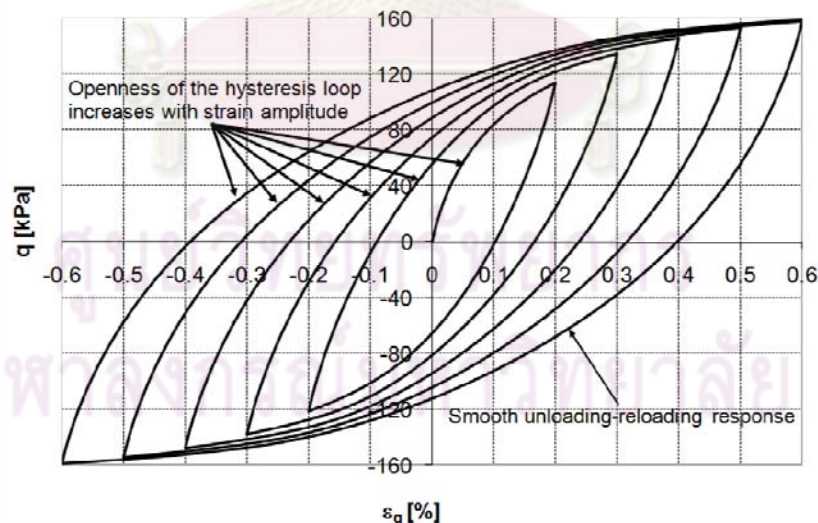
Figure 3.24 Closed hysteresis loop response of non-linear KHMCC model.
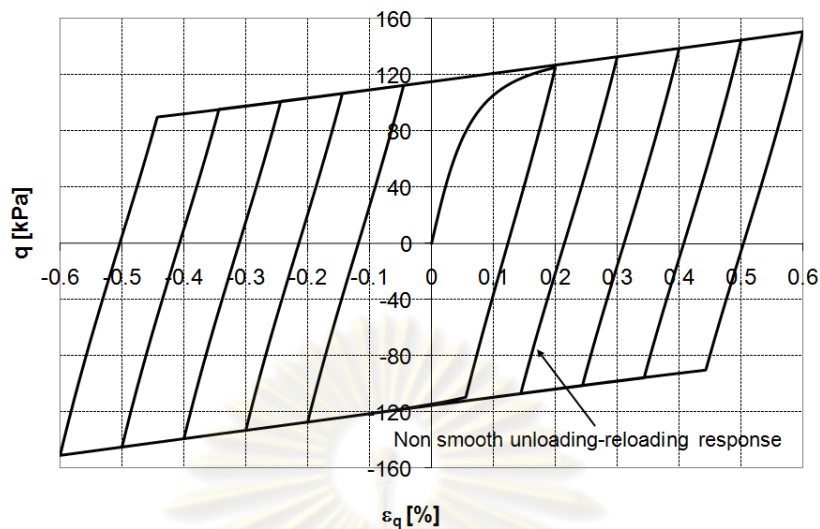
Figure 3.25 Closed hysteresis loop response of MCC model.
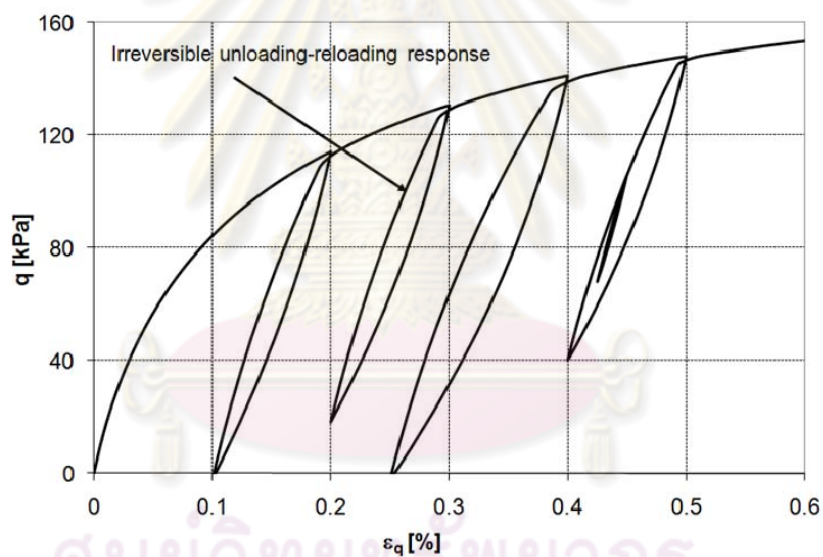
Figure 3.26 Unloading-reloading undrained stress-strain response of non-linear KHMCC model.
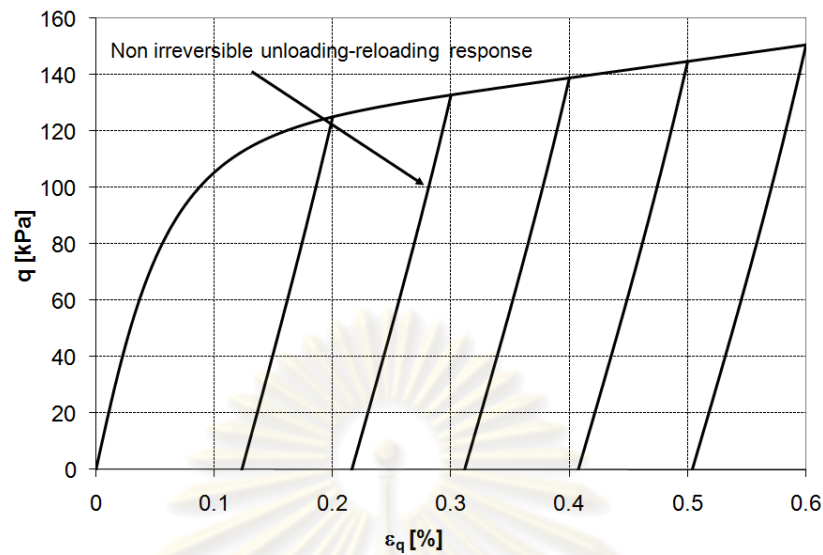
Figure 3.27 Unloading-reloading undrained stress-strain response of MCC model.

3.6   Summary

Formulation of the non-linear KHMCC model in triaxial and general stress variables as well as an approach to determine the necessary parameters obtained from experimental tests for regulating small-strain stiffness characteristic in form of power function of pressure has been presented. The stiffness factor for the kinematic hardening has been made as power function of initial preconsolidation pressure. Further, some important issues on the numerical implementation of this model have been discussed, including incremental stress-strain response algorithm, numerical integration of hardening functions, effect of time increment and number of yield surfaces. The rate-dependent multisurface hyperplasticity algorithm using strain driven forward-Euler integration scheme is employed in this study to reduce complexity of treatment from numerical error. It is also shown that the numerical stability of rate-dependent algorithm is clearly affected by the increment of time step. It is observed that the stress-strain response smoother when the number of yield surfaces is increased. Numerical study also indicate that running time of multiple kinematic hardening model increases linearly against increasing number of yield surfaces. However, availability of high-speed computer can significantly reduce time computation. Validation of the numerical model implementation against analytical solution of simple idealised undrained triaxial test show that the model has been successfully implemented. Finally, numerical demonstrations show that the non-linear KHMCC model can demonstrate some important aspects in soil mechanics such as small-strain stiffness, effects of immediate past stress history behaviour, a hysteresis loop and smooth transition of stiffness during unloading-reloading cycles. Nevertheless, the anisotropy can be loosely explained by

the immediate stress past. The softening behaviour should be explored in the future in order to realize the promising features of the model on soil destructure. In the next chapter the developed model will be compare with experimental data of clay soils.

CHAPTER IV.   SOME COMPARISONS WITH EXPERIMENTAL DATA OF CLAY SOILS

4.1   Introduction

The development of non-linear KHMCC model under triaxial and general stress condition has been presented in Chapter 3. Though several demonstrations to show features of the developed model have been presented, comparisons this model to experimental data has not been carried out.

This chapter presents comparisons of the developed model with some experimental on clay soils. The comparisons are performed using single-element calculation.

4.2   Loading Path Dependence and Non-Linear Stiffness at Small-Strain

4.2.1   Introduction

Detailed experimental investigations on the stress-strain response of overconsolidated soil have also shown characteristics dependence on both non-linearity and most recent loading paths (Jardine et al., 1984; Atkinson et al., 1990; Stallebrass and Taylor, 1997; and Houlsby, 1999). The effect of current loading history has also been observed by a different experimental approach (Jardine, 1985; Jardine, 1992; and Smith et al., 1992). They found that there are zones exist at small-strain and its can change in both of shape and size as the soil is subjected to different loading histories.

The importance of these two behaviours in predicting load-deformation on soil-structure interaction problems have been observed with many cases in the field (Jardine et al., 1986; Jardine et al., 1991; Gunn, 1993, and Addenbrooke, 1997).

This section presents a comparison of experimental results of current state and loading history dependence in overconsolidated clay with non-linear KHMCC model prediction. An experimental undrained triaxial test on Speswhite kaolin (Stallebrass & Taylor, 1997) has been selected. This experimental have been conducted to show a non-linearity and current state and loading history dependence on relative directions of the current and previous loading paths in overconsolidated clay. Model validation is performed with response of tangent shear stiffness against stresses. Further, the experimental result of unloading-reloading at small-strain is also compared to model prediction. In addition, study about effect of number of yield surfaces against stress-strain response is carried out.

4.2.2 Model Comparison

Atkinson (1990), Jardine (1985, 1992), Smith et al. (1992), Stallebrass and Taylor (1997) and Houlsby (1999) observed an additional influence on the stress-strain behaviour that is the loading paths dependence or immediate stress history of soil described by the most recent loading, which may take the form of an extended period of rest or a sudden change in the direction of the stress path. They found that there are zones exist at small-strain and its can change in both of shape and size as the soil is subjected to different loading histories.

Stallebrass (1990) and Stallebrass and Taylor (1997) have been conducted experimental undrained triaxial test on Speswhite kaolin and simulated the results using Three-Surface Kinematic Hardening (3-SKH) model (Atkinson and Stallebrass, 1991). They plotted the results with tangent shear stiffness G_t against deviatoric stress q as shown in Figure 4.1. Table 2 shows 3-SKH soil model parameter in this simulation.
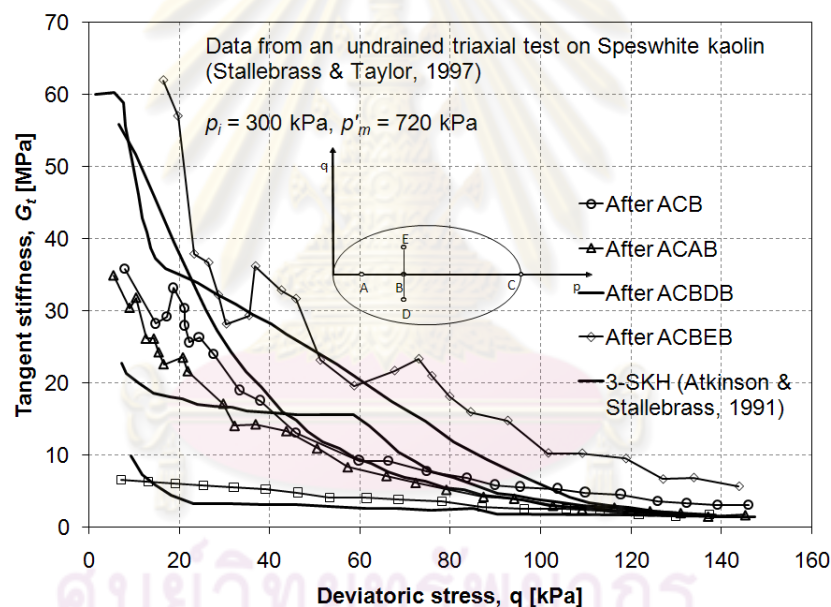
Figure 4.1 Prediction of tangent stiffness G_t-deviatoric stress q of 3-SKH model compared with experimental results (after Stallebrass and Taylor, 1997).

Table 4.1 Summary of 3-SKH model parameters of Speswhite Kaolin (after Stallebrass and Taylor, 1997)

M	λ^*	e_{cs}	κ^*	$G \ [kPa]$	T	S	ψ
0.89	0.073	1.994	0.005	$1964p^{0.65}R_o^{0.2}$	0.25	0.08	2.5

In this study, we simulated the experimental with a given series of stress points (A, B, C, D, and E) as shown in Figure 4.2. Four cases of consolidated stress path are given i.e. ACB, ACAB, ACBDB, and ACBEB represent a sudden change in the direction of the stress path before undrained shearing stage at point B, which have OCR

of 2.4 (p_0 = 300 kPa and p_m = 720 kPa). Also shown in Figure 4.2, all stress histories located within a bounding yield surface.
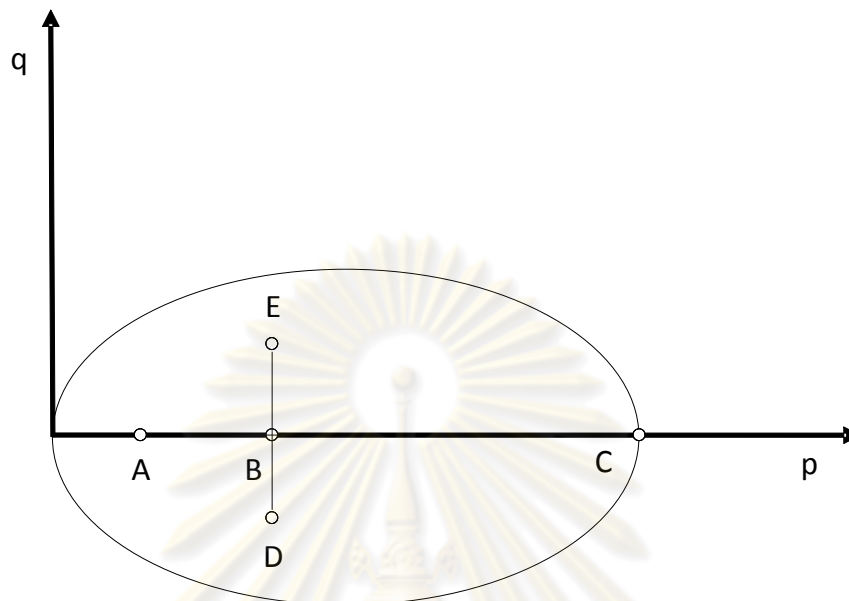
Figure 4.2 Series of stress point with different stress paths for over consolidated clay.

In this simulation, the small-strain stiffness parameters g, k and n are obtained using stiffness relationships in Table 4.1 normalised to Equation (3.46) with 1 atm (100 kPa) as a reference pressure. Equation (4.1) shows the small-strains stiffness relationship used in this simulation. Then the constant k can be determined using Equation (3.44) with poisson ratio ν of 0.3. The kinematic hardening parameter a is determined from small parametric study of actual stress-strain curve as shown in Figure 4.3.Table 4.2 summarises non-linear KHMCC model in this simulation.

$$\frac{G}{p_r} = 467 \left(\frac{p}{p_r} \right)^{0.65} \tag{4.1}$$

Figures 4.4 and 4.5 show the fields of yield surfaces at initial condition and after the four different stress paths.

Table 4.2 Summary of non-linear KHMCC model parameters of Speswhite kaolin

k	1012	
g	467	dimensionless material constant
n	0.65	
M	0.89	Slope of critical state line in q-p plane
a	15	Kinematic hardening parameter
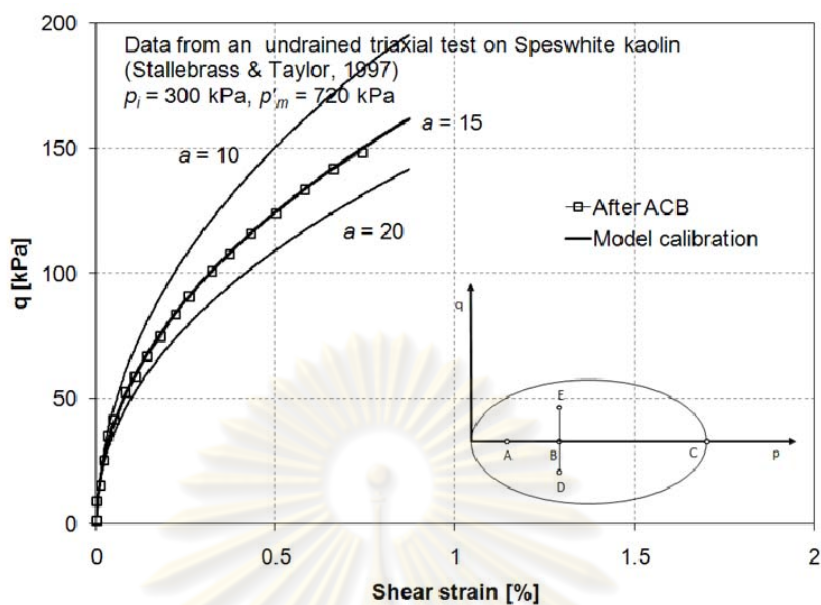
Figure 4.3 Parametric study of kinematic hardening parameter *a*.
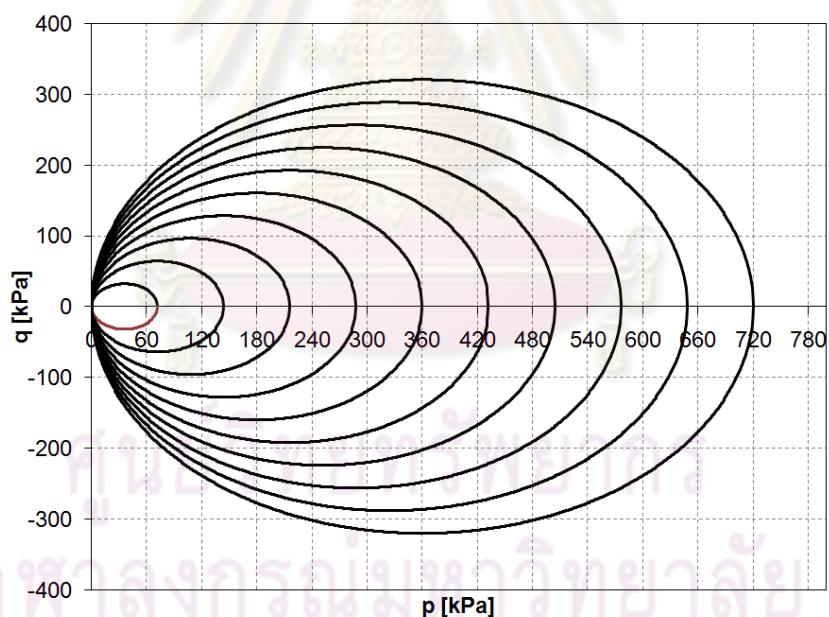
Figure 4.4 Position of yield surfaces at initial condition.

Figure 4.6 shows the comparison result which show plot of normalised tangent shear stiffness G_t against the deviatoric stress. This plot shows clearly that the small-strain stiffness is affected by loading path history. Prediction of the model is also in a good agreement with the experimental result. However, some irregularities appear in the curve are a result from numerical discretisation. Figure 4.7 shows four undrained stress paths response from non-linear KHMCC. It is obvious that the non-linear KHMCC

model can predict the loading paths dependence during undrained shear. Finally, model is verified to simulate unloading-reloading behaviour at small-strain compared with the experimental test data as shown in Figure 4.8. The model prediction shows that it can model a non-recoverable strain during unloading reloading response. It also shows that stiffness reduction for larger stress change is in good agreement with experimental result. The simulations using 100 numbers of yield surfaces, except the unloading-reloading response is carried out using 50 numbers of yield surfaces. This simple computation is performed by Intel Pentium M 1.6 GHz.

(a)   (b)

(c)   (d)
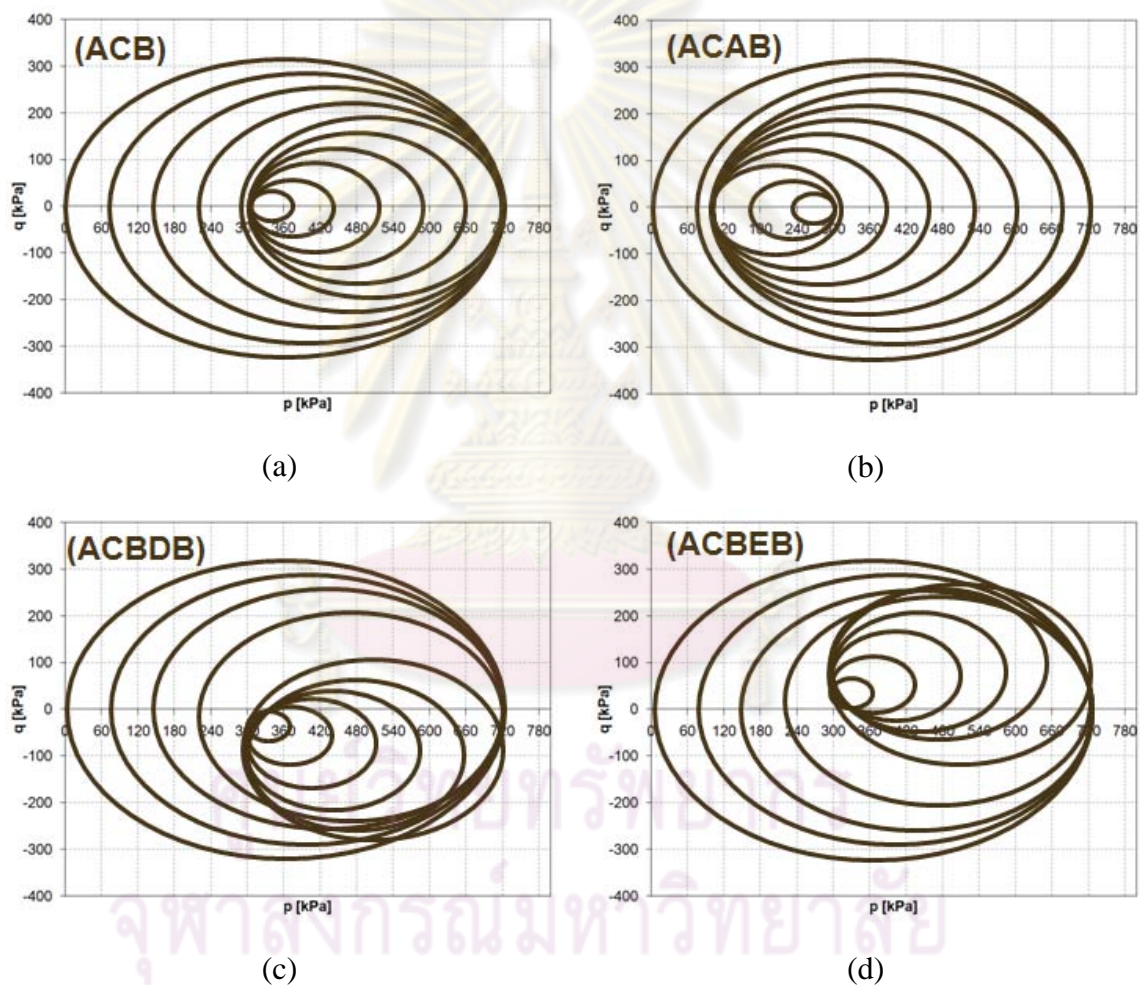
Figure 4.5 Position of yield surfaces after four different stress histories.

4.2.3   *Effect of number of yield surfaces*

This numerical study aims to see the effect of number of yield surfaces in the response of different stress paths and try to find the optimum number of yield surfaces according to obtain accurate result. The numerical study is performed using 1, 2, 10 and

100 yield surfaces, and the effect is shown in stress-strain and stress path responses in Figures 4.9 and 4.10.
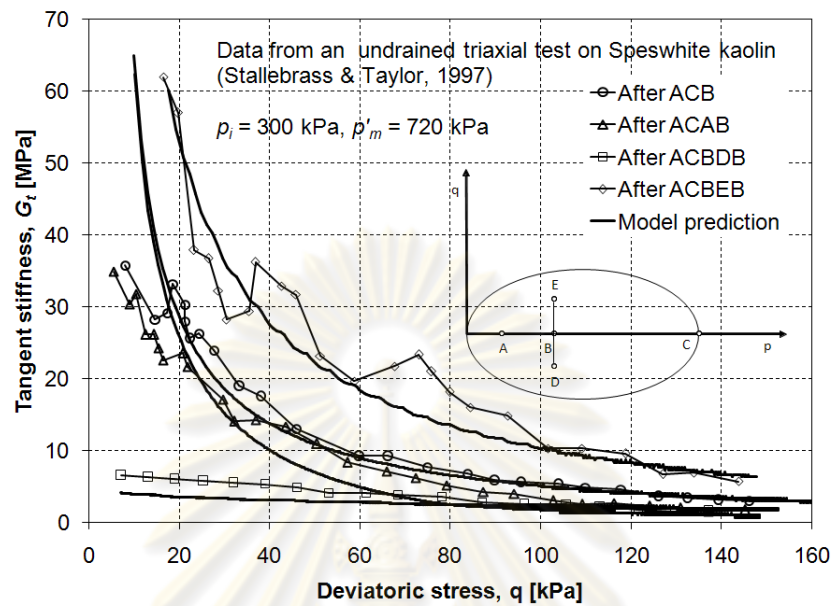
Figure 4.6 Prediction of tangent stiffness G_t-deviatoric stress q of non-linear KHMCC model compared with experimental results.
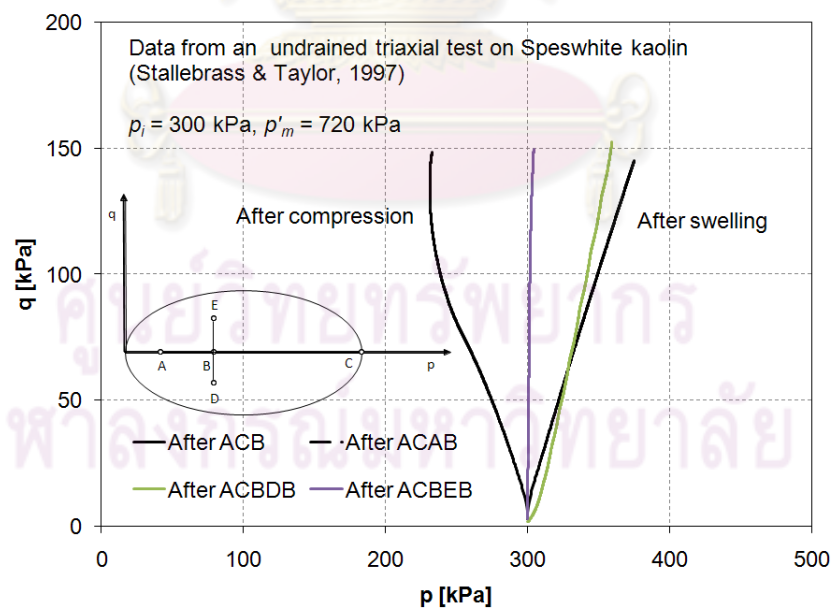
Figure 4.7 Prediction of stress paths of non-linear KHMCC model after different loading histories.
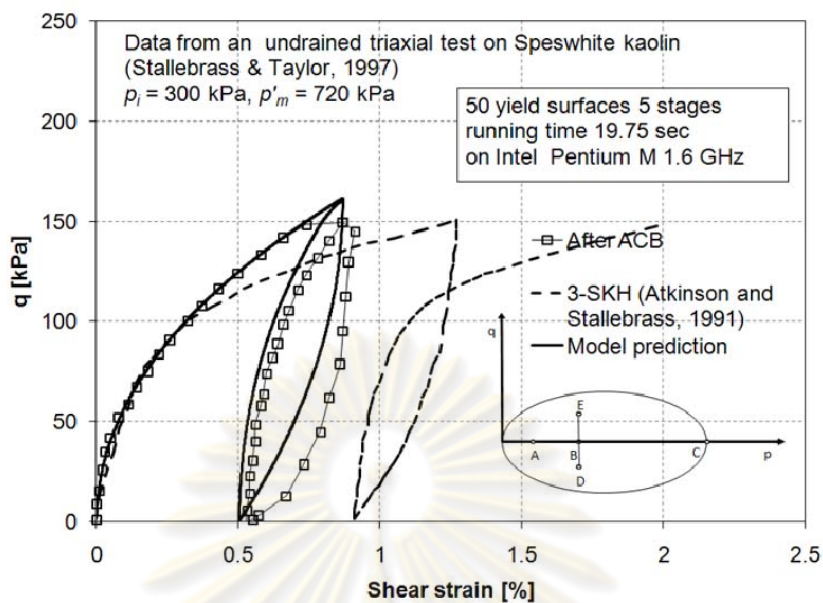
Figure 4.8 Prediction of unloading-reloading response at small-strain of non-linear KHMCC model compared with experimental result.
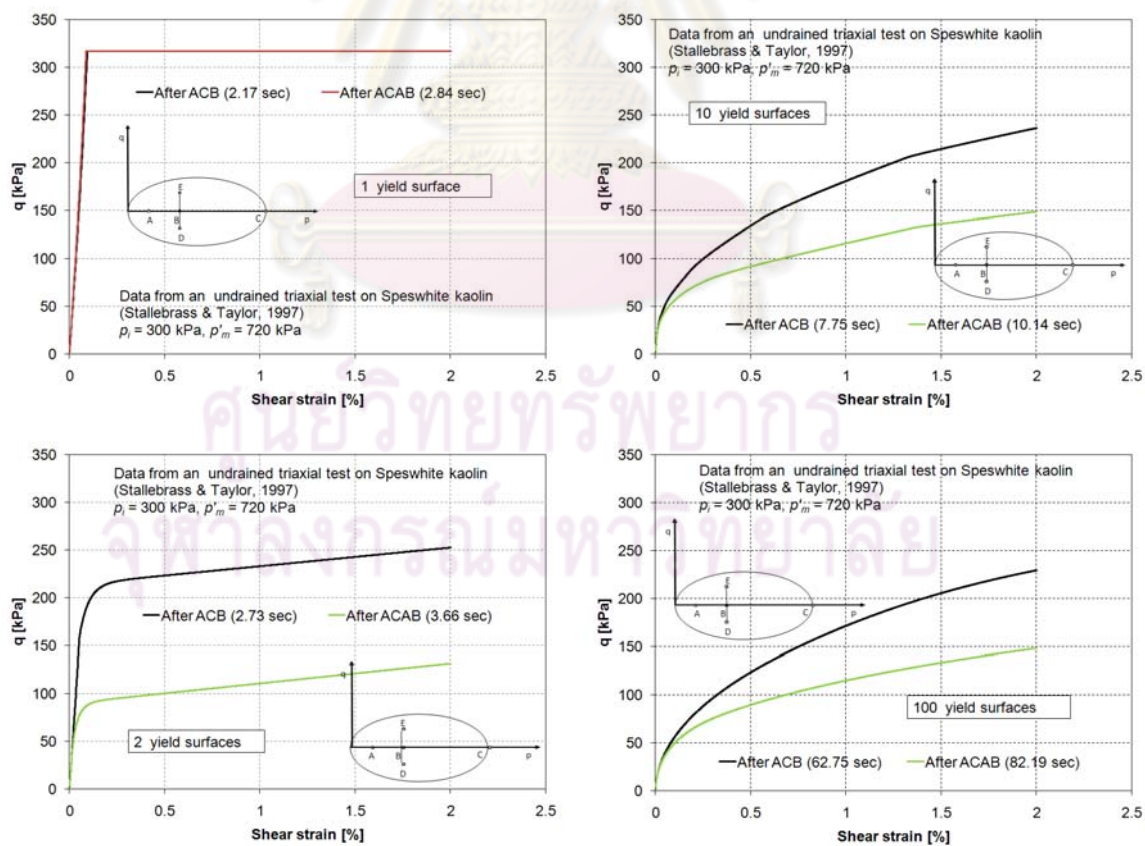
Figure 4.9 Effect of number of yield surfaces on the stress-strain response.
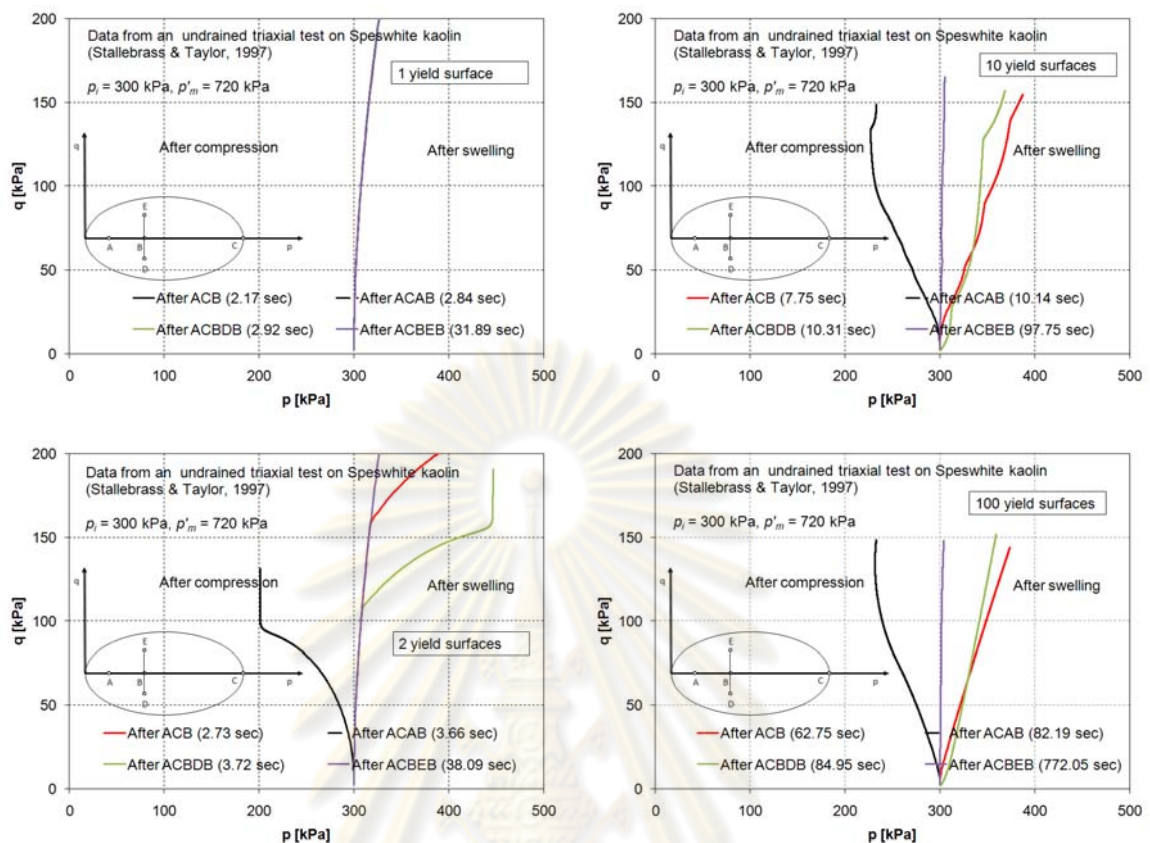
Figure 4.10 Effect of number of yield surfaces on the stress paths response.

It is clearly shown in the Figures 4.9 and 4.10 that the stress-strain and stress path responses are influenced by number of yield surfaces. It can concluded that 20 number of yield surfaces are adequate to obtain accurate result.

4.3 Response of K_0-consolidated Undrained Direct Simple Shear (CK_0UDSS) Test of Bangkok Clay

4.3.1 Introduction

The purpose of a simple shear test is to determine shear strength parameters and the stress-strain behaviour of soils under loading conditions that closely simulate plane strain and allow for the principal axes of stresses to rotate. The stress states in soils for many geotechnical problems are akin to simple shear. Ladd (1991) presented a well-known simple illustration of stress condition of soil during staged construction of embankment on clay as shown in Figure 4.11. The soil mass beneath embankment is assumed in the triaxial compression (TC) condition; on the other hand, the soil mass around the toe slope of the embankment is assumed in the triaxial extension (TE)

condition. However, the soil mass between these two conditions can accurately simulated using the direct simple shear (DSS) test.
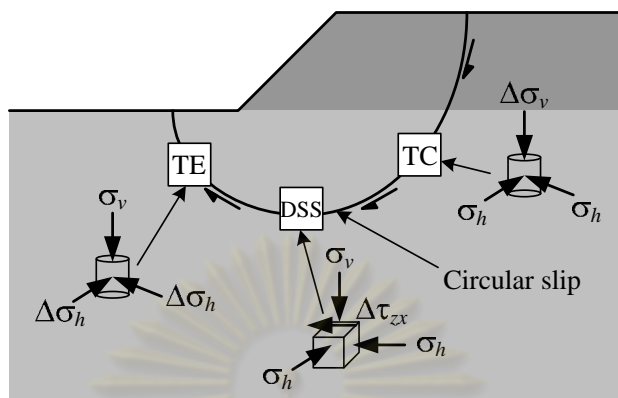
Figure 4.11 Stress conditions during staged construction of embankment on clay (after Likitlersuang et al., 2008).

This section presents a comparison of experimental results of K_0-consolidated Undrained Direct Simple Shear (CK_0UDSS) Test of Bangkok Clay (Konkong, 2007) with non-linear KHMCC model prediction. Model prediction of stress-strain and stress-paths response is compared to experimental data of monotonic simple shear response of normally consolidated Bangkok Clay

4.3.2 Review of Experimental Works

The soil laboratory tests were carried out using Geonor H12 DSS apparatus (NGI-type) at Chulalongkorn University. The specimens were prepared in cylindrical shape whose vertical side is enclosed by a wire reinforced rubber membrane. During the consolidation state, the samples were one-dimensional (K_0) consolidated by applying the normal (vertical) effective stress (σ'_{vc}) (see Figure 4.12). These tests were conducted at a strain rate of 5% per hour. A computer interfaced data acquisition system has been set up to obtain a continuous record of test data. A full time-histories of horizontal shear stress (τ), change (decrease or increase) in vertical stresses that equal to induced excess pore water pressure, Δu) and horizontal shear strain (γ) have been monitored.
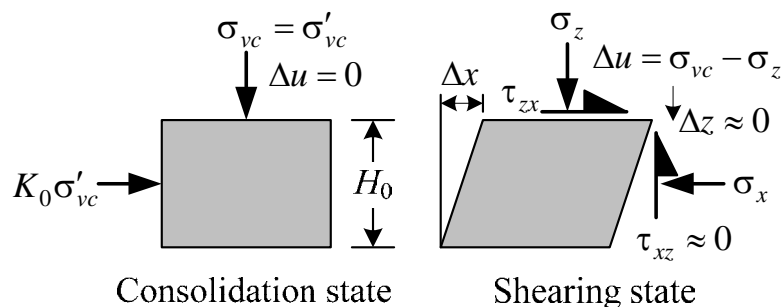
Figure 4.12 Stresses imposed on sample under direct simple shear test (after Likitlersuang et al., 2008).

Table 4.3 Index properties of soil samples (After Konkong, 2007)

Index Properties	Values
Moisture content (%)	59 – 62
Liquid Limit , LL (%)	78 – 83
Plastic Limit, PL (%)	41 – 44
Plasticity Index, PI (%)	37 – 39
Specific Gravity, Gs	2.64
Unit Weight, γ (t/m^3)	1.633

A K_0-consolidated undrained direct simple shear tests (CK_0UDSS) with constant-volume was conducted on the samples. In constant-volume DSS test, volume of the sample is essentially constrained against changes during shear. It has been shown on a normally consolidated clay that change in applied vertical stress required to maintain the volume constant is equal to developed pore pressure in an undrained DSS test as Degroot (1992). Initially, the samples were consolidated to various effective axial consolidation stress (σ'_{vc}) level, between 200 to 500 kPa. The preconsolidation pressure or maximum past stress (σ'_{vm}) of the clay was predicted about 130 kPa. Therefore, consolidation of samples to σ'_{vc} above 130 kPa essentially assured that all the samples tests were normally consolidated. The stress-strain and stress-path response of these tests are presented in Figures 4.13 and 4.14, respectively.
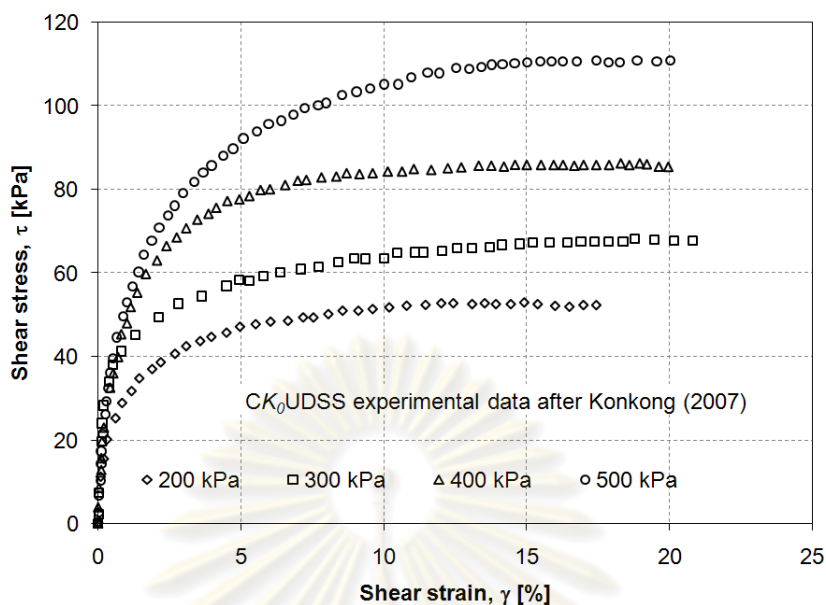
Figure 4.13 Stress-strain curves of CK_0UDSS tests of Bangkok Clay (After Konkong, 2007)
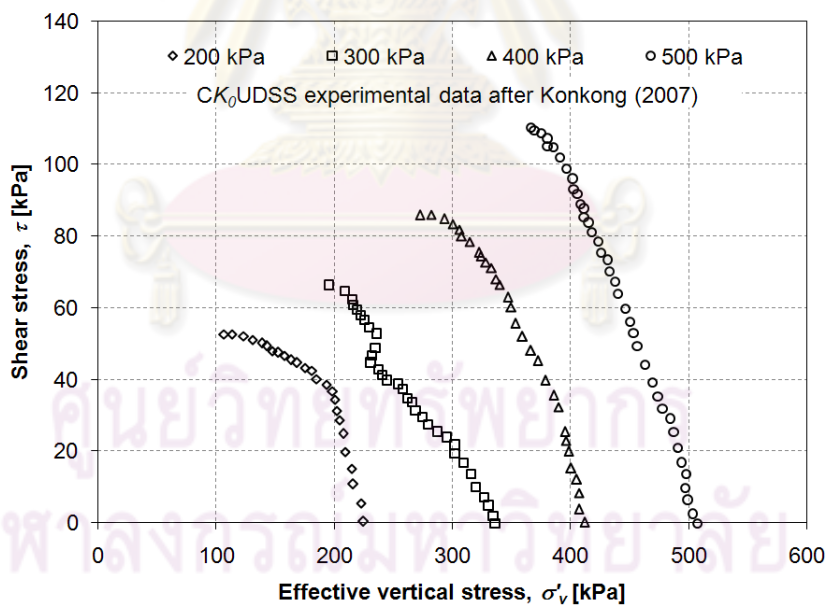
Figure 4.14 Stress-paths curves of CK_0UDSS tests of Bangkok Clay (After Konkong, 2007)

4.3.3 Model Comparison

In this validation, both linear ($n = 1$) and non-linear KHMCC ($n \neq 1$) model are used to predict the stress-strain response CK_0UDSS tests of Bangkok Clay. Table 4.4

and Table 4.5 summarise linear and non-linear KHMCC model parameters. For linear KHMCC model, dimensionless material constants are directly obtained from observation of stress-strain response of CK_0UDSS of Bangkok Clay, whereas for non-linear KHMCC model are obtained based on relationship between initial stiffness and pressure of Bangkok Clay proposed by Techavorasinskun et. al. (2002) as shown in Equation (4.2) after normalised into Equation (3.46).

$$\frac{G}{p_r} = 242 \left(\frac{p}{p_r} \right)^{0.6} \qquad (4.2)$$

The constant k is obtained from Equation (3.44) with $v = 0.41$ (typical value of K_0 of Bangkok clay is around 0.68 (Shibuya *et. al.*, 2001)). The slope of critical line (M) is observed from the undrained stress paths in Figure 4.9, and relationships in Equation (3.40). Finally, kinematic hardening parameter a is determined from procedures which are explained in the previous section as shown in Figure 4.15.
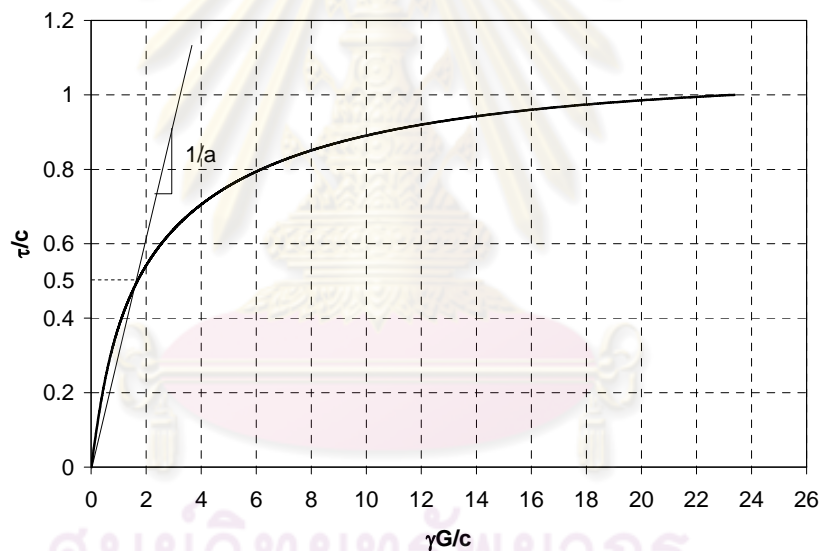
Figure 4.15 Determination of parameter *a*

Figure 4.16 to Figure 4.19 show comparisons between model prediction and experimental results of CK_0UDSS of Bangkok Clay.

Table 4.4 Summary of linear KHMCC parameters of Bangkok Clay

Parameters	Values	Physical meaning
k	300	small-strain dimensionless material constant
g	61	

n	1.0	
M	0.82	Slope of critical state line in q-p plane
a	3.6	Kinematic hardening parameter

Table 4.5 Summary of non-linear KHMCC parameters of Bangkok Clay

Parameters	Values	Physical meaning
k	1200	small-strain dimensionless material constant
g	242	
n	0.6	
M	0.82	Slope of critical state line in q-p plane
a	8.8	Kinematic hardening parameter
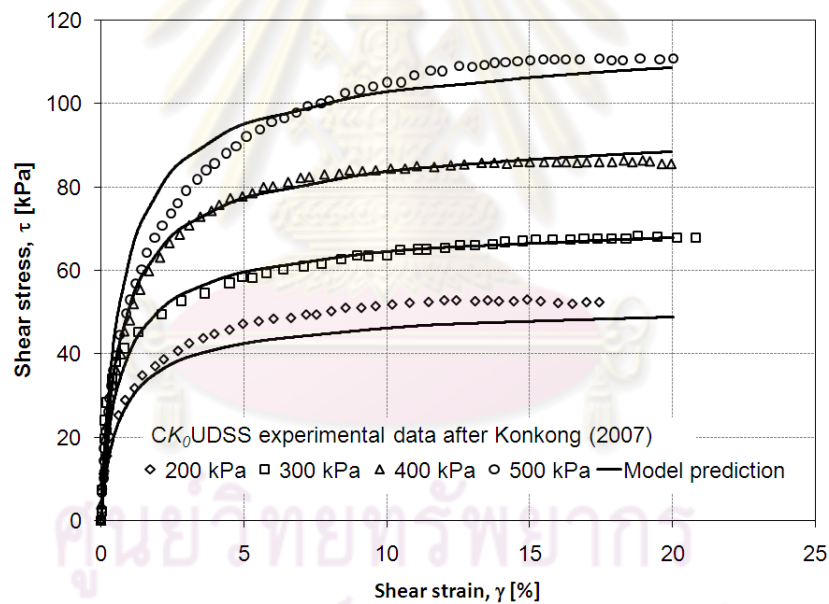
Figure 4.16 Linear KHMCC model prediction of stress-strain curves of CK_0UDSS tests of Bangkok Clay
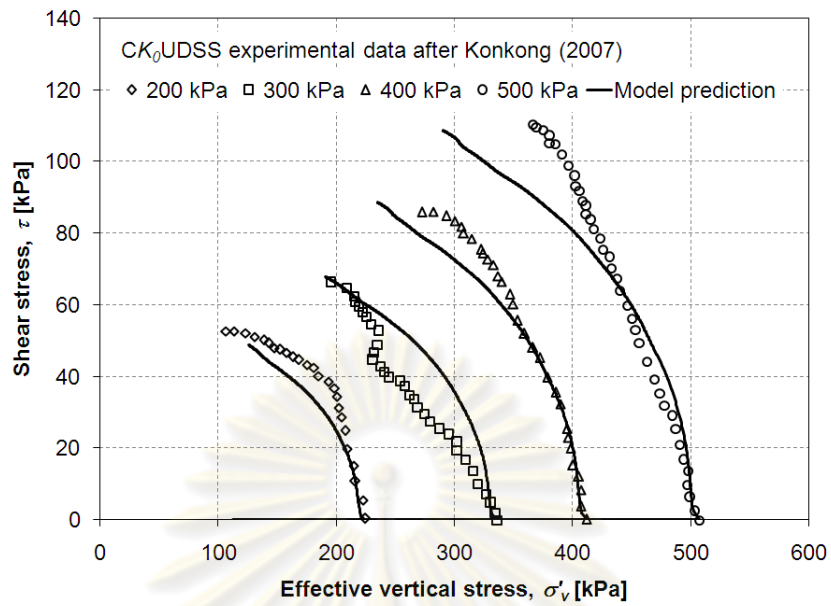
Figure 4.17 Linear KHMCC model prediction of stress-paths of CK_0UDSS tests of Bangkok Clay
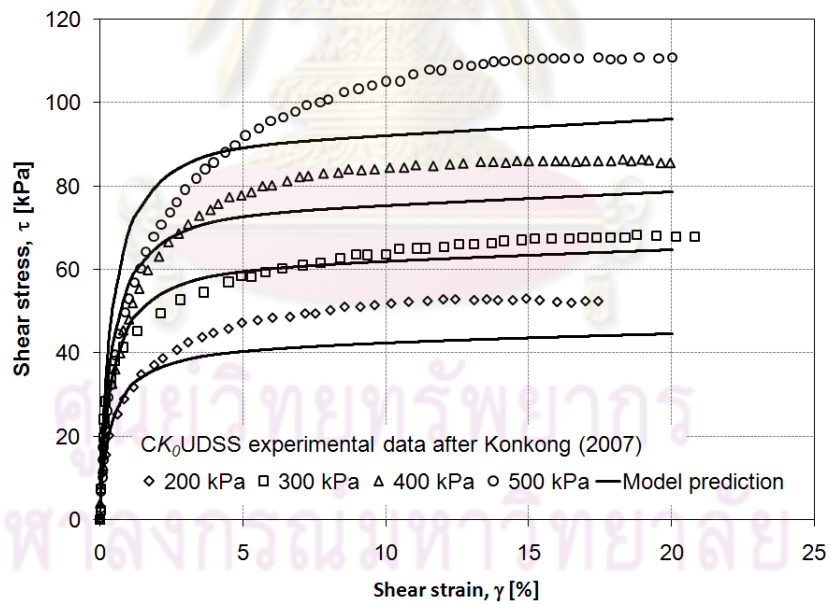
Figure 4.18 Non-linear KHMCC model prediction of stress-strain curves of CK_0UDSS tests of Bangkok Clay
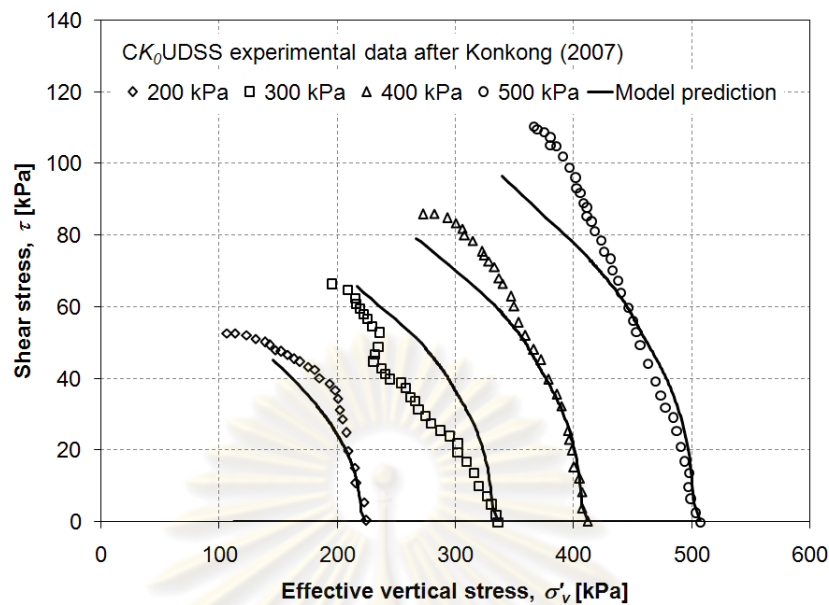
Figure 4.19 Non-linear KHMCC model prediction of stress-paths of CK_0UDSS tests of Bangkok Clay

The model predictions show that the model provides a good prediction on the stress-strain and stress path curve. However, non-linear KHMCC model gives lower strength and stiffer response compared with linear model. These models can also offer the effect of confining pressure on stiffness.

4.4 Small-Strain Undrained Compression Behaviour of Bangkok Clay

4.4.1 Introduction

Small-strain undrained compression of Bangkok Clay is investigated in the laboratory using advanced triaxial apparatus which is incorporated local axial and radial strain measurement and bender element system (Yimsiri et al., 2009; Ratananikom, 2009). Isotropically consolidated undrained triaxial compression tests are carried out on both vertically- and horizontally-cut undisturbed specimens to investigate anisotropic behaviour of Bangkok Clay. This section presents comparison between prediction of non-linear KHMCC model against some observed small-strain characteristics behaviour of Bangkok Clay, i.e.: small-strain shear modulus and modulus during undrained compression shearing.

4.4.2 *Review of Experimental Works*

Undisturbed samples were taken from Lad-Prao at depth 0f 10-13 m BGL. The index and physical properties is summarised in Table 4.6.

Table 4.6 Index properties of soil samples (after Yimsiri et al., 2009)

Index Properties	Values
Water content (%)	45 – 60
Liquid Limit , LL (%)	77
Plastic Limit, PL (%)	31
Total Unit Weight, γ (kN/m^3)	16.1 – 17.3

There are four tests were conducted as shown in Table 4.7. The specimens were initially isotropically consolidated to 1 or 2 times of their in-situ isotropic stress. To ensure the test was conducted in fully drainage condition, the constant-rate-stress consolidation was employed at constant rate of 0.05 kPa/min. Then, the strain-controlled condition was applied during undrained compression loading stage with external axial strain rate of approximately 0.15%/hr. This condition was slow enough to prevent a high pore pressure occurred throughout the specimen.

Further, during isotropic consolidation, the small-strain shear modulus G_{vh} and G_{hh} are measured from the vertically-cut and horizontally-cut specimen, respectively.

Table 4.7 Triaxial test program (after Yimsiri et al., 2009)

Test No.	Depth (m)	e_0	p'_0	Direction
CIUC-1V	10.9	1.69	80	Vertical
CIUC-2V	13.1	1.27	100	Vertical
CIUC-5V	13.1	1.31	200	Vertical
CIUC-5H	12.3	12.3	180	Horizontal

The empirical equation in the form suggested by Hardin & Black (1968) is proposed to fit the relationships between G_{max} and p' as shown in Equations (4.3) and (4.4).

$$\frac{G_{vh}}{F(e)} = 6942 p'^{0.102} \tag{4.3}$$

$$\frac{G_{hh}}{F(e)} = 6593 p'^{0.102} \tag{4.4}$$

where $F(e) = \frac{(2.973 - e)^2}{1 + e}$

These results indicate small degree of small-strain shear modulus anisotropy.

4.4.3 Model Comparison

Table 4.8 summarises non-linear KHMCC model. The constant k is obtained from Equation (3.44) with $v = 0.41$ (typical value of K_0 of Bangkok clay is around 0.68 (Shibuya *et. al.*, 2001)). The slope of critical line (M) is observed from the undrained stress response. Finally, kinematic hardening parameter a is determined from procedures which are explained in the previous section. We use data from Test No. CIUC-1V and CIUC-2V in this comparison.

Table 4.8 Summary of non-linear KHMCC model parameters

Test No.	G_{max}	p_r [kPa]	g	k	n	M	a	Direction
CIUC-1V	$\dfrac{G_{vh}}{p_r} = 154\left(\dfrac{p'}{p_r}\right)^{0.102}$	40	154	804	0.102	1.6	6	Vertical
CIUC-2V	$\dfrac{G_{vh}}{p_r} = 264\left(\dfrac{p'}{p_r}\right)^{0.102}$	50	264	1383	0.102	1.8	6	Vertical

Figure 4.20 and Figure 4.21 show comparison of stress-strain and stiffness degradation curves between model prediction and experimental results.
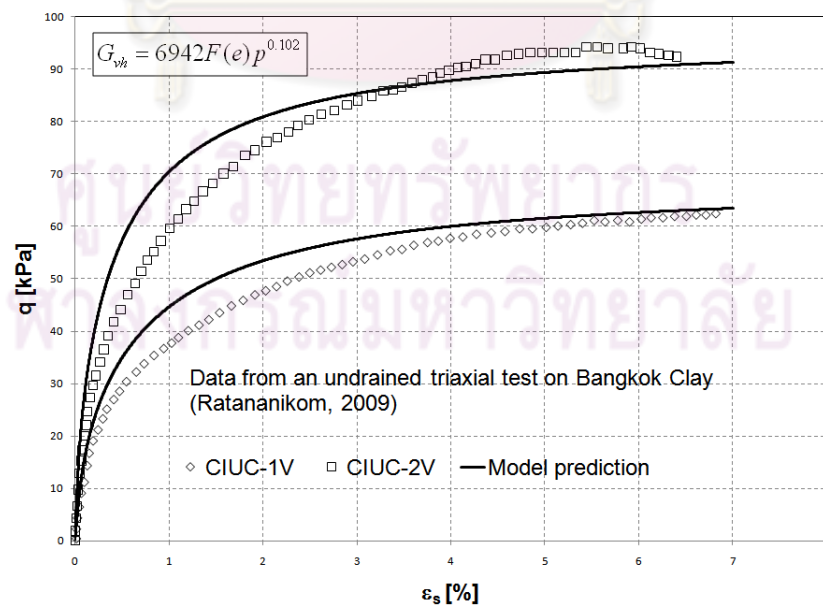
Figure 4.20 Comparison of stress-strain curves between model prediction and experimental results

The graph shows "Data from an undrained triaxial test on Bangkok Clay (Ratananikom, 2009)" with equation $G_{vh} = 6942F(e)p^{0.102}$. The y-axis is "Normalised secant shear modulus G_s/p'_0" and x-axis is "ε_s [%]". Legend: CIUC-1V, CIUC-2V, Model prediction.
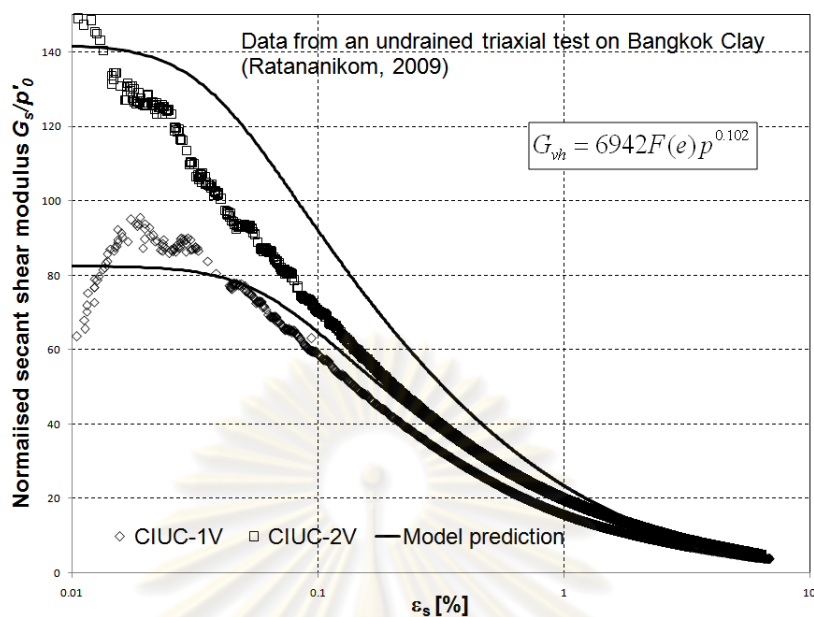
Figure 4.21 Comparison of stiffness degradation curves between model prediction and experimental results

The model prediction shows that the model provides a good prediction on the undrained strength and small-strain shear modulus. The model can also offer the effect of confining pressure on initial stiffness and give a smooth change of stiffness from elastic to plastic behaviour.

4.5   Summary

A comparison between non-linear KHMCC model prediction and experimental results have been presented. Model comparison with small-strain experimental on overconsolidated clay soil (Stallebrass and Taylor, 1997) clearly shows that the developed model with small number of parameters can accurately simulate the key features of small-strain characteristic. Unloading-reloading response of model prediction shows a non-recoverable strain and loading path dependence which are good agreement with the experimental observation.

Model comparison with CK_0UDSS tests of Bangkok Clay (Konkong, 2007) also show that the developed model provides a good prediction on the stress-strain and stress path curve. The model can also offer the effect of confining pressure on stiffness.

Further comparison with small-strain undrained compression test of Bangkok Clay (Yimsiri et al., 2009; Ratananikom, 2009) clearly shows that model prediction provides a good prediction on the undrained strength and small-strain shear modulus. The model can also offer the effect of confining pressure on initial stiffness and give a smooth change of stiffness from elastic to plastic behaviour.

For further application into actual geotechnical engineering boundary value problems, the developed model should be implemented to finite element code. In next chapter a rate-dependent continuous hyperplasticity finite element algorithm is employed.

ศูนย์วิทยทรัพยากร
จุฬาลงกรณ์มหาวิทยาลัย

CHAPTER V.   RATE-DEPENDENT CONTINUOUS HYPERPLASTICITY FINITE ELEMENT ALGORITHM

5.1   Introduction

There are two groups of material behaviour usually involved in the finite element calculation, i.e.: a rate-independent material that is the response is the irrespective of the strain rate or shows some small dependence on the strain rate; and a rate-dependent material that is the state of stress and strain exhibit a time dependence. The first material group can consist of materials such as linear elastic material, non-linear elastic and elasto-plastic material; and second group can consist of linear viscous material, non-linear viscous and elasto-viscoplastic material.

We will not go in detail in these subjects, but in this chapter we will describe rate-independence as the particular case of rate-dependent behaviour to obtain significant simplifications in numerical calculation. A rate-independent finite element calculation can be carried out using a rate-dependent algorithm with an artificial very small viscosity (Owen and Hinton, 1980; Smith and Griffiths, 1998; and Potts and Zdravkovic, 1999).

5.2   Basic Finite Element

The finite element method usually involves the following steps:

(1) Discretisation of the problem into finite number of elements.

The most popular element is isoparametric element which is both the element displacement and geometry are expressed using similar interpolation functions in terms of natural coordinate.

(2) Selection of nodal displacement as primary variables.

Stresses and strains are secondary quantities which are calculated from the nodal displacement.

(3) Derivation of element equations.

To establish the element stiffness matrix, numerical integration such as Gauss Quadrature integration is used, so that stresses and strains are determined at integration points.

(4) Assembly of element equations into global equations.

Because usually global equations have large matrix size, some strategies have been proposed to develop efficient storage algorithm such as skyline method.

(5) Formulation of boundary conditions.

(6) Solving of global equations.

To solve the global equations, Gauss elimination is usually adopted in the calculation.

Figure 5.1 shows the general steps for finite element calculation. The basic finite element theory is based on the assumption of linear material behaviour. As described in Chapter 2 soils do not behave in such a manner, soils behave in such a highly non-linear way. It means that strength and stiffness depending on stress and strain levels. So that, several solution schemes are available to deal with the non-linear constitutive models. Next section describes briefly some solution strategies usually applied in the finite element method. Explanation will be emphasised on the rate-dependent solution scheme or some references call by visco-plastic solution.
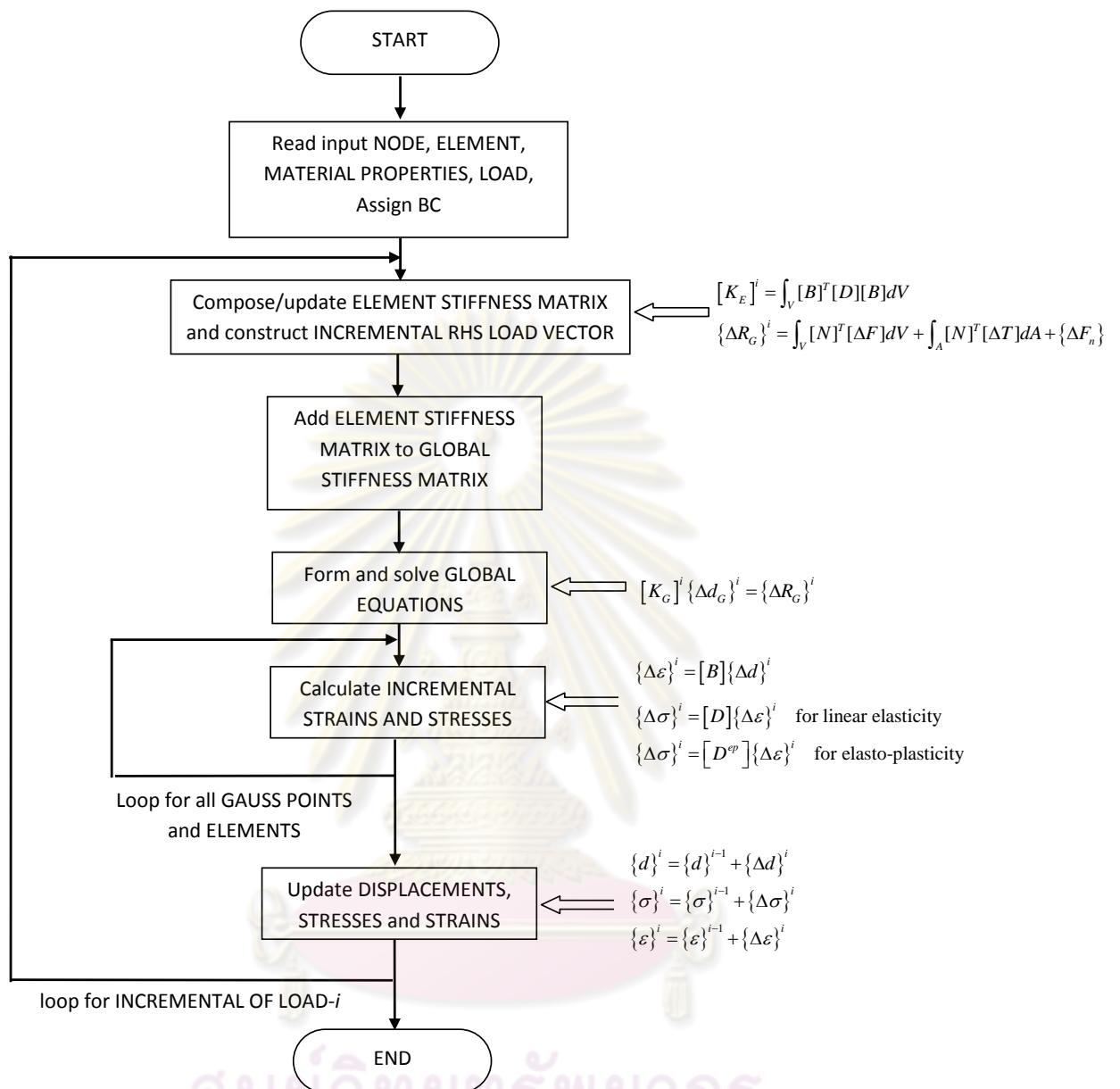
Figure 5.1 General finite element calculation steps

5.3   Non-Linear Finite Element

Principally, the non-linearity of the material can be simply approximated by small increment of piece-wise linear approximation. Some solution schemes are basically proposed to deal with the larger increment of loading (displacement), according to reduce computing time, of course, with an acceptable accuracy.

If the soil is non-linear elastic and/or elasto-plastic, the constitutive matrix [*D*] in Figure 5.1 is no longer constant, but changes with stress and/or strain during

incremental of loading (displacement). Figure 5.2 illustrates several solution schemes for non-linear finite element method.
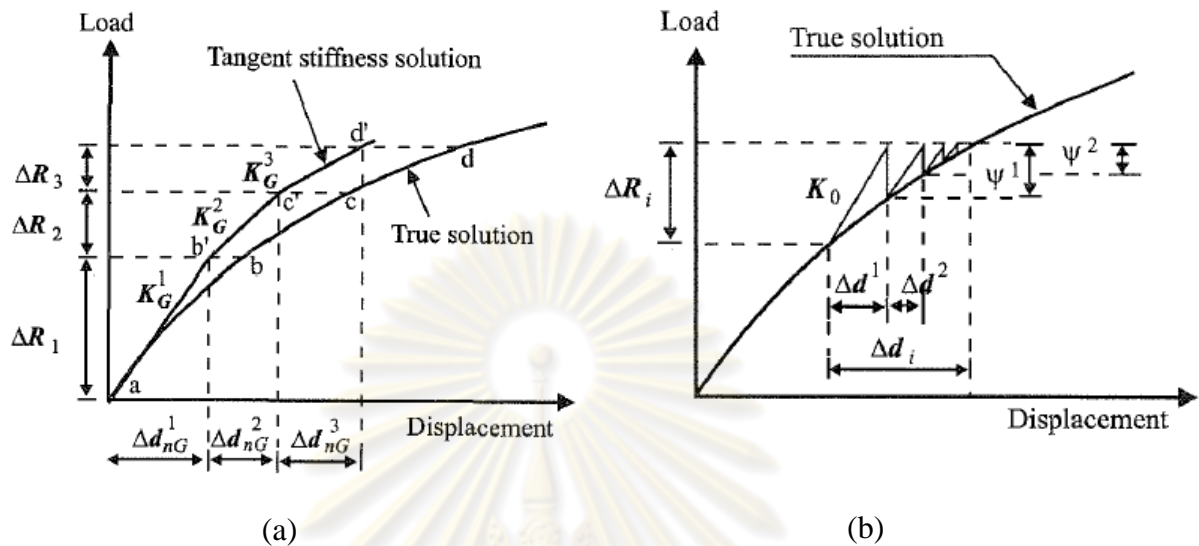
Figure 5.2 Several solution schemes for non-linear finite element (a) tangent stiffness method, (b) Modified Newton Raphson (Potts and Zdravkovic, 1999)

Due to the non-linearity of constitutive behaviour, the governing finite element equation is reduced to the following incremental form:

$$\left[K_G \right]^i \left\{ \Delta d_G \right\}^i = \left\{ \Delta R_G \right\}^i \tag{5.1}$$

where $\left[K_G \right]^i$ is the incremental global stiffness matrix, $\left\{ \Delta d_G \right\}^i$ is the vector of incremental nodal displacement, $\left\{ \Delta R_G \right\}^i$ is the vector of incremental nodal forces and i is the increment number. Regarding to obtain a solution of a boundary value problem (BVP), the Equation (5.1) must be solved for each increment. Then, the final solution is obtained by summing the results of each increment. The incremental global stiffness matrix $\left[K_G \right]^i$ is not constant, but varies over an increment of loading (displacement). As stated before, this variation can be simply accounted by using very large number of small increments. Hence, the solution of Equation (5.1) is not straightforward and different solution strategies exist, to ensure the solution satisfying the four basic requirements of BVP: equilibrium, compatibility, constitutive behaviour and boundary conditions.

In tangent stiffness method or variable stiffness method (Figure 5.2a), the incremental global stiffness matrix $\left[K_G \right]^i$ is assumed to be constant over each increment and is calculated using the current stress state at the beginning of each increment. It is

clearly shows that in order to obtain accurate solution to highly non-linear problems, many small solution increments are required. The solution obtained using this method can drift from the true solution and may not fulfil the basic solution requirements.

The Modified Newton Raphson (MNR) method uses an iterative technique to solve Equation (5.1). The first iteration is essentially similar with the tangent stiffness method. However, the predicted incremental displacements are used to calculate the residual load ψ as illustrated in Figure 5.1b. Further, Equation (5.1) is solved again with this residual load, $\{\psi\}$, forming the incremental RHS vector:

$$\left[K_G\right]^i \left(\{\Delta d_G\}^i\right)^{j+1} = \{\psi\}^j \tag{5.2}$$

The superscript j refers to the iteration number and $\{\psi\}^0 = \{\Delta R_G\}^i$. This process is repeated until the residual load is small. The incremental displacements are equal to the sum of the iterative displacements.

5.4   Rate-dependent method
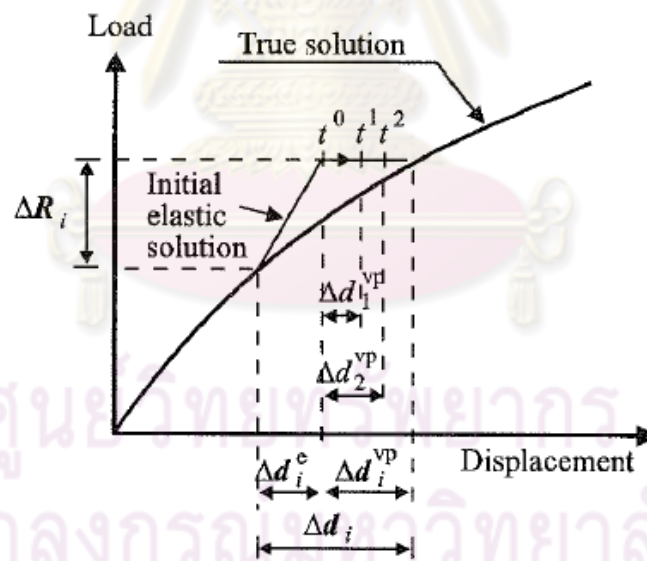
Figure 5.3 Rate-dependent solution scheme for non-linear finite element (Potts and Zdravkovic, 1999)

This method was originally developed for rate-dependent materials (linear elasto-viscoplastic materials). However, in its further application this method is also used to calculate the response of rate-independent materials (non-linear elastic and elasto-plastic materials), see for detail Owen and Hinton (1980); Zienkiewicz and Cormeau (1974).

The process of this method illustrates in Figure 5.3. At the beginning of increment, the incremental global stiffness matrix $[K_G]^i$ is assembled using elastic constitutive matrix $[D]$, so that the visco-plastic strain increment vector at $t = t_0$ is $\{\Delta\varepsilon^{vp}\}_{t=t0}^i = 0$. It means that at the first increment of load and at $t = 0$ the Equation (5.1) is solved using linear elastic relationships and can be re-written using Equation (5.3), according to obtain a first estimate of the nodal displacement.

$$[K_G]_t^i \{\Delta d_G\}_t^i = \{\Delta R_G\}_t^i \tag{5.3}$$

The calculated displacements are correct if the resulting stress state lies within the yield surface, it means that the behaviour is elastic. If the resulting stress states outside the yield surface, the stress state can only be sustained for as short time and visco-plastic straining occurs and increases with time, until the visco-plastic strain rate is insignificant. At this point, the accumulated visco-plastic strain and associated stress change are equal to the incremental plastic strain and stress change respectively. The flowchart of this method for elasto-plastic finite element is presented in Figure 5.4. From this we can develop flowchart for continuous hyperplasticity finite element as shown in Figure 5.5.

5.5   Summary

Rate-independence as the particular case of rate-dependent behaviour can be carried out using an artificial very small viscosity (Owen and Hinton, 1980; Smith and Griffiths, 1998; and Potts and Zdravkovic, 1999). There are other several solution schemes available to deal with the non-linear constitutive models such as Tangent Stiffness and Modified Newton Raphson Method. Some of them are basically proposed to deal with the larger increment of loading (displacement), according to reduce computing time, of course, with an acceptable accuracy and to satisfy the four basic requirements of BVP: equilibrium, compatibility, constitutive behaviour and boundary conditions. However, the advantage of the rate-dependent algorithm is that we can actually define μ as a "true" viscosity coefficient for analysing or modelling actual creep behaviour.

```
                          ┌──────────┐
                          │  START   │
                          └────┬─────┘
                               │
          ┌────────────────────▼────────────────────┐
          │  Read input NODE, ELEMENT, MATERIAL      │
          │  PROPERTIES, LOAD, Assign BC, {Δε^vp}^{t=t0}=0 │
          └────────────────────┬────────────────────┘
  (A)───────────────────────────┘
```

Read input NODE, ELEMENT, MATERIAL PROPERTIES, LOAD, Assign BC, $\left\{\Delta\varepsilon^{vp}\right\}^{t=t0}=0$

Compose/update ELEMENT STIFFNESS MATRIX and construct INCREMENTAL RHS LOAD VECTOR

$$\left[K_E\right]_t^i = \int_V [B]^T[D][B]dV$$

$$\left\{\Delta R_G\right\}_t^i = \int_V [N]^T[\Delta F]dV + \int_A [N]^T[\Delta T]dA + \left\{\Delta F_n\right\}$$

Add ELEMENT STIFFNESS MATRIX to GLOBAL STIFFNESS MATRIX

Form and solve GLOBAL EQUATIONS

$$\left[K_G\right]_t^i \left\{\Delta d_G\right\}_t^i = \left\{\Delta R_G\right\}_t^i$$

Calculate INCREMENTAL STRAINS AND STRESSES

$$\left\{\Delta\varepsilon\right\}_t^i = [B]\left\{\Delta d\right\}_t^i$$

$$\left[\Delta\sigma\right]_t^i = [D]\left(\left\{\Delta\varepsilon\right\}_t^i - \left\{\Delta\varepsilon^{vp}\right\}_t^i\right)$$

Add INCREMENTAL STRESSES at time t to accumulated stress from previous increment load

$$\left\{\sigma\right\}_t^i = \left\{\sigma\right\}_t^{i-1} + \left[\Delta\sigma\right]_t^i$$

$F\left(\sigma_t^i\right) < 0$

Evaluate $F\left(\sigma_t^i\right)$

$F\left(\sigma_t^i\right) \geq 0$

loop for all GAUSS POINTS

End of GAUSS POINTS

loop for all GAUSS POINTS

Calculate VISCO-PLASTIC STRAIN RATE and update INCREMENTAL VISCO-PLASTIC STRAIN

$$\left\{\Delta\varepsilon^{vp}\right\}_{t+1}^i = \left\{\Delta\varepsilon^{vp}\right\}_t^i + \Delta t\left\{\dot\varepsilon^{vp}\right\}_t^i$$

Calculate INCREMENTAL VISCO-PLASTIC STRESS and NODAL FORCE EQUIVALENT

$$\left\{\Delta\sigma^{vp}\right\}_t^i = [D]\Delta t\left\{\dot\varepsilon^{vp}\right\}_t^i$$

$$\left\{\Delta f\right\}_t^i = \sum_{\text{all gauss points}} [B]^T\left\{\Delta\sigma^{vp}\right\}_t^i$$

End of GAUSS POINTS

Update INCREMENTAL RHS LOAD VECTOR $\left\{\Delta R_G\right\}$

$$\left\{\Delta R_G\right\}_{t+1}^i = \left\{\Delta R_G\right\}_t^i + \sum_{\text{all elements}} \int_V \left\{\Delta f\right\}_t^i dV$$

loop for all ELEMENTS

No

Evaluate $\left\{\dot\varepsilon^{vp}\right\}_t^i \approx 0$

loop for TIME STEPPING-t

Yes

(B)

Figure 5.4 Rate-dependent elasto-plastic finite element calculation steps

ศูนย์วิทยทรัพยากร

จุฬาลงกรณ์มหาวิทยาลัย

START

Read input NODE, ELEMENT, MATERIAL PROPERTIES, LOAD, Assign BC, $\{\Delta\alpha\}^{t=t0} = 0$

A

Compose/update ELEMENT STIFFNESS MATRIX and construct INCREMENTAL RHS LOAD VECTOR

$$[K_E]_t^i = \int_V [B]^T [D][B] dV$$

$$\{\Delta R_G\}_t^i = \int_V [N]^T [\Delta F] dV + \int_A [N]^T [\Delta T] dA + \{\Delta F_n\}$$

Add ELEMENT STIFFNESS MATRIX to GLOBAL STIFFNESS MATRIX

Form and solve GLOBAL EQUATIONS

$$[K_G]_t^i \{\Delta d_G\}_t^i = \{\Delta R_G\}_t^i$$

Calculate INCREMENTAL STRAINS AND STRESSES

$$\{\Delta\varepsilon\}_t^i = [B]\{\Delta d\}_t^i \quad ; \quad \{\dot\alpha\}_t^i = \left\{\frac{\partial w}{\partial\hat\chi}\right\}_t^i$$

$$[\Delta\sigma]_t^i = \left[-\frac{\partial^2 E}{\partial\sigma^2}\right]\left(\{\Delta\varepsilon\}_t^i - \left(\int_0^1\left[-\frac{\partial^2 E}{\partial\hat\alpha\,\partial\sigma}\right]\{\dot\alpha\}_t^i d\eta\right)\Delta t\right)$$

Add INCREMENTAL STRESSES at time t to accumulated stress from previous increment load

$$\{\sigma\}_t^i = \{\sigma\}_t^{i-1} + [\Delta\sigma]_t^i$$

$$\{\chi\}_t^i = \{\sigma\}_t^i - H_p\{\Delta\alpha_p\}_t^i - \frac{2}{3}H_q\{\Delta\alpha'\}_t^i$$

$F(\chi_t^i) < 0$

Evaluate $F(\chi_t^i)$

$F(\chi_t^i) \geq 0$

loop for N YIELD SURFACES and for all GAUSS POINTS

End of GAUSS POINTS

loop for N YIELD SURFACES and for all GAUSS POINTS

Calculate PLASTIC STRAIN RATE and update INCREMENTAL PLASTIC STRAIN

$$\{\Delta\alpha\}_{t+1}^i = \{\Delta\alpha\}_t^i + \Delta t\{\dot\alpha\}_t^i$$

Calculate INCREMENTAL PLASTIC STRESS and NODAL FORCE EQUIVALENT

$$\{\Delta\sigma^{vp}\}_t^i = [D]\Delta t\{\dot\alpha\}_t^i$$

$$\{\Delta f\}_t^i = \sum_{\text{all gauss points}} [B]^T\{\Delta\sigma^{vp}\}_t^i$$

End of GAUSS POINTS

Update INCREMENTAL RHS LOAD VECTOR $\{\Delta R_G\}$

$$\{\Delta R_G\}_{t+1}^i = \{\Delta R_G\}_t^i + \sum_{\text{all elements}}\int_V\{\Delta f\}_t^i dV$$

loop for all ELEMENTS

No

loop for TIME STEPPING-t

Evaluate $\{\dot\alpha\}_t^i \approx 0$

Yes

B

Figure 5.5 Rate-dependent continuous hyperplasticity finite element calculation steps

CHAPTER VI. CONCLUSIONS AND DEVELOPMENT FOR FUTURE RESEARCH

6.1   Conclusions

As stated in the Chapter 1 Introduction, this study is expected to provide a theoretical background and numerical implementation for those who are interested in the advancement of critical state soil model and may give a light to model the complicated behaviours of soils observed from advanced small-strain laboratory testing under the framework of hyperplasticity. Followings are concluding remarks from this study.

6.1.1   Recent Issues on the Soil Behaviour

It is believed that soil is one of natural material which behaves very complex. The study of soil behaviour increases since progressive developments of advanced soil laboratory tests such as directional shear cell (Arthur & Menzies, 1972), hollow cylinder apparatus (High et al., 1983) and bender element system (e.g. Viggiani & Atkinson, 1995); and the instrumented soil tests such as strain gauges, electrolevels, proximity (Hird & Yung, 1989) and local-deformation transducer.

Many experimental findings are addressed to pre-failure deformation behaviour which is in the past just assumed as a linear elastic relationships. In fact, in soils the true linear elastic region is often negligibly small and plastic yielding starts almost immediately with straining. Some findings from experimental investigations can be summarised as follows:

 (1) The stress-strain characteristic of soils is non-linear and irreversible, in that the initial soil stiffness or small-strain tangent stiffness depends on the stress level. It is also affected by other variables, such as the voids ratio, anisotropic stress state, and/or the preconsolidation pressure (Hardin, 1978; Houlsby & Wroth, 1991; Viggiani, 1992; Rampello *et al*., 1994) and others.

 (2) Soil behaviour is affected by orientation or its deposited direction, so that soil is classified as an anisotropic material (Seah, 1990; Zdravkovic, 1996; Zdravkovic & Jardine, 2000) and others.

 (3) Soil has a "memory", so that the stress-stain behaviour of soil is depends on the current state and stress history or consolidation history (after Casagrande, 1932; Holtz & Kovacs, 1981); and recent stress history (Som, 1968; Atkinson, 1973, 1990).

(4) Initial stress-strain behaviour of many soils is much stiffer than indicated by conventional strain (intermediate to large strain) measurement. It also exhibits a non-linear behaviour (Jardine, Symes and Burland, 1984).

(5) Soils exhibit time dependent behaviour as well as plastic deformation, so that soils are also called as viscous material (Mitchell and Soga, 2005).

6.1.2 *Recent Advanced Soil Constitutive Models*

Many advanced soil constitutive models based on different concepts have been proposed. In fact, it is believed that each model can be valid within its own local realm, and that no universal constitutive model has yet been developed that is valid for all materials under all conditions. There are three major categorises of recent advanced soil models which are addressed to weak point of critical state models, i.e.: bounding surface model, multiple surfaces model and hypoplasticity.

Although, in principally the bounding surface models more efficient than multiple surfaces, but they still have three important shortcomings i.e: (1) They often require the choice of a number of somewhat arbitrary functions; (2) often the functions without obvious physical meaning; (3) they usually fail to describe the effects of the immediate past history.

Multiple surface models are the most promising approach, but they also still have some drawbacks, i.e.: (1) they result in a large number of material parameters to be specified; (2) they also result in considerable amount of computation; (3) many of them are inherently complex.

Hypoplasticity model, which is only developed and discussed within few researches and has two shortcomings: (1) The constitutive model basically is not based on definite physical meanings, (2) The relation between stress rate tensor and stretching tensor is nonlinear, which make it very difficult to solve boundary value problems because an explicit stiffness matrix based on this model cannot be obtained easily and it has no any evidence of solving this problem mathematically and numerically.

Another issue is that since constitutive models relate to physical phenomena, they must be developed without violate certain principles or axioms that govern the physical phenomena such as the laws of thermodynamics. Hyperplasticity framework which is developed by multiple surfaces describes the behaviour of soils both for clay and sand, associative or non associative flow within a rigorous, compact, and consistent framework using thermodynamics principles.

The other reasons are this framework models could be developed without the need for additional *ad hoc* assumptions and procedures, and it makes considerable use of potential function and multiple internal variables to predict entire stress-strain

response of a material subject to a specified sequence of stress or strain increment. Furthermore, some drawbacks of multiple surfaces can be eliminated by introducing an infinite number of internal variables. This idea leads to the concept of an internal function rather than internal variables.

6.1.3   *Model Development and Numerical Implementation*

The main reason to develop a continuous hyperplasticity non-linear KHMCC model is fact that the stress-strain characteristic of soils is non-linear and irreversible, in that the initial soil stiffness or small-strain tangent stiffness depends on the stress level. Formulation of elastic part of non-linear KHMCC's Gibbs free energy in form of power function of pressure is addressed to incorporate this behaviour. An approach to determine the necessary parameters obtained from experimental tests for regulating small-strain stiffness characteristic in form of power function of pressure has been presented. For simplicity, the stiffness factor for the kinematic hardening has been made as power function of initial preconsolidation pressure.

The rate-dependent multisurface hyperplasticity algorithm using strain driven forward-Euler integration scheme is employed in this study to reduce complexity of treatment from numerical error. It is also shown that the numerical stability of rate-dependent algorithm is clearly affected by the increment of time step. It is observed that the stress-strain response smoother when the number of yield surfaces is increased. Numerical study also indicate that running time of multiple kinematic hardening model increases linearly against increasing number of yield surfaces. However, availability of high-speed computer can significantly reduce time computation.

Validation of the numerical model implementation against analytical solution of simple idealised undrained triaxial test concludes that the model has been successfully implemented. Finally, numerical demonstrations show that the non-linear KHMCC model can demonstrate some important aspects in soil mechanics such as small-strain stiffness, effects of immediate past stress history behaviour, a hysteresis loop and smooth transition of stiffness during unloading-reloading cycles. Dependence of small-strain stiffness on pressure is clearly shown. This model can explains the fact that the openness of the hysteresis loop increases with strain amplitude. Model response on unloading-reloading behaviour also shows non-recoverable strain amplitude.

6.1.4   *Some Comparisons to Experimental Data of Clay Soils*

Model comparisons with experimental data are performed using single-element calculation. There are three experimental data has been used to validate the model performance, i.e.: small-strain experimental on overconsolidated clay soil (Stallebrass

and Taylor, 1997), CK_0UDSS tests of Bangkok Clay (Konkong, 2007), and small-strain undrained compression test of Bangkok Clay (Yimsiri et al., 2009; Ratananikom, 2009).

An experimental undrained triaxial test on Speswhite kaolin (Stallebrass & Taylor, 1997) has been selected to show performance of the developed model in characterising a loading path dependence and non-linearity at small-strain in overconsolidated clay. Model comparison clearly shows that the developed model with small number of parameters can accurately simulate the key features of small-strain characteristic. A plot of tangent shear stiffness against stresses response from the developed model clearly shows a dependence of small-strain with stress level which is good agreement with the experimental observation. The model response give a better prediction than 3-SKH model might be because the developed model using higher number of yield surfaces. However, the strong point from the developed model is we can generate more number of yield surfaces, theoretically infinite number of yield surfaces, in easy way by introducing an internal function. Furthermore, unloading-reloading response of model prediction shows a non-recoverable strain and loading path dependence which are a good agreement with the experimental observation.

Model comparison with monotonic loading of CK_0UDSS tests of Bangkok Clay (Konkong, 2007) also show that the developed model provides a good prediction on the stress-strain and stress path curve. The model can also offer the effect of confining pressure on stiffness.

Further comparison with small-strain undrained compression test of Bangkok Clay (Yimsiri et al., 2009; Ratananikom, 2009) clearly shows that model prediction provides a good prediction on the undrained strength and small-strain shear modulus. The model can also offer the effect of confining pressure on initial stiffness and give a smooth change of stiffness from elastic to plastic behaviour.

6.1.5   *Rate-dependent Continuous Hyperplasticity Finite Element Algorithm*

There are other several solution schemes available to deal with the non-linear constitutive models such as Tangent Stiffness mehod, Modified Newton Raphson and rate-dependent or visco-plastic method. Some of them are basically proposed to deal with the larger increment of loading (displacement), according to reduce computing time, of course, with an acceptable accuracy and to satisfy the four basic requirements of BVP: equilibrium, compatibility, constitutive behaviour and boundary conditions.

Rate-independence as the particular case of rate-dependent behaviour can be carried out using an artificial very small viscosity (Owen and Hinton, 1980; Smith and Griffiths, 1998; and Potts and Zdravkovic, 1999). This method was originally developed for rate-dependent materials (linear elasto-viscoplastic materials).

However in this study, the rate-dependent finite element algorithm is employed according to consider an actual rate-dependent problem in soil mechanics such in creep behaviour. We can actually define μ as a "true" viscosity coefficient for this kind of analysis.

6.2 Development for Future Research

Although, the developed model can describe almost all important pre-failure deformation behaviours in both normally and overconsolidated clay such as recent stress history behaviour, non-linearity at small-strain, initial stiffness dependence on pressure, as well as rate effect or rate-dependent behaviour (because this model is developed using rate-dependent calculation, it means that we can actually define μ as a "true" viscosity coefficient). But it still has several important shortcomings and requires further work in the future are as follows:

(1) Strength prediction of developed model for soils on dry side of CSL is over prediction; this is because the model is developed based on the CSSM. The softening behaviour should be explored in the future in order to realize the promising features of the model on soil destructure.

(2) To investigate applicability of other integration schemes according to reduce steps of calculation and to improve accuracy when employing large increment of loading (displacement). Thirapong et al. (2009) has been initially investigated the applicability of consistent integration scheme to kinematic hardening multisurface hyperplasticity in one-dimensional problem using Iwan model. They concluded that this scheme can raise high accuracy despite of large increments as shown in Figure 6.1.
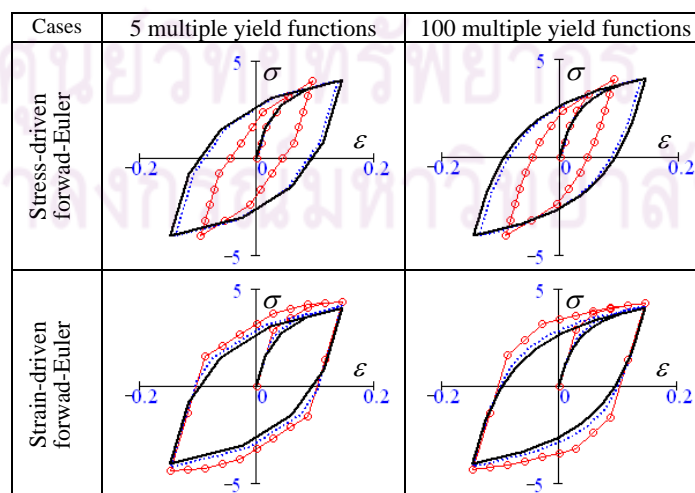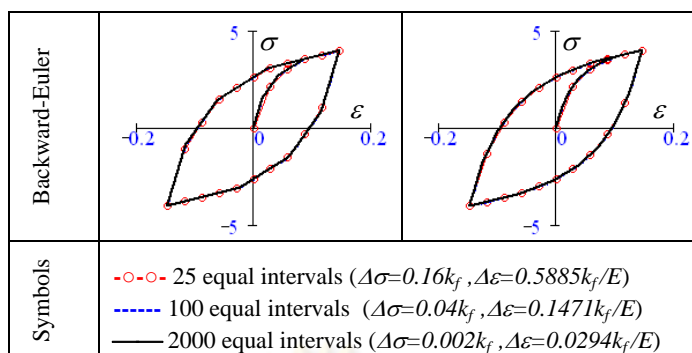
Figure 6.1 Comparisons of analysed results obtained from stress-driven/strain-driven forward-Euler schemes and backward-Euler scheme with variation on numbers of multiple yield functions and sizes of stress/strain increments (Thirapong et al., 2009)

Further research development for applying this algorithm in continuous hyperplasticity framework should be encouraged.

(3) Although the hysteresis loop and unloading-reloading response is predicted well by the developed model, further work should be carried out to see performance of developed model in larger problem of cyclic loading.

(4) Implementation of the developed model into finite element code should be conducted in the future to evaluate performance of the developed model in real geotechnical boundary value problems. The developed rate-dependent continuous hyperplasticity finite element algorithm can be used in this future work.

REFERENCES

Addenbrooke, T.I., Potts, D.M., and Puzrin, A.M. (1997), "The influence of pre-failure soil stiffness on the numerical analysis of tunnel construction", Geotechnique, Vol. 47, No. 3, pp. 693-712

Apriadi, Dedi, Likitlersuang, Suched, Pipatpongsa, Thirapong and Ohta, Hideki (2009), "On the numerical implementation of hyperplasticity non-linear kinematic hardening modified cam clay model", The IES Journal Part A: Civil & Structural Engineering, Vol. 2, No. 3, pp. 187-201

Arthur, J.R.F. and Menzies, B.K. (1972), "Inherent anisotropy in a sand", Geotechnique, Vol. 22, No. 1, pp. 115–129

Atkinson, J.H., Richardson, D., and Stallebrass, S.E. (1990), "Effect of recent stress history on stiffness of overconsolidated soil", Geotechnique, Vol. 40, pp. 531-540

Atkinson, J.H. and Sallfors, G. (1991), "Experimental determination of stress-strain-time characteristics in laboratory and in-situ tests", Proc. of X ECSMFE, Florence, (Eds. Associazione Geotecnica Italiana), pp. 915-956 Rotterdam: A. A. Balkema

Atkinson, J.H. and Stallebrass, S.E. (1991), "A model for recent stress history and non-linearity in the stress-strain behaviour of overconsolidated soil", Proc. 7th Int. Cof. On Computer Methods and Advances in Geomechanics, Cairns, Vol. 1, pp. 555-560

Borja, R.I. et al. (2003), "On the numerical integration of three-invariant elastoplastic constitutive models", Comput. Methods Appl. Mech. Engrg. 192, pp. 1227–1258

Chen, W.F. and Baladi, G.Y. (1985), "Soil plasticity: theory and implementation", Elsevier Science Publisher B.V., NY

Collins, I.F. and Houlsby G.T. (1997), "Application of thermomechanical principles to the modelling of geotechnical materials", Proc. Royal Society of London, Series A, Vol. 453, pp. 1975-2001

Cormeau, I.C. (1975), "Numerical stability in quasi-static elasto-viscoplasticity", Int. J. Num. Meth. Eng., Vol. 9, No. 1, pp. 109-127

Dafalias, Y. and Herrmann, L.R. (1982), "Bounding surface formulation of soil plasticity", Soil Mechanics Cyclic and Transient Loads (G. N. Pande and O. C. Zienkiewicz, eds), Chapter 10, pp 253-282, New York, John Wiley & Sons

Desai, C.S. and Siriwardane, H.J. (1984), "Constitutive laws for engineering materials with emphasis on geologic materials", Prentice-Hall, Inc., NJ

Drucker, D. C. and Prager, W. (1952), "Soil mechanics and plastic analysis or limit design", Quarterly of Applied Mechanics, Vol. 10(2), pp. 157-165

Einav, I., Puzrin, A.M and Houlsby, G.T. (2000), "Continuous hyperplastic models for overconsolidated clays", Proc. Symp. on Mathematical Models in Geomechanics, Scilla di Reggio Calabria, 19-22 Sept., Vol. 37, No. 5/6, pp. 515-523

Graham, J. and Houlsby, G.T. (1983), "Anisotropic elasticity of a natural clay", Geotechnique, Vol. 33, No. 2, pp. 165-180

Gunn, M.J. (1993), "The prediction of surface settlement profiles due to tunnelling. In Predictive soil mechanics", Proc. Wroth Memorial Symp. Oxford (Eds G.T. Houlsby and A.N. Schofield), London: Thomas Telford, pp. 304–316

Hardin, B. O. (1978), "The nature of stress–strain behaviour for soils. Earthquake engineering and soil dynamics", Proceedings of the ASCE Geotechnical Engineering Division Specialty Conference, Pasadena, pp. 3–90

Hight, D.W, Gens, A. & Symes, M.J. (1983), "The development of a new hollow cylinder apparatus for investigating the effects of principal stress rotation in soils", Geotechnique 33(4), pp. 355-383

Hight, D.W, Gens, A. & Symes, M.J. (1983), "The development of a new hollow cylinder apparatus for investigating the effects of principal stress rotation in soils", Geotechnique, Vol. 33, No. 4, pp. 355-383

Hird, C.C. and Yung, P.C.Y. (1989), "The use of proximity transducer for local strain measurement in triaxial tests", Geotechnical Testing Journal, Vol. (12), No. 4, pp. 353-369

Houlsby, G.T. (1981), "A study of plasticity theories and their applicability to soils", Ph.D. Thesis, University off Cambridge.

Houlsby, G.T. (1985), "The use of a variable shear modulus in elastic–plastic models for clays", Computers and Geotechnics 1, pp. 3–13

Houlsby, G. T. & Wroth, C.P. (1991), "The variation of the shear modulus of a clay with pressure and overconsolidation ratio", Soils Found. 31, No. 3, pp. 138–143.

Houlsby, G.T. (1999), "A model for the variable stiffness of undrained clay", Proc. Int. Symp. on Pre-Failure Deformation of Soils, Torino, 26-29 September, Balkema, ISBN 9058090760, Vol. 1, pp. 443-450

Houlsby, G.T. and Puzrin, A.M. (1999), "An approach to plasticity based on generalised thermodynamics", Proc. of the International Symposium on Hypoplasticity, Horton, Greece, pp. 23 3-245

Houlsby, G.T. and Puzrin, A.M. (2000), "A thermomechanical framework for constitutive models for rate-independent dissipative materials", International Journal of Plasticity, Vol. 16 No. 9, pp. 1017-1047

Houlsby, G.T. and Puzrin, A.M. (2002), "Rate-dependent plasticity models derived from potential functions", Journal of Rheology, Vol. 46, No. 1, pp. 113-126.

Houlsby, G.T., Amoroso, A., and Rojas, E. (2005), "Elastic moduli of soils dependent on pressure: a hyperplastic formulation", Geotechnique, Vol. 55, No. 5, pp. 383-392

Houlsby, G.T. and Puzrin, A.M. (2006), "Principles of hyperplasticity: an approach to plasticity theory based on thermodynamics principles", Springer-Verlag London Limited, London

Iizuka,A. and Ohta,H. (1987), "A determination procedure of input parameters in elasto-viscoplastic finite element analysis", Soils and Foundations, Vol.27, No.3, pp.71-87

Iwan, W.D. (1967), "On the class of models for the yielding behavior of continuous and composite systems", Transactions of the American Society of Mechanical Engineers, Journal of Applied Mechanics, Vol. 34, pp. 612-617

Jardine, R.J., Symes, M.J., and Burland, J.B. (1984), "The measurement of soil stiffness in the triaxial apparatus", Geotechnique, Vol. 34, No. 3, pp. 323-340

Jardine, R.J. (1985), "Investigations of pile-soil behaviour with special reference to the foundations offshore structures", Ph.D. thesis, University of London

Jardine, R.J., Potts, D.M., Fourie, A.B., and Burland, J.B. (1986), "Studies of the influence of non-linear stress-strain characteristics in soil-structure interaction", Geotechnique, Vol. 36, No. 3, pp. 377-396

Jardine, R.J., St John, H.D., Hight, D.W. & Potts, D.M. (1991), "Some practical applications of a non-linear ground model", Proc. 10th Eur. Conf. On Soil Mech. and Found. Engng, Florence, 1, pp. 223-228.

Jardine, R.J. (1992), "Some observations on the kinematic nature of soil stiffness", Soils Foundations, Japan Soc. Soil Mech. and Fdn Engng, 32, No. 2, pp. 111-124

Kohata, Y., Tatsuoka, F., Wang, Lo, Jiang, G. L., Hoques, E. & Kodaka, T. (1997), "Modelling the non-linear deformation properties of stiff geomaterials", Geotechnique, 47, No. 3, pp. 563–580

Kolymbas, D. (1977), "A rate-dependent constitutive equation for soils", <u>Mech. Res. Comm.</u>, Vol. 4, pp. 367-372

Kolymbas, D. (2000), "Introduction to hypoplasticity", <u>Advances in geotechnical engineering and tunnelling</u>, volume 1, Balkema

Konkong, N. (2007), "Cyclic undrained shear behaviour of bangkok clay using direct simple shear apparatus", <u>Master Thesis</u>, Chulalongkorn University

Ladd C.C. (1991), "Stability Evaluation during Staged Construction". The Twenty-Second Karl Terzaghi Lecture, <u>Journal of Geotechnical Engineering</u>, ASCE, Vol. 117, No. 4, pp. 540-615

Likitlersuang, S. and Houlsby, G.T. (2003), "A hyperplasticity model for clay behaviour: an application to bangkok clay," <u>D.Phil. Thesis</u>, Oxford University.

Likitlersuang, S. and Houlsby, G.T. (2006), "Development of hyperplasticity model for soil mechanics", <u>International Journal for Numerical and Analytical Method in Geomechanics</u>, No. 30, pp. 229-254.

Likitlersuang, S. and Houlsby, G.T. (2007), "Predictions of a continuous hyperplasticity model for bangkok clay", <u>Geomechanics and Geoengineering</u>, Volume 2, Issue 3, pp. 147 - 157

Matsuoka, H. and T. Nakai (1974), "Stress-deformation and strength characteristics of soil under three different principal stresses" <u>Proceedings, JSCE</u>, no. 232, Dec, 1974, pp. 59-70

Mitchell, J.K. and Soga, K. (2005), "Fundamentals of soil behavior", 3rd Edition, John Wiley and Sons, 577pp, New York

Mroz, Z. (1967), "On the description of anisotropic workhardening", <u>J. Mech. Phys. Solids</u>, Vol. 15, pp. 163-175

Mroz, Z. and Norris, V.A. (1982), "Elastoplastic and viscoplastic constitutive models for soils with application to cyclic loading", <u>Soil Mechanics Cyclic and Transient Loads (G. N. Pande and O. C. Zienkiewicz, eds)</u>, Chapter 8, pp. 173-218, New York, John Wiley & Sons

Owen, D.R.J. and Hinton, E. (1980), "Finite element in plasticity: Theory and Practice", Pineridge Press, Swansea

Pennington, D. S., Nash, D. F. T. & Lings, M. L. (1997), "Anisotropy of G0 shear stiffness in Gault clay", <u>Geotechnique</u>, Vol. 47, No. 3, pp. 391–398

Potts, D.M., and Ganendra, D. (1994), "An evaluation of substepping and implicit stress point algorithm", <u>Comput. Methods Appl. Mech. Engrg.</u>, Vol.119, pp. 341-354

Potts, D.M. and Zdravkovic, L. (1999), "Finite element analysis in geotechnical engineering Volume I, II": Theory and Application, Tomas Telford, ISBN 0727727532

Potts, D.M. (2003), "Numerical analysis: a virtual dream or practical reality?", Geotechnique, Vol. 53, No. 6, pp. 535-573

Prevost, J.H. (1978), "Plasticity theory for soil stress-strain behaviour", Proceedings of the American Society of Civil Engineers, Journal of the Engineering Mechanics Division, Vol. 104, No. EM5, October, pp. 1177-1194

Puzrin, A.M. and Burland, J.B. (1996), "A logarithmic stress-strain function for rocks and soils", Geotechnique, Vol. 46, No. 1, pp. 157-164

Puzrin, A.M. and Burland, J.B. (1998), "Non-linear model of small-strain behaviour of soils", Geotechnique, Vol. 48, No. 2, pp. 217-233

Puzrin, A.M. and Houlsby, G.T. (2001a), "Strain-based plasticity models for soils and the BRICK model as an example of hyperplasticity approach", Geotechnique, Vol. 51, No. 2, pp. 169-172

Puzrin, A.M. and Houlsby, G.T. (2001b), "Fundamentals of kinematic hardening hyperplasticity", International Journal of Solids and Structures, Vol. 38, pp 377 1-3794

Puzrin, A.M. and Houlsby, G.T. (2001c) "On the non-intersection dilemma in multi-surface plasticity", Geotechnique, Vol. 51, No. 4, pp. 369-372

Puzrin, A.M. and Houlsby, G.T. (2001d), "A thermomechanical framework for rate-independent dissipative materials with internal functions", International Journal of Plasticity, Vol. 17, pp. 1147-1165

Puzrin, A.M. and Houlsby, G.T. (2003), "Rate-dependent hyperplasticity with internal functions", Proceedings of the American Society of Civil Engineers, Journal of the Engineering Mechanics Division, Vol. 129, No. 3, March, pp. 252-263

Rampello, S., Silvestri, F. & Viggiani, G. (1994), " The dependence of G0 on stress state and history in cohesive soils", Proc. 1st Int. Conf. on pre-failure deformation characteristics of geomaterials, Sapporo 2, pp. 1155–1160

Rampello. S., Viggiani, G. M. B. & Amorosi, A. (1997), "Small-strain stiffness of reconstituted clay compressed along constant triaxial effective stress ratio paths", Geotechnique, Vol. 47, No. 3, pp. 475–489

Ratananikom, W. (2009), "Pre failure stress strain behaviour and strength of Bangkok Clay", Ph.D. Thesis, Chulalongkorn University, Thailand (In prep).

Roscoe, K. H., Schofield, A. N. and Thurairajah, A. (1963), "Yielding of clays in state wetter than critical" Geotechnique, Vol. 13, No. 3, pp. 211-240

Roscoe, K.H. and Burland, J.B. (1968), "On the generalised behaviour of 'wet' clay", Engineering Plasticity, (Heyman, J. and Leckie, F.A. eds.), Cambridge University Press, pp. 535-610

Schofield, A.N. and Wroth, C.P. (1968), "Critical state soil mechanics", McGraw Hill, London

Seah, T.H. (1990), "Anisotropy of normally consolidated Boston blue clay", Sc.D. Thesis, MIT.

Shibuya, S., Tamrakar, S.B., and Theramast, N. (2001), "Geotechnical site characterization on engineering properties of Bangkok Clay", Geotechnical Engineering, SEAGS, Vol. 32, No. 3, pp. 139-151

Smith, I.M. and Griffiths, D.V. (1998), "Programming the finite element method", Third Ed., John Wiley and Sons, Ltd., England

Smith, P.R., Jardine, R.J., and Hight, D.W. (1992), "The yielding of Bothkennar clay", Geotechnique, Vol. 42, No. 2, pp. 257-274

Soga, K., Nakagawa, K., and Mitchell, J.K. (1995), "Measurement of stiffness degradation characteristics of clays using a torsional shear device", First International Conference on Earthquake Geotechnical Engineering, Tokyo, Nov. 14-16, pp. 107-112

Stallebrass, S.E. (1990), "The effect of recent stress history on the deformation of overconsolidated soils", Ph.D. thesis, City University

Stallebrass, S.E., and Taylor, R.N. (1997), "The development and evaluation of a constitutive model for the prediction of ground movements in overconsolidated clay", Geotechnique, Vol. 47, No. 2, pp. 235-254

Tanizawa, F., Teachavorasinskun, S., Yamaguchi, J., Sueoka, T. & Goto, S. (1994), "Measurement of shear wave velocity of sand before liquefaction and during cyclic mobility", Proceedings of the international symposium on pre-failure deformation characteristics of geomaterials (eds S. Shibuya, T. Mitachi and S. Miura), Vol. 1, pp. 63–68. Rotterdam: Balkema

Teachavorasinskun, S., Thongchim, P., and Lukkunaprasit, P. (2001), "Shear modulus and damping ratio of clay during undrained cyclic loading", Geotechnique, Vol 51, No. 5, pp. 467-470

Teachavorasinskun, S. and Amornwithayalax, T. (2002) "Elastic shear modulus of Bangkok clay during undrained triaxial compression", Geotechnique, Vol. 52, No. 7, pp. 537-540

Thirapong Pipatpongsa, Dedi, Apriadi, Suched, Likitlersuang, Hideki, Ohta (2009), "Consistent integration for Iwan spring model under multisurface hyperplasticity framework", <u>JSCE Annual Meeting 2009</u>, pp.1281-1282, Fukuoka

Viggiani, G. (1992), "Small-strain stiffness of fine grained soils", <u>Ph.D. thesis</u>, City University, London

Viggiani, G. and Atkinson, J.H. (1995) "Stiffness of fine-grained soil at very small strains", <u>Geotechnique</u>, Vol. 45, No. 2, pp. 249-265

Yimsiri, S. and Soga, K. (2001), "Anisotropy of highly-overconsolidated clay in small- and intermediate-strain levels", <u>Proc. of the 14th Southeast Asian Geotechnical Conference, 14th SEAGC</u>, Hong Kong

Yimsiri, S., Ratananikom, W. and Likitlersuang, S. (2009), "Investigation of some anisotropic characteristic of Bangkok Clay", <u>Proc. of the 17th International Conferecne on Soil Mechanics & Geotechnical Engineering , Alexandria</u>, Egypt

Zdravkovic, L. (1996), "The stress-strain-strength anisotropy of a granular medium under general stress conditions", <u>PhD. Thesis</u>, Imperial College of Science, Technology and Medicine, University of London

Zdravkovic, L. and Jardine, R.J. (2000), "Undrained anisotropy of K-0-consolidated silt", <u>CAN GEOTECH J</u>, Vol. 37, pp. 178 – 200

Ziegler, H. (1983), "An introduction to thermomechanics", North Holland, Amsterdam

ศูนย์วิทยทรัพยากร
จุฬาลงกรณ์มหาวิทยาลัย

APPENDICES

```
$debug
program NonlinearKHMCC2D
!*****************************************************************************************************
!* WHEN YOU USE THIS PROGRAM, PLEASE CITE THE FOLLOWING PAPER IN YOUR REFERENCE.
!* 1. Likitlersuang, S. and Houlsby, G.T.
!*    "Development of Hyperplasticity Model for Soil Mechanics",
!*     Int. Journal for Numerical and Analytical Method in Geomechanics, No. 30, pp 229 - 254, 2006
!* 2. Apriadi, Dedi, Likitlersuang, Suched, Pipatpongsa, Thirapong, Ohta, Hideki
!*    "On The Numerical Implementation Of Nonlinear Kinematic Hardening Modified Cam Clay Model"*
!*     The IES Journal Part A: Civil & Structural Engineering, Vol.2, No.3, pp.187-201, August, 2009.
!*  AND IF YOU FIND A BUG, PLEASE LET US KNOW:
!*   Dedi Apriadi, e-mail: dedia@geotech.pauir.itb.ac.id
!*    Suched Likitlersuang e-mail: Suched.L@eng.chula.ac.th
!*****************************************************************************************************
use material_pro
use PORTLIB
implicit none
double precision, external :: macaulay,delta
double precision :: p,q,px0,s_vm,pmax,chidev_temp,sdev_temp,ev,es,epsdev_temp
double precision, allocatable ::
eps(:),sdev(:),epsdev(:),chi(:,:),chidev(:,:),chi_ii(:),alphadev(:,:),alpha_ii(:)
integer :: nstage,nstep_calc
integer :: istage,istep,i,j,iv,jv,kv,plot_inc
integer, allocatable ::   nstep(:),cont(:)
double precision, allocatable :: tt(:,:),dt(:),s_max(:)
double precision, allocatable :: AA(:,:),iAA(:,:),BB(:,:,:),CC(:,:),D(:,:,:),H(:)
integer(2) :: ihr, imin, isec, i100th
real(4) runtime, TA(2)
character*80 f_inp,f_out
character*4  command
character*4  title(20)
!*******************************************Heading
write(*,*) '2-D HYPERPLASTICITY NON-LINEAR KINEMATIC HARDENING MODIFIED CAM CLAY MODEL'
write(*,*) 'Coded by Dedi Apriadi 2007/2009 - Bangkok/Tokyo'
write(*,*) ''
call id()
write(*,*) ''
write(*,*)'Enter your main input file: '
read (*,*) f_inp
write(*,*)'Enter your main output file: '
read (*,*) f_out
open (unit=3,file=f_inp,status='old')
open (unit=9,file=f_out,form="formatted",action="readwrite")
open (unit=2,file="stress.out",form="formatted",action="readwrite")
open (unit=4,file="strain.out",form="formatted",action="readwrite")
open (unit=5,file="state.out",form="formatted",action="readwrite")
write(2,*)'2-D HYPERPLASTICITY NON-LINEAR KINEMATIC HARDENING MODIFIED CAM CLAY MODEL'
write(2,*)'Coded by Dedi Apriadi 2007/2009 - Bangkok/Tokyo'
write(2,*)''
write(4,*)'2-D HYPERPLASTICITY NON-LINEAR KINEMATIC HARDENING MODIFIED CAM CLAY MODEL'
write(4,*)'Coded by Dedi Apriadi 2007/2009 - Bangkok/Tokyo'
write(4,*)''

write (9,*)
'============================================================================================
============================='
write (9,*) '  Step Stage  SIG_xx         SIG_yy         SIG_zz         SIG_xy         EPS_xx
Eps_yy        Eps_zz         Eps_xy'
write (9,*)
'============================================================================================
============================='
write(5,*)'============================================================================================
============================='
write(5,*)'Nth Yield   step stage      Hp             Hq             alphap        alphaq          c
Chi_p        Chi_q'
write(5,*)'============================================================================================
============================='

read(3,'(20A4)')title
read(3,*)command

do while (command.ne.'STOP')

    do_command: select case (command)        ! branch to command

    case ('CONT')
    !----------------------------------------------------------
            call GETTIM (ihr, imin, isec,i100th)
            write(*,FMT='(A,I2,A,I2,A,I2)')' Started at ',ihr,':',imin,':',isec
            print*,''

            write(2,FMT='(A,I2,A,I2,A,I2)')' Started at ',ihr,':',imin,':',isec
```

```
                write(2,*)''

                write(4,FMT='(A,I2,A,I2,A,I2)')' Started at ',ihr,':',imin,':',isec
                write(4,*)''

                read (3,*)nv,nstage,plot_inc,n
                read (3,*)flag
                print*, n,'  NUMBER OF YIELD SURFACES'
                print*, nstage,'  STAGES'
                print*,''

                print*, 'allocating memories........'
                allocate(tt(nstage,nv))
                allocate(dt(nstage))
                allocate(nstep(nstage))
                allocate(cont(nstage))
                allocate(s_max(nv))

                allocate(eps(nv))
                allocate(sdev(nv))
                allocate(epsdev(nv))
                allocate(alphadev(nv,n))
                allocate(alpha_ii(n))
                allocate(chi_ii(n))
                allocate(chidev(nv,n))
                allocate(hp(n))
                allocate(hq(n))
                allocate(c(n))
                allocate(eta(n))
                allocate(y(n))
                allocate(sig(nv))

                allocate(alpha(nv,n))
                allocate(chi(nv,n))

                allocate(AA(nv,nv))
                allocate(iAA(nv,nv))
                allocate(BB(nv,nv,n))
                allocate(CC(nv,n))
                allocate(D(nv,nv,n))
                allocate(H(nv))
                allocate(RH(nv))
                allocate(LH(nv,nv))
                allocate(dsigma(nv))
        read(3,*)command


        case ('MATE')
    !-------------------------------------------------------------
                print*, 'reading material properties........'
                if (flag==1) then
                        read (3,*) K,r,ap,bp          !K=K; G=gp
                        read (3,*) gx,aq,bq,M
                else if (flag==2) then               !K=K; G=G
                        read (3,*) K,r,ap,bp
                        read (3,*) G,aq,bq,M
                else if (flag==3) then
                        read (3,*) kx,r,ap,bp          !K=kp'0,G=gp
                        read (3,*) gx,nx,aq,bq,M
                else if (flag==4) then                     !K=kp'0^n pa^(1-n);G=gp'0^n pa^(1-n) DA
2007
                        read (3,*) kx,r,ap,bp
                        read (3,*) gx,nx,aq,bq,M   !elastic stiffness or small-strain stiffness
                end if
        read(3,*)command

        case ('INIT')
    !-------------------------------------------------------------
                print*, 'reading initial condition........'
                read(3,*) s_vm,sig(1),sig(2),sig(3),sig(4)
                do iv=1,nv                                    !initial total volumetric and deviatoric
strain
                        eps(iv)=0.0d0            !eps(1)=eps_xx, eps(2)=eps_yy, eps(3)=eps_zz,
eps(4)=2*eps_xy
                end do
                read(3,*)command

        case ('LOAD')
    !-------------------------------------------------------------
                print*, 'reading loading condition........'
                read (3,*) mu
                do istage=1,nstage
                        read (3,*) istage, cont(istage)
                        read (3,*) (tt(istage,iv),iv=1,nv)
```

```fortran
                        read (3,*) dt(istage),nstep(istage)
                end do
                read(3,*)command

        case ('CALC')
    !------------------------------------------------------------
                print*, 'CALCULATING........'
                deta=1.0d0/real(n)
                s_max(1)=s_vm
                s_max(2)=s_vm
                s_max(3)=s_vm
                pmax=(s_max(1)+s_max(2)+s_max(3))/3.0d0
                p=(sig(1)+sig(2)+sig(3))/3.0d0
                q=sig(1)-sig(3)
                ev=eps(1)+eps(2)+eps(3)
                es=2.0d0/3.0d0*(eps(1)-eps(3))
                px0=pmax/2.0d0
                pr=p

                !Initialisation
                do iv=1,nv
                        do i=1,n
                                chidev(iv,i)=0.0d0
                                alphadev(iv,i)=0.0d0
                        end do
                end do

                dgdp_eta_p=0.0d0
                dgdp_eta_q=0.0d0
                do j=1,n
                        dgdp_eta_p=dgdp_eta_p+(1-r*eta(j))**bp/(2.0d0*(ap-1.0d0))
                        dgdp_eta_p=dgdp_eta_q+(1-r*eta(j))**bq/(2.0d0*(aq-1.0d0))
                end do

                do iv=1,nv        !initial alpha  for all flags except 5
                        do j=1,n
                                eta(j)=real(j)/real(n)
                                if (flag==1) then
                                        hp(j)=K*(1.0d0-r*eta(j))**bp/(2.0d0*(ap-1.0d0)) ! Dr.
Suched 2006

                                else if (flag==2) then
                                        hp(j)=K*(1.0d0-r*eta(j))**bp/(2.0d0*(ap-1.0d0))
                                else if(flag==3) then
                                        hp(j)=kx*pmax*(1.0d0-r*eta(j))**bp/(2.0d0*(ap-1.0d0))

                                else if (flag==4) then
                                        hp(j)=kx*pr**(1-nx)*pmax**nx*(1.0d0-
r*eta(j))**bp/(2.0d0*(ap-1.0d0))   !Dedi Apriadi 2007 for non linear hardening
                                end if
                                if (iv<=3) then
                                        alpha(iv,j)=px0/(3.0d0*hp(j))
                                else
                                        alpha(iv,j)=0.0d0
                                end if
                        end do
                end do

                do iv=1,nv
                        do i=1,n
                                eta(i)=real(i)/real(n)
                                if (flag==1) then
                                        hq(i)=3.0d0*gx*p*(1.0d0-eta(i))**bq/(2.0d0*(aq-1.0d0))
        !Suched 2006
                                else if (flag==2) then
                                        hq(i)=3.0d0*G*(1.0d0-eta(i))**bq/(2.0d0*(aq-1.0d0))
                                else if(flag==3) then
                                        hq(i)=3.0d0*gx*p*(1.0d0-eta(i))**bq/(2.0d0*(aq-1.0d0))
         !w/ K=kp'0; G=g p
                                else if (flag==4) then
                                        hq(i)=3.0d0*gx*pr**(1-nx)*pmax**nx*(1.0d0-
eta(i))**bq/(2.0d0*(aq-1.0d0))
                                end if
                                alpha_ii(i)=alpha(1,i)+alpha(2,i)+alpha(3,i)
                                alphadev(iv,i)=alpha(iv,i)-(alpha_ii(i)/3.0d0)*delta(iv)
                                sdev(iv)=sig(iv)-p*delta(iv)
                                epsdev(iv)=eps(iv)-(ev/3.0d0)*delta(iv)
                                c(i)=hp(i)*alpha_ii(i)*eta(i)
                                if(iv<=3) then
                                        chi(iv,i)=sig(iv)-hp(i)*alpha_ii(i)-
2.0d0*hq(i)*alphadev(iv,i)/3.0d0
                                else
                                        chi(iv,i)=sig(iv)-hq(i)/3.0d0*alphadev(iv,i)
                                end if
                                chi_ii(i)=(chi(1,i)+chi(2,i)+chi(3,i))/3.0d0
```

```
                                chidev_temp=0.0d0
                                chidev(iv,i)=chi(iv,i)-chi_ii(i)*delta(iv)
                                if(iv<=3) then
                                        chidev_temp=chidev_temp+chidev(iv,i)**2
                                else
                                        chidev_temp=chidev_temp+2.0d0*chidev(iv,i)**2
                                end if
                                y(i)=sqrt(chi_ii(i)**2+1.50d0*chidev_temp/M**2)-c(i)
                        end do
                end do

                istep=0
                istage=1

                !Input documentation
                write(2,'(1x,20A4)')title
                write(2,*)''
                write(2,'(" NUMBER OF YIELD SURFACES",I5)') n
                write(2,'(" NUMBER OF STAGES",I5)') nstage
                write(2,*)''
                write(2,*)'MATERIAL PROPERTIES'

                write(2,'(" Dimensionless material constants: g=",D10.5,"  k=",D10.5,"  n=",D10.5)')
gx,kx,nx
                write(2,'(" Critical state parameter: M=",D10.5)') M
                write(2,'(" Kinematic hardening parameter: a=",D10.5)') ap
                write(2,*)''

                write(4,'(1x,20A4)')title
                write(4,*)''
                write(4,'(" NUMBER OF YIELD SURFACES",I5)') n
                write(4,'(" NUMBER OF STAGES",I5)') nstage
                write(4,*)''
                write(4,*)'MATERIAL PROPERTIES'

                write(4,'(" Dimensionless material constants: g=",D10.5,"  k=",D10.5,"  n=",D10.5)')
gx,kx,nx
                write(4,'(" Critical state parameter: M=",D10.5)') M
                write(4,'(" Kinematic hardening parameter: a=",D10.5)') ap
                write(4,*)''

                !Output documentation
                write (2,*)
'==============================================================================='
                write (2,*) ' Step Stage     Sxx          Syy          Szz          Sxy          p
q'
                write (2,*)
'==============================================================================='

                write (4,*)
'==============================================================================='
                write (4,*) ' Step Stage  EPS_xx       EPS_yy       EPS_zz       EPS_xy          Ev
Es'
                write (4,*)
'==============================================================================='

                write (unit=9,FMT='(I5,I5,D12.5,D12.5,D12.5,D12.5,D12.5,D12.5,D12.5,D12.5)')
istep,istage,sig(1),sig(2),sig(3),sig(4),eps(1),eps(2),eps(3),eps(4)
                write (unit=2,FMT='(I5,I5,D12.5,D12.5,D12.5,D12.5,D12.5,D12.5)')
istep,istage,sig(1),sig(2),sig(3),sig(4),p,q
                write (unit=4,FMT='(I5,I5,D12.5,D12.5,D12.5,D12.5,D12.5,D12.5)')
istep,istage,eps(1),eps(2),eps(3),eps(4),ev,es

        do istage=1,nstage
                if (istage==1) then
                        nstep_calc=nstep(istage)/plot_inc
                else if (istage>1) then
                        nstep_calc=nstep(istage)/plot_inc
                end if
                print*, '          stage',istage
                do istep=1,nstep_calc         !strain increment =
(nstep*dt)/(nstep(istage)/cut)
                        do i=1,plot_inc
        !with nstep = total axial/deviatoric strain rate
                                do iv=1,nv
        !nstep*dt = total axial/deviatoric strain
                                        do j=1,n
                                                eta(j)=real(j)/real(n)
                                                if (flag==1) then
                                                        hq(j)=3.0d0*gx*p*(1.0d0-
eta(j))**bq/(2.0d0*(aq-1.0d0))     !Suched 2006

                                                else if (flag==3) then
                                                        hq(j)=3.0d0*gx*p*(1.0d0-
eta(j))**bq/(2.0d0*(aq-1.0d0))
```

```fortran
                                                                end if

        alpha_ii(j)=alpha(1,j)+alpha(2,j)+alpha(3,j)
                                                        alphadev(iv,j)=alpha(iv,j)-
(alpha_ii(j)/3.0d0)*delta(iv)
                                                        sdev(iv)=sig(iv)-p*delta(iv)
                                                        epsdev(iv)=eps(iv)-(ev/3.0d0)*delta(iv)
                                                        c(j)=hp(j)*alpha_ii(j)*eta(j)
                                                        if(iv<=3) then
                                                                chi(iv,j)=sig(iv)-
hp(j)*alpha_ii(j)-2.0d0*hq(j)*alphadev(iv,j)/3.0d0
                                                        else
                                                                chi(iv,j)=sig(iv)-
hq(j)/3.0d0*alphadev(iv,j)
                                                        end if

        chi_ii(j)=(chi(1,j)+chi(2,j)+chi(3,j))/3.0d0
                                                        chidev_temp=0.0d0
                                                        chidev(iv,j)=chi(iv,j)-
chi_ii(j)*delta(iv)
                                                        if(iv<=3) then

        chidev_temp=chidev_temp+chidev(iv,j)**2
                                                        else

        chidev_temp=chidev_temp+2.0d0*chidev(iv,j)**2
                                                        end if
        y(j)=sqrt(chi_ii(j)**2+1.50d0*chidev_temp/M**2)-c(j)
                                                                end do
                                                        end do

                                                        call make_dgda(alphadev,alpha_ii,chi)
                                                        call make_d2gds2(p,sdev,AA)
                                                        call make_d2gdsda(BB)
                                                        call make_dwdchi(chidev,chi_ii,CC)

                                                        do iv=1,nv
                                                                do j=1,n
                                                                        do jv=1,nv
                                                                                D(jv,iv,j)=BB(jv,iv,j)*CC(iv,j)
                                                                        end do
                                                                end do
                                                        end do

                                                        do iv=1,nv
                                                                H(iv)=SUM(D(iv,1:nv,1:n)) !integration of [BB] x
[CC] in respect to eta
                                                        end do
                                                        do iv=1,nv
                                                                if (cont(istage)==1) then
        RH(iv)=SUM(AA(iv,1:nv)*tt(istage,iv))*dt(istage)+H(iv)*deta*dt(istage)  !for stress control
                                                                else if (cont(istage)==2) then
                                                                        !RH(iv)=(tt(istage,iv)-
H(iv)*deta)*dt(istage)  !for strain control
                                                                        RH(iv)=(tt(istage,iv)-
H(iv)*deta)*dt(istage)  !for strain control
                                                                endif
                                                        end do
                                                        do iv=1,nv
                                                                do kv=1,nv
                                                                        LH(iv,kv)=AA(iv,kv)
                                                                end do
                                                        end do
                                                        if (cont(istage)==1) then              !for stress control
                                                                sdev_temp=0.0d0
                                                                epsdev_temp=0.0d0
                                                                do iv=1,nv
                                                                        sig(iv)=sig(iv)+tt(istage,iv)*dt(istage)
                                                                        eps(iv)=eps(iv)+RH(iv)
                                                                        if (iv==4) then

        sdev_temp=sdev_temp+2.0d0*sdev(iv)**2

        epsdev_temp=epsdev_temp+2.0d0*epsdev(iv)**2

                                                                        else
                                                                                sdev_temp=sdev_temp+sdev(iv)**2

        epsdev_temp=epsdev_temp+epsdev(iv)**2

                                                                        end if
                                                                end do
                                                                p=(sig(1)+sig(2)+sig(3))/3.0d0
```

```fortran
                                          if (sdev(1)<0.0d0) then  !just for triaxial
condition
                                                  q=-(3.0d0/2.0d0*sdev_temp)**0.5
                                          else
                                                  q=(3.0d0/2.0d0*sdev_temp)**0.5
                                          end if

                                          if (epsdev(1)<0.0d0) then  !just for triaxial
condition
                                                  es=-(2.0d0/3.0d0*epsdev_temp)**0.5
                                          else
                                                  es=(2.0d0/3.0d0*epsdev_temp)**0.5
                                          end if

                                          ev=eps(1)+eps(2)+eps(3)
                             else if (cont(istage)==2) then      !for strain control
                                          call lufactor
                                          sdev_temp=0.0d0
                                          epsdev_temp=0.0d0
                                          do iv=1,nv
                                                  sig(iv)=sig(iv)+dsigma(iv)
                                                  eps(iv)=eps(iv)+tt(istage,iv)*dt(istage)
                                                  if (iv==4) then

        sdev_temp=sdev_temp+2.0d0*sdev(iv)**2

        epsdev_temp=epsdev_temp+2.0d0*epsdev(iv)**2

                                                  else
                                                          sdev_temp=sdev_temp+sdev(iv)**2

        epsdev_temp=epsdev_temp+epsdev(iv)**2
                                                  end if
                                          end do
                                          p=(sig(1)+sig(2)+sig(3))/3.0d0
                                          if (sdev(1)<0.0d0) then  !just for triaxial
condition
                                                  q=-(3.0d0/2.0d0*sdev_temp)**0.5
                                          else
                                                  q=(3.0d0/2.0d0*sdev_temp)**0.5
                                          end if

                                          if (epsdev(1)<0.0d0) then  !just for triaxial
condition
                                                  es=-(2.0d0/3.0d0*epsdev_temp)**0.5
                                          else
                                                  es=(2.0d0/3.0d0*epsdev_temp)**0.5
                                          end if

                                          ev=eps(1)+eps(2)+eps(3)
                                 endif

                             do iv=1,nv
                                  do j=1,n

        alpha(iv,j)=alpha(iv,j)+CC(iv,j)*dt(istage)
                                  end do
                             end do
                          end do
                          write
(unit=9,FMT='(I5,I5,D12.5,D12.5,D12.5,D12.5,D12.5,D12.5,D12.5,D12.5)')
istep,istage,sig(1),sig(2),sig(3),sig(4),eps(1),eps(2),eps(3),eps(4)
                          write (unit=2,FMT='(I5,I5,D12.5,D12.5,D12.5,D12.5,D12.5,D12.5)')
istep,istage,sig(1),sig(2),sig(3),sig(4),p,q
                          write (unit=4,FMT='(I5,I5,D12.5,D12.5,D12.5,D12.5,D12.5,D12.5)')
istep,istage,eps(1),eps(2),eps(3),eps(4),ev,es

                          do i=1,n
                                  !write
(unit=2,FMT='(I5,I10,I5,D15.5,D15.5,D15.5,D15.5,D15.5,D15.5,D15.5,D15.5,D15.5,D15.5)')
i,istep,istage,hp(i),hq(i),temp_alpha(1,i),temp_alpha(2,i),c(i),chi(1,i),chi(2,i),CC(1,i),CC(1,i),
y(i)
                          end do
                     end do
              end do

              deallocate(tt)
              deallocate(dt)
              deallocate(nstep)
              deallocate(cont)
              deallocate(s_max)

              deallocate(eps)
```

```
                      deallocate(sdev)
                      deallocate(epsdev)
                      deallocate(alphadev)
                      deallocate(alpha_ii)
                      deallocate(chi_ii)
                      deallocate(chidev)
                      deallocate(hp)
                      deallocate(hq)
                      deallocate(c)
                      deallocate(eta)
                      deallocate(y)
                      deallocate(sig)

                      deallocate(alpha)
                      deallocate(chi)

                      deallocate(AA)
                      deallocate(iAA)
                      deallocate(BB)
                      deallocate(CC)
                      deallocate(D)
                      deallocate(H)
                      deallocate(RH)
                      deallocate(LH)
                      deallocate(dsigma)
            read(3,*)command

            case default
      !-----------------------------------------------------------
                  print*, command
            print*, 'Command not recognized; please read manual'
            stop

            end select do_command

end do

call GETTIM (ihr, imin, isec,i100th)
write(*,*) ''
write(*,FMT='(A,I2,A1,I2,A1,I2)')' Finished at ',ihr,':',imin,':',isec
runtime = DTIME(TA)
write(*,FMT='(A,F10.2,A)')' Running time ',runtime,' seconds'

write (2,*) '============================================================================='
write(2,*) ''
write(2,FMT='(A,I2,A1,I2,A1,I2)')' Finished at ',ihr,':',imin,':',isec
write(2,FMT='(A,F10.2,A)')' Running time ',runtime,' seconds'

write (4,*) '============================================================================='
write(4,*) ''
write(4,FMT='(A,I2,A1,I2,A1,I2)')' Finished at ',ihr,':',imin,':',isec
write(4,FMT='(A,F10.2,A)')' Running time ',runtime,' seconds'

close (3)
close (2)
close (4)
close (5)
close(9)

stop
end program NonlinearKHMCC2D

double precision function macaulay(x)
        implicit none
        double precision, intent(in) :: x
        macaulay=(x+ABS(x))/2.0d0
end function macaulay

double precision function delta(i)    !Kronecker's delta
implicit none
integer, intent(in) :: i
if((i==1).or.(i==2).or.(i==3)) then
        delta=1.0d0
else
        delta=0.0d0
end if
end function delta
```

BIOGRAPHY

Dedi Apriadi received the B.Eng and M.Eng. degrees in Geotechnical Engineering from Bandung Institute of Technology in 1995 and 1999, respectively. He has been a Research Assistant at Geotechnical Engineering Laboratory, Bandung Institute of Technology since 1996. Since October 2006, he joined a Ph.D. sandwich program between Chulalongkorn University, Thailand and Tokyo Institute of Technology, Japan supported by AUN/SEED-Net JICA. During his Ph.D. study, he has already submitted 10 papers with his advisors. Two of the papers received the Student Award for Outstanding paper and Best Presentation from 21st KKCNN Civil Engineering Symposium in Singapore and Certificate of Appreciation from Vice President of Asian ISSMGE from 6th Asian Young Geotechnical Engineers Conference in India, respectively. His research interests include constitutive modelling of geomaterials, computational geotechnics and geotechnical earthquake engineering. He is a member of Japan Society of Civil Engineers (JSCE) and Indonesia Society of Geotechnical Engineers (HATTI).

ศูนย์วิทยทรัพยากร
จุฬาลงกรณ์มหาวิทยาลัย